CHAPTER 1

Residence Time Distributions

E. BRUCE NAUMAN

Rensselaer Polytechnic Institute

1-1 INTRODUCTION

The concept of residence time distribution (RTD) and its importance in flow processes first developed by Danckwerts (1953) was a seminal contribution to the emergence of chemical engineering science. An introduction to RTD theory is now included in standard texts on chemical reaction engineering. There is also an extensive literature on the measurement, theory, and application of residence time distributions. A literature search returns nearly 5000 references containing the concept of residence time distribution and some 30 000 references dealing with residence time in general. This chapter necessarily provides only a brief introduction; the references provide more comprehensive treatments.

The residence time distribution measures features of ideal or nonideal flows associated with the bulk flow patterns or *macromixing* in a reactor or other process vessel. The term *micromixing*, as used in this chapter, applies to spatial mixing at the molecular scale that is bounded but not determined uniquely by the residence time distribution. The bounds are extreme conditions known as *complete segregation* and *maximum mixedness*. They represent, respectively, the least and most molecular-level mixing that is possible for a given residence time distribution.

Most of this handbook treats *spatial mixing*. Suppose that a sample of fluid is collected and analyzed. One may ask: Is it homogeneous? Standard measures of homogeneity such as the striation thickness in laminar flow or the coefficient of variation in turbulent flow can be used to answer this question quantitatively. In this chapter we look at a different question that is important for continuous flow systems: When did the particles, typically molecules but sometimes larger particles, enter the system, and how long did they stay? This question

Handbook of Industrial Mixing: Science and Practice, Edited by Edward L. Paul, Victor A. Atiemo-Obeng, and Suzanne M. Kresta
ISBN 0-471-26919-0

involves *temporal mixing*, and its quantitative answer is provided by the RTD (Danckwerts, 1953).

To distinguish between spatial and temporal mixing, suppose that a flow system is fed from separate black and white streams. If the effluent emerges uniformly gray, there is good spatial mixing. For the case of a pipe, the uniform grayness corresponds to good mixing in the radial direction. Now suppose that the pipe is fed from a single stream that varies in shade or grayness. The effluent will also vary in shade unless there is good temporal mixing. In the context of a pipe, spatial mixing is equivalent to *radial mixing*, and temporal mixing is equivalent to *axial mixing*.

In a batch reactor, all molecules enter and leave together. If the system is isothermal, reaction yields depend only on the elapsed time and on the initial composition. The situation in flow systems is more complicated but not impossibly so. The counterpart of the batch reaction time is the age of a molecule. Aging begins when a molecule enters the reactor and ceases when it leaves. The total time spent within the boundaries of the reactor is known as the *exit age*, or *residence time*, t. In real flow systems, molecules leaving the system will have a variety of residence times. The distribution of residence times provides considerable information about homogeneous isothermal reactions. For single first-order reactions, knowledge of the RTD allows the yield to be calculated exactly, even in flow systems of arbitrary complexity. For other reaction orders, it is usually possible to calculate fairly tight limits, within which the yield must lie (Zwietering, 1959). If the system is nonisothermal or heterogeneous, the RTD cannot predict reaction yield directly, but it still provides a general description of the flow that is not easily obtained by velocity measurements.

Residence time experiments have been used to explore the hydrodynamics of many chemical processes. Examples include fixed and fluidized bed reactors, chromatography columns, two-phase stirred tanks, distillation and absorption columns, and trickle bed reactors.

1-2 MEASUREMENTS AND DISTRIBUTION FUNCTIONS

Transient experiments with inert tracers are used to determine residence time distributions. In real systems, they will be actual experiments. In theoretical studies, the experiments are mathematical and are applied to a dynamic model of the system. Table 1-1 lists the types of RTDs that can be measured using tracer experiments. The simplest case is a *negative step change*. Suppose that an inert tracer has been fed to the system for an extended period, giving $C_{in} = C_{out} = C_0$ for $t < 0$. At time $t = 0$, the tracer supply is suddenly stopped so that $C_{in} = 0$ for $t > 0$. Then the tracer concentration at the reactor outlet will decrease with time, eventually approaching zero as the tracer is washed out of the system. This response to a negative step change defines the *washout function*, W(t). The responses to other standard inputs are shown in Table 1-1. Relationships between the various functions are shown in Table 1-2.

Table 1-1 Residence Time Distribution Functions

Name	Symbol	Input Signal	Output Signal	Physical Interpretation	Properties
Washout function	$W(t)$	Negative step change in tracer, concentration from an initial value of C_0 to a final value of 0	$W(t) = C_{out}(t)/C_0$	$W(t)$ is the fraction of particles that remained in the system for a time greater than t.	$W(0) = 1$ $W(\infty) = 0$ $dW/dt \leq 0$
Cumulative distribution function	$F(t)$	Positive step change in tracer concentration from an initial value of 0 to a final value of C_∞	$F(t) = C_{out}(t)/C_\infty$	$F(t)$ is the fraction of particles that remained in the system for a time less than t.	$F(0) = 0$ $F(\infty) = 1$ $dF/dt \geq 0$
Differential distribution function	$f(t)$ or $E(t)$	Sharp impulse of tracer	$f(t) = \dfrac{C_{out}(t)}{\int_0^\infty C_{out}(t)\,dt}$	$f(t)\,dt$ is the fraction of particles that remained in the system for a time between t and $t + dt$.	$f(t) \geq 0$ $\int_0^\infty f(t)\,dt = 1$
Convolution integral	$C_{out}(t)$	Any time-varying tracer concentration	$C_{out}(t) = \int_{-\infty}^{t} C_{in}(\theta) f(t-\theta)\,d\theta$ $= \int_0^\infty C_{in}(t-\theta) f(\theta)\,d\theta$	The output signal is a damped response that reflects the entire history of inputs.	$[C_{out}]_{max} \leq [C_{in}]_{max}$

Table 1-2 Relationships between the Functions and Moments of the RTD

Definition	Mathematical Formulation
Relations between the distribution functions	$f(t) = \dfrac{dF}{dt} = -\dfrac{dW}{dt}$
	$F(t) = \displaystyle\int_0^t f(t')dt'$
	$W(t) = \displaystyle\int_t^\infty f(t')dt'$
Moments about the origin	$\mu_n = \displaystyle\int_0^\infty t^n f(t)\,dt = n\int_0^\infty t^{n-1}W(t)\,dt$
First moment = mean residence time	$\bar{t} = \displaystyle\int_0^\infty tf(t)\,dt = \int_0^\infty W(t)\,dt$
Moments about the mean	$\mu_n' = \displaystyle\int_0^\infty (t-\bar{t})^n f(t)\,dt = n\int_0^\infty (t-\bar{t})^{n-1}W(t)\,dt + (-\bar{t})^n$
Dimensionless variance of the RTD	$\sigma^2 = \dfrac{\mu_2'}{\bar{t}^2} = \dfrac{\displaystyle\int_0^\infty (t-\bar{t})^2 f(t)\,dt}{\bar{t}^2} = \dfrac{2\displaystyle\int_0^\infty tW(t)\,dt}{\bar{t}^2} - 1$

A good input signal, usually a negative step change, must be made at the reactor inlet. The mixing-cup average concentration of tracer molecules must be accurately measured at the outlet. If the tracer has a background concentration, it is subtracted from the experimental measurements. The flow properties of the tracer molecules must be similar to those of the reactant molecules, and the change in total flow rate must be insignificant. It is usually possible to meet these requirements in practice. The major theoretical requirement is that the inlet and outlet streams have unidirectional flows, so that once the molecules enter the system they stay in until they exit, never to return. Systems with unidirectional inlet and outlet streams are *closed* so that a molecule enters the system only once and leaves only once. Most systems of chemical engineering importance are closed to a reasonable approximation.

Among RTD experiments, washout experiments are generally preferred since $W(\infty) = 0$ will be known a priori but $F(\infty) = C_0$ must usually be measured. The positive step experiment will also be subject to errors caused by changes in C_0 during the course of the experiment. However, the positive step change experiment requires a smaller amount of tracer since the experiment will be terminated before the outlet concentration fully reaches C_0. Impulse response experiments that measure f(t) use still smaller amounts.

The RTD can be characterized by its moments as indicated in Table 1-2. The most important moment is the first moment about the mean, known as the *mean*

residence time and usually denoted as $\bar{t}$:

$$\bar{t} = \int_0^\infty tf(t)\,dt = \int_0^\infty W(t)\,dt = \frac{\text{mass inventory in the system}}{\text{mass flow rate through the system}} = \frac{\text{hold-up}}{\text{throughput}} \quad (1\text{-}1)$$

Thus $\bar{t}$ can be found from inert tracer experiments. It can also be found from measurements of the system inventory and throughput. Agreement of the $\bar{t}$'s calculated by these two methods provides a good check on experimental accuracy. Occasionally, eq. (1-1) is used to determine an unknown volume or an unknown density from inert tracer data.

Roughly speaking, the first moment, $\bar{t}$, measures the size of an RTD, while higher moments measure its shape. One common measure of shape is the dimensionless second moment about the mean, also known as the *dimensionless variance*, σ^2 (see Table 1-2). In piston flow, all particles have the same residence time, so $\sigma^2 = 0$. This case is approximated by highly turbulent flow in a pipe. In an ideal continuous flow stirred tank reaction, $\sigma^2 = 1$. Well-designed reactors in turbulent flow have a σ^2 value between 0 and 1, but laminar flow reactors can have $\sigma^2 > 1$.

Note that either W(t) or f(t) can be used to calculate the moments. Use the one that was obtained directly from an experiment. If moments of the highest possible accuracy are desired, the experiment should be a negative step change to get W(t) directly.

1-3 RESIDENCE TIME MODELS OF FLOW SYSTEMS

Figure 1-1 shows the washout functions for some flow systems. The time scale in this figure has been converted to dimensionless time, $t/\bar{t}$. This means that the integrals of the various washout functions all have unit mean so that the various flow systems can be compared independent of system size.

1-3.1 Ideal Flow Systems

The ideal cases are the *piston flow reactor* (PFR), also known as a *plug flow reactor*, and the *continuous flow stirred tank reactor* (CSTR). A third kind of ideal reactor, the *completely segregated CSTR*, has the same distribution of residence times as a normal, perfectly mixed CSTR. The washout function for a CSTR has the simple exponential form

$$W(t) = e^{-t/\bar{t}} \quad (1\text{-}2)$$

A CSTR is said to have an *exponential distribution* of residence times. The washout function for a PFR is a negative step change occurring at time $\bar{t}$:

$$W(t) = \begin{cases} 1 & t < \bar{t} \\ 0 & t > \bar{t} \end{cases} \quad (1\text{-}3)$$

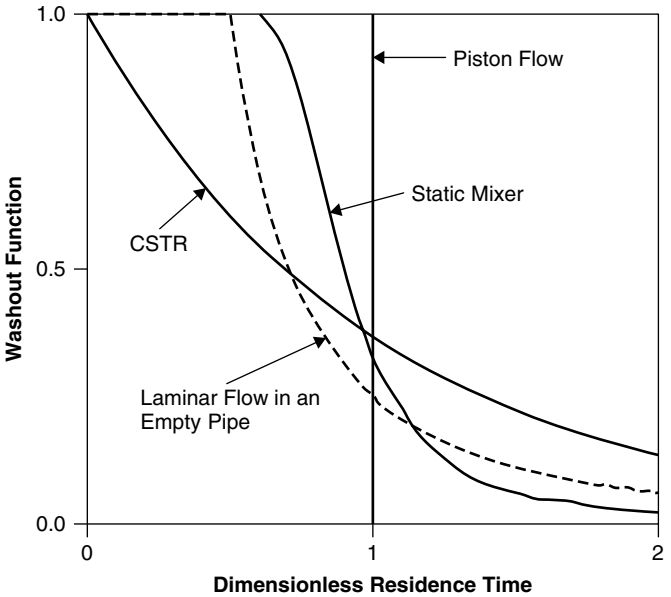

Figure 1-1 Residence time washout functions for various flow systems.

The derivative of a step change is a delta function, and $f(t) = \delta(t - \bar{t})$. Thus, a piston flow reactor is said to have a *delta distribution* of residence times. The variances for these ideal cases are $\sigma^2 = 1$ for a CSTR and $\sigma^2 = 0$ for a PFR, which are extremes for well-designed reactors in turbulent flow. Poorly designed reactors and laminar flow reactors with little molecular diffusion can have σ^2 values greater than 1.

1-3.2 Hydrodynamic Models

The curve for laminar flow in Figure 1-1 was derived for a parabolic velocity profile in a circular tube. The washout function is

$$W(t) = \begin{cases} 1 & t < \bar{t}/2 \\ \dfrac{\bar{t}^2}{4t^2} & t > \bar{t}/2 \end{cases} \tag{1-4}$$

Equation (1-4) is a theoretical result calculated from a hydrodynamic model, albeit a very simple one. It has a sharp *first appearance time*, t_{first}, where the washout function first falls below 1.0. Real systems, such as that for the static mixer illustrated in Figure 1-1, may have a fuzzy first appearance time. For the fuzzy case, a 5% response time [i.e., $W(t) = 0.95$] is used instead. Table 1-3 shows first appearance times for some laminar flow systems.

Table 1-3 First Appearance Times in Laminar Flow Systems

Geometry	$t_{first}/\bar{t}$
Equilateral–triangular ducts	0.450
Square ducts	0.477
Straight, circular tubes	0.500
Straight, circular tubes (5% response)	0.513
16 element Kenics mixer (5% response)	0.598
Helically coiled tubes	0.613
Annular flow	0.500–0.667
Parabolic flow between flat plates	0.667
40 element Kenics mixer (5% response)	0.676
Single-screw extruder	0.750
Helical coils with changes in the direction of centrifugal force	>0.85

Flow patterns in the Kenics static mixer are too complicated to determine the residence time distribution analytically. Instead, experimental measurements were fit to a simple model. The model used for the Kenics mixer in Table 1-3 assumes regions of undisturbed laminar flow separated by planes of complete radial mixing, there being one mixing plane for every four Kenics elements. Simpler models are useful for systems in turbulent flow.

A system with a sharp first appearance time and $\sigma^2 < 1$ can be approximated as a PFR in series with a CSTR. This model is used for residence times in a fluidized bed reactor. If the system has a fuzzy first appearance time and $\sigma^2 \approx 1$, the tanks-in-series model or the axial dispersion model can be used. These models are used for tubular reactors in turbulent flow. The tanks-in-series is also used when the physical system consists of CSTRs in series, and it may be a good approximation for a single CSTR with dual Rushton turbines.

Tubular polymerization reactors frequently show large deviations from the parabolic velocity profile of constant viscosity laminar flow. The velocity profile of a polymerizing mixture can be calculated by combining the equations of motion with the convective diffusion equations for heat and mass, but direct experimental verification of the calculations is difficult. One way of testing the results is to compare an experimental residence time distribution to the calculated distribution. There is a one-to-one correspondence between velocity profile and RTD for well-developed diffusion-free flows in tubes. See Nauman and Buffham (1983) for details.

1-3.3 Recycle Models

High rates of external recycle have the same effect on the RTD as high rates of internal recycle in a stirred tank. The recycle system in Figure 1-2*a* can represent a loop reactor or it can be a model for a stirred tank. The once-through RTD must be known. In principle, it can be measured by applying a step change at the reactor inlet, measuring the outlet response, and then destroying the tracer before it has

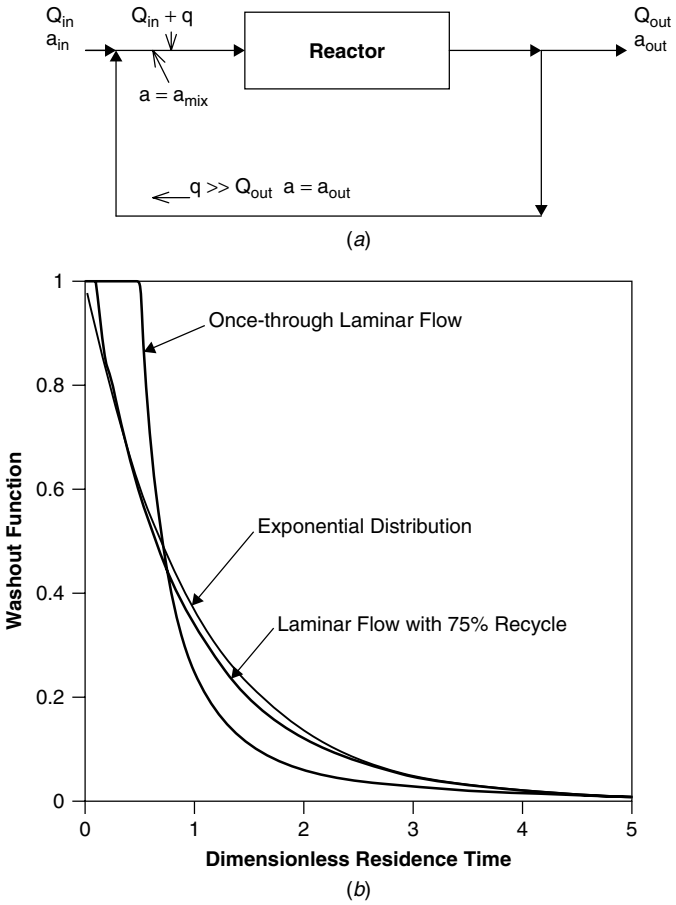

Figure 1-2 Recycle reactor: (*a*) flow diagram; (*b*) washout function for a 3 : 1 recycle ratio.

a chance to recycle. A more elaborate analysis allows its estimation from tracer experiments performed on the entire system. In practice, mathematical models for the once-through distribution are generally used. The easiest way of generating the composite distribution is by simulation. As a specific example, suppose that the reactor in Figure 1-2*a* is a tube in laminar flow so that the once-through distribution is given by eq. (1-4). Results of a simulation for a recycle ratio of $q/Q = 3$ are shown in Figure 1-2*b*. This first appearance time for a reactor in a recycle loop is the first appearance time for the once-through distribution divided by $q/Q + 1$. It is thus 0.125 in Figure 1-2*b* and declines rather slowly as the recycle ratio is increased. However, even at $q/Q = 3$, the washout function is remarkably close to the exponential distribution of a CSTR. More conservative estimates for the recycle ratio necessary to approach the behavior of a CSTR range from 6 to 100. The ratio selected, of course, depends on the application.

1-4 USES OF RESIDENCE TIME DISTRIBUTIONS

The most important use of residence time theory is its application to equipment that is already built and operating. It is usually possible to find a tracer together with injection and detection methods that will be acceptable to a plant manager. The RTD is measured and then analyzed to understand system performance. In this section we focus on such uses. The washout function is assumed to have an experimental basis. Calculations using it will be numerical in nature or will be analytical procedures applied to a model that reproduces the data accurately. Data fitting is best done by nonlinear least squares using untransformed experimental measurements of W(t), F(t), or f(t) versus time, t. Eddy diffusion in a turbulent system justifies exponential extrapolation of the integrals that define the moments in Table 1-2. For laminar flow systems, washout experiments should be continued until at least five times the estimated value for $\bar{t}$. The dimensionless variance has limited usefulness in laminar flow systems.

1-4.1 Diagnosis of Pathological Behavior

An important use of residence time measurements is to diagnose abnormalities in flow. The first test is whether or not $\bar{t}$ has its expected value (i.e., as the ratio of inventory to throughput). A lower-than-expected value suggests fouling or stagnancy. A higher value is more likely to be caused by experimental error.

The second test supposes that $\bar{t}$ is reasonable and compares the experimental washout curve to what would be expected for the physical design. Suppose that the experimental curve is initially lower than expected; then the system exhibits *bypassing*. If the tail of the distribution is higher than expected, the system exhibits *stagnancy*. Bypassing and stagnancy often occur together. If an experimental washout function initially declines faster than expected, it must eventually decline more slowly since the integrals under the experimental and model curves must both be $\bar{t}$. Bypassing and stagnancy are most easily distinguished when the system is near piston flow and the idealized model is a step change. They are harder to distinguish in stirred tanks because the comparison is made to an exponential curve. When a stirred tank exhibits either bypassing or stagnancy, $\sigma^2 > 1$. Extreme stagnancy will give a mean residence time less than that calculated as the ratio of inventory to throughput. Bypassing or stagnancy can be modeled as vessels in parallel. A stirred tank might be modeled using large and small tanks in parallel. To model bypassing, the small tank would have a residence time lower than that of the large tank. To model stagnancy, the small tank would have a longer residence time. The *side capacity model* shown in Figure 1-3 can also be used and is physically more realistic than a parallel connection of two isolated tanks.

1-4.2 Damping of Feed Fluctuations

One generally beneficial consequence of temporal mixing is that fluctuations in component concentrations will be damped. The extent of the damping depends on

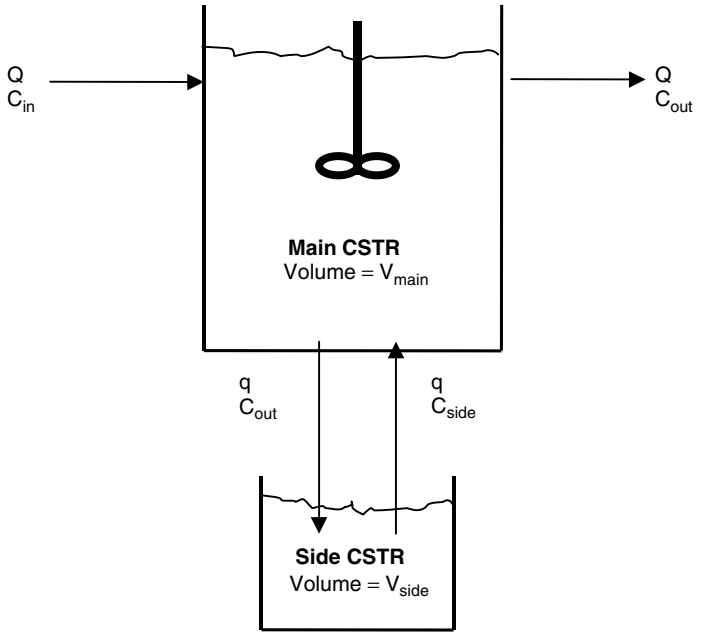

Figure 1-3 Side capacity model for bypassing or stagnancy in a CSTR.

the nature of the input signal and the residence time distribution. The following pair of convolution integrals applies to an inert tracer that enters the system with time-varying concentration $C_{in}(t)$:

$$C_{out}(t) = \int_0^\infty C_{in}(t - t')f(t')\,dt' = \int_{-\infty}^{t} C_{in}(t)f(t - t')\,dt' \qquad (1\text{-}5)$$

A piston flow reactor causes pure dead time: a time delay of $\bar{t}$ and no damping. A CSTR acts as an exponential filter and provides good damping provided that the period of the disturbance is less than $\bar{t}$. If the input is sinusoidal with frequency ω, the output will also be sinusoidal, but the magnitude or amplitude of the ripple will be divided by $\sqrt{1 + (\omega\bar{t})^2}$. Damping performance is not sensitive to small changes in the RTD. The true CSTR, the recycle reactor shown in Figure 1-3, and a recently designed axial static mixer give substantially the same damping performance (Nauman et al., 2002).

1-4.3 Yield Prediction

In this section we outline the use of RTDs to predict the yield of homogeneous isothermal reactions, based on the pioneering treatments of Danckwerts (1953) and Zwietering (1959) and a proof of optimality due to Chauhan et al. (1972). If there are multiple reactants, the feed stream is assumed to be premixed.

1-4.3.1 First-Order Reactions. Suppose that the reaction is isothermal, homogeneous, and first order with rate constant k. Then knowledge of the RTD allows the reaction yield to be calculated. The result, expressed as the fraction unreacted, is

$$\frac{a_{out}}{a_{in}} = \int_0^\infty e^{-kt} f(t)\, dt = 1 - k\int_0^\infty e^{-kt} W(t)\, dt \tag{1-6}$$

Here, a_{in} and a_{out} are the inlet and outlet concentrations of a reactive component, A, that reacts according to A $\rightarrow$ products. Use the version of eq. (1-6) that contains the residence time function actually measured, W(t) or f(t).

Equation (1-6) provides a unique estimate of reaction yields because the first-order reaction extent depends only on the time that the molecule has spent in the system and not on interactions or mixing with other molecules. Reactions other than first order give more ambiguous results because the RTD does not measure spatial mixing between molecules that can affect reaction yields.

1-4.3.2 Complete Segregation. A simple generalization of eq. (1-6) is

$$a_{out} = \int_0^\infty a_{batch}(t) f(t)\, dt = 1 - k\int_0^\infty a_{batch}(t) W(t)\, dt \tag{1-7}$$

where $a_{batch}(t)$ is the concentration in a batch reactor that had initial concentration a_{in}. This equation can be used to calculate the conversion of any reaction. It assumes an extreme level of local segregation; there is no mixing at all between molecules that entered the system at different times. Molecules that enter together leave together and remain in segregated packets while in the system. Figure 1-4*a* illustrates this possibility for a completely segregated CSTR.

1-4.3.3 Maximum Mixedness. The micromixing extreme opposite to complete segregation is maximum mixedness and is the highest amount of molecular level mixing that is possible with a fixed residence time distribution. The conversion of a unimolecular but otherwise arbitrary reaction in a maximum mixedness reactor is found by solving Zwietering's differential equation (Zwietering, 1959):

$$\frac{da}{d\lambda} + \frac{f(\lambda)}{W(\lambda)}[a_{in} - a(\lambda)] + R_A = 0 \tag{1-8}$$

where $R_A = R_A(a)$ is the reaction rate. The boundary condition is that a must be bounded for all $\lambda > 0$. The outlet concentration, a_{out}, is found by evaluating the solution at $\lambda = 0$. For the special case of an exponential distribution, the solution of eq. (1-8) reduces to that obtained from a steady-state material balance on a perfectly mixed CSTR. A maximally mixed CSTR is the classic CSTR of reaction engineering. In the case of a delta distribution, eqs. (1-7) and (1-8) give the same answer. Reactors in which the flow is piston flow or near piston flow are insensitive to micromixing.

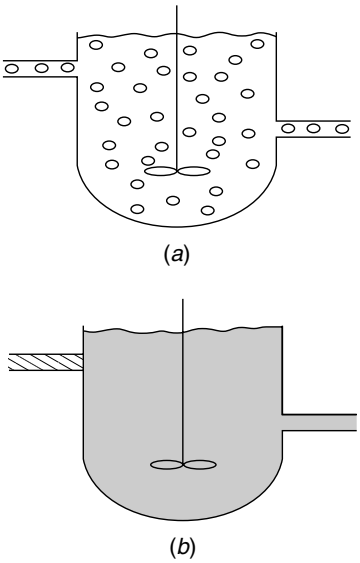

Figure 1-4 Extremes of micromixing in a stirred tank reactor: (*a*) Ping-Pong balls circulating in an agitated vessel, the completely segregated stirred tank reactor; (*b*) molecular homogeneity, the perfectly mixed CSTR.

1-4.3.4 Yield Limits. Equations (1-7) and (1-8) provide absolute limits on the conversion of most unimolecular reactions and many reactions involving multiple reactants, provided that the feed is premixed. There are three ideal reactors: piston flow, the perfectly mixed CSTR, and the completely segregated CSTR. Calculate the yields for all three types and the yield for a real system will usually lie within the limits of these yields. Measure the residence time distribution and eqs. (1-7) and (1-8) will provide closer limits. This is illustrated in the worked example that follows. A unique calculation of yield for any reaction other than first order is impossible based only on residence time data. It requires a micromixing model such as those developed by Bourne and co-workers (Baldyga et al., 1997). Such models are needed especially when the feed is unmixed or when there is a complex reaction with one or more fast steps. A CSTR cannot be considered well mixed unless the (internal) recycle ratio is very high and molecular-level mixing by molecular diffusion is rapid.

Example 1-1. You have been asked to improve the performance of an existing polymerization reactor. Initially, you know only that it operates at an input flow rate of 10 000 lb/hr, gives a conversion of $62 \pm 1\%$ at a nominal operating temperature of 140°C, and reportedly once gave a higher conversion. The reactor drawings show a complicated arrangement of stirring paddles and cooling coils. The design intent was to approximate piston flow, but a detailed hydrodynamic analysis would be impractical. The drawings do show the working volume of

the reactor, and you calculate that the fluid inventory should be about 12 500 lb. Thus you estimate $\bar{t} = 1.25$ hr.

The company library contains the original kinetics study for the polymerization, and it seems to have been done well. The major reaction is a self-condensation with rate eq. $R_A = -ka^2$, where $a_{in}k = 4\ hr^{-1}$ at 140°C. The fraction unreacted in an isothermal batch reactor at t would be

$$\frac{a_{out}}{a_{in}} = \frac{1}{1 + a_{in}kt}$$

assuming that piston flow in the plant reactor gives $a_{out}/a_{in} = 0.167$, just like the batch reactor.

For a CSTR at maximum mixedness, $a_{out}/a_{in} = 0.358$. In principle, this result is found by solving eq. (1-8), but the result is the same as for a perfectly mixed CSTR.

For a segregated stirred tank, $a_{out}/a_{in} = 0.299$. This result is found by solving eq. (1-7) subject to an exponential distribution of residence times. The measured result, $a_{out}/a_{in} = 0.38$, is worse than any of the ideal reactors! There are several possibilities:

1. The RTD lies outside the normal region. In particular, there may be bypassing.
2. The laboratory kinetics are wrong.
3. The kinetics are right, but the calculated value for $a_{in}k\bar{t}$ is too high. This in turn leads to two main possibilities: (a) The actual temperature is lower than the measured temperature; or (b) the estimated value of $\bar{t}$ is too high.

The good engineer will consider all these possibilities and a few more. Temperature errors are very common, particularly in viscous, low thermal conductivity systems typical of polymers; and they lead to sizable errors in concentration. However, measured temperatures are usually lower than actual rather than higher.

Suppose you decide that the original kinetic study was sound, that there are no apparent changes in the process chemistry, and that the analytical techniques are accurate. This makes flow distribution or mixing a likely culprit. Besides, you would like to see just how that strange agitation/cooling system performs from a flow viewpoint.

Suppose you find an inert hydrocarbon that is not normally present in the system, which is easily detected by gas chromatography and can be tolerated in the product stream. You arrange for the tracer injection port and the product sampling ports to be installed during a maintenance shutdown. It is important that the tracer be well mixed in the inlet stream. Otherwise, it might channel though the system and give nonrepresentative results. You accomplish this by injecting the tracer at the suction side of the transfer pump that is feeding the reactor. You also dissolve a little polymer in the tracer stream to match its viscosity more closely to that of the reactor feed. Having carefully prepared, you perform

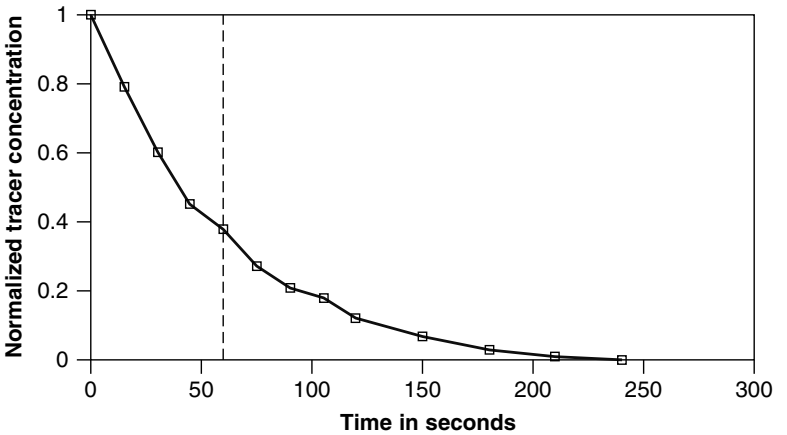

Figure 1-5 Experimental RTD data for Example 1-1.

a tracer washout experiment and obtain the results shown in Figure 1-5. The mean residence time is determined by integrating under the experimental washout curve and gives $\bar{t} = 59$ s. This is much less than the calculated value of 1.25 hr. You arrange for the reactor to be opened and find that it is partially filled with cross-linked polymer. When this is removed, the conversion increases to 74%: $a_{out}/a_{in} = 0.26$. A new residence time experiment gives $\bar{t} = 1.25$ hr as expected, and shows that the washout curve closely matches that for two stirred tanks in series:

$$f(t) = \frac{4t \exp(-2t/\bar{t})}{\bar{t}}$$

Now eqs. (1-7) and (1-8) can be used to calculate more precise limits on reactor performance. The results are $a_{out}/a_{in} = 0.290$ for complete segregation and $a_{out}/a_{in} = 0.287$ for maximum mixedness. Thus, as is typical of most industrial reactions, the extremes of micromixing provide tight limits on conversion. Since the actual result is outside these limits, something else is wrong. Quite likely it is the measured temperature that now seems too low.

1-4.4 Use with Computational Fluid Dynamic Calculations

Although they are increasingly popular, computational fluid dynamic (CFD) calculations are notoriously difficult to validate: Model equations may be available to the user, but the source code is typically proprietary, experimental data for comparison may be impossible to obtain, and the sheer volume of data available from the simulations makes complete and meaningful validations extremely difficult. Velocity measurements are difficult. Pressure drop measurements are easy but insensitive to the details of the flow. The RTD is a more sensitive test, but it is not unique since the RTD is derived from a flow-averaged velocity profile

rather than the spatially resolved velocities that are predicted by CFD. Further, an experimental RTD will include effects of eddy or molecular diffusion that are not reliability captured by current CFD codes. Most CFD codes use convergence acceleration techniques that cause numerical diffusion that is an artifact of the computation. Numerical diffusion mimics molecular or eddy diffusion, although to an indeterminate extent.

Modern CFD codes are used routinely to calculate residence time distributions in complex flow systems such as static mixers. Care must be taken to sample according to flow rate rather than spatial position, and the number of particles must be surprisingly large for accurate results, particularly for the chaotic flow fields found in motionless mixers. The simulation of the recycle curve in Figure 1-2*b* used 2^{18} tracer particles. The tail of the washout functions provides a demanding test for freedom from numerical diffusion. In the complete absence of diffusion, residence time distributions in laminar flow have slowly decreasing tails that give infinite variances. Specifically, they have algebraic tails for which W(t) decreases as t^{-2} so that all moments higher than the first diverge. Diffusion will cause the distributions to have rapidly decreasing exponential tails. The conclusion is that improvements in CFD codes and still faster computers are needed for accurate design calculations in complex geometries. Residence time calculations will be a useful tool for their validation. The situation becomes even more difficult when the equations of motion are combined with convective diffusion equations to estimate reactions yields and heat transfer. We anticipate significant near-term improvements in CFD codes, but they are now at the cutting edge of technology and have not yet become everyday tools for the practicing engineer.

1-5 EXTENSIONS OF RESIDENCE TIME THEORY

Residence time measurements are easiest in single-phase systems having one inlet and one outlet, but extensions to more complex cases are discussed in the General References. The RTD can be measured by component on an overall basis. Individual RTD's per inlet, per outlet, and per phase can also be measured. Most of the concepts discussed in this chapter can be applied to unsteady-state systems. The material leaving the systems at any time will have a time-dependent distribution of residence time. Analytical and numerical solutions are possible for a variable-volume CSTR, allowing calculation of time-dependent RTDs and reaction yields in a system subject to fluctuations in flow rate. For isothermal, solid-catalyzed reactions, the contact time distribution is the analog of the residence time distribution. It can be measured using adsorbable tracers. The results can be used to predict reaction yields or the upper and lower bounds of reaction yields. The thermal time distribution applies to nonisothermal homogeneous systems. It is a conceptual tool useful for optimizing the performance of nonisothermal tubular reactors and extruder reactors. Improved CFD codes will allow its calculation in static mixers and other complex geometries used for simultaneous heat transfer and reactor.

NOMENCLATURE

Roman Symbols

a	concentration of component A
a_{batch}	concentration of component A in a batch reactor
a_{in}	inlet reactant concentration
a_{mix}	reactant concentration after the mixing point in a recycle reactor
a_{out}	outlet reactant concentration
C	concentration of inert tracer
C_{in}	inlet tracer concentration
C_{out}	outlet tracer concentration
f	differential distribution function of residence times
F	cumulative distribution function of residence times
k	reaction rate constant
q	internal flow rate or recycle flow rate
Q	volumetric flow rate through the system
R_A	reaction rate of component A
t	residence time
t_{first}	first appearance time
$\bar{t}$	mean residence time
V	volume
W	residence time washout function

Greek Symbols

λ	residual life, the time variable in Zwietering's differential equation
μ_n	n^{th} moment of the residence time distribution
σ^2	dimensionless variance or residence times
ω	frequency of input disturbance
Θ	dummy variable of integration

REFERENCES

Baldyga, J., J. R. Bourne, and S. J. Hearn (1997). Interaction between chemical reactions and mixing on various scales, *Chem. Eng. Sci.*, **52**, 458–466.

Chauhan, S. P., J. P. Bell, and R. J. Adler (1972). On optimal mixing in continuous homogeneous reactors, *Chem. Eng. Sci.*, **27**, 585–591.

Danckwerts, P. V. (1953). Continuous flow systems: distribution of residence times, *Chem. Eng. Sci.*, **2**, 1–13.

Nauman, E. B., D. Kothari, and K. D. P. Nigam (2002). Static mixers to promote axial mixing, *Chem. Eng. Res. Des.*, **80**(A6), 681–685.

Zwietering, T. N. (1959). The degree of mixing in continuous flow systems, *Chem. Eng. Sci.*, **11**, 1–15.

In addition to the references above, the concepts introduced in this chapter are discussed at length in:

Nauman, E. B., and B. A. Buffham (1983). *Mixing in Continuous Flow Systems*, Wiley, New York.

Much of the material is also available in:

Nauman, E. B. (1981). Invited review: residence time distributions and micromixing, *Chem. Eng. Commun.*, **8**, 53.

Scale-up issues related to RTDs are discussed in:

Nauman, E. B. (2002). *Chemical Reactor Design, Optimization and Scaleup*, McGraw-Hill, New York.

CHAPTER 2

Turbulence in Mixing Applications

SUZANNE M. KRESTA
University of Alberta

ROBERT S. BRODKEY
Ohio State University

2-1 INTRODUCTION

Turbulence is central to much of liquid mixing technology and all of the typical processes (reaction, mass transfer, heat transfer, liquid–liquid dispersion, gas dispersion, solids suspension, and fluid blending) are dramatically affected by its presence. An understanding of the nature of turbulence is needed to deal with the interactions between turbulent fluctuations and mixing processes. Without an understanding of these basic physical phenomena, reliable predictions of performance can be difficult to achieve. Simple scale-up rules can be hopelessly inadequate. Unfortunately, the physics of turbulence still evades a general mechanistic description; and the flow in a stirred tank is complicated further by recirculation, strong geometric effects, and instabilities on several scales of motion. In this chapter we focus on providing a physical understanding of both turbulence and the tools that we use to understand its effects on process results.

The primary objective is to translate our current understanding of turbulence into an engineering context, providing the reader with a set of tools that can be used to solve practical mixing problems. In each section we begin with discussion of a central concept in turbulence and follow this with application of the idea to a practical problem, putting the concept into a practical context. Several facets of the turbulence problem are examined, in order to:

- Provide an engineering description of turbulence in terms of length and time scales.

Handbook of Industrial Mixing: Science and Practice, Edited by Edward L. Paul, Victor A. Atiemo-Obeng, and Suzanne M. Kresta
ISBN 0-471-26919-0

- Illustrate the implications of these length and time scales for industrial mixing operations.
- Review the implications of isotropy and other approximate theoretical treatments.
- Consider the nature and implications of various experimental measures of the flow.
- Summarize the strengths and limitations of turbulence models and computational fluid dynamics (CFD) in general in the context of the design of mixing equipment.

In this chapter the topic of turbulence is broken down into four sections. First, in Section 2-2, the application of turbulence scaling principles to reactor design is discussed, to clarify for the reader the role played by the turbulent motions. In Section 2-3 we dig deeper into the description of turbulence, considering the various time and length scales involved in the description of turbulent flow, the scaling arguments that are used for engineering estimates, and how these estimates are related to the flow field. The information that is lost in the time averages and scaling arguments is revisited from the perspective of experimental and theoretical approximations of the flow in Section 2-4. Finally, the mathematical approach to the problem, the modeling of turbulence, is discussed in Section 2-5. The text is aimed at readers with no advanced training in fluid mechanics, and explanations of theoretical concepts are liberally interspersed with examples. Those with more experience will find summaries at the end of each section; they may also find a review of the more subtle concepts useful. Although the chapter can be read from beginning to end, it is also designed for independent reference to a specific subtopic. We begin by clarifying the initial definitions that we will need to discuss turbulence and the mixing operation.

2-2 BACKGROUND

2-2.1 Definitions

These definitions are provided for the readers' reference. The case of B being mixed into a continuous A is used for the purpose of illustration.

2-2.1.1 Turbulence. An exact mechanistic definition of turbulence is limited by our understanding of its nature. Indeed, there can be no exact definition until we have exact understanding. However, as engineers, we need a working definition to ensure that we are all talking about the same thing.

We first look at the history of this moving target. The first historical phase was phenomenological theories where turbulence was defined by specific mechanistic concepts developed by researchers such as Prandtl. This led, for example, to the Prandtl mixing length. Taylor then suggested that statistical theory be applied to develop a more general view of turbulence. He proposed that the mechanism of turbulence is so complex that we cannot formulate a general model on which to

base an analysis unless we restrict the meaning of turbulent motion to an irregular fluctuation about a mean value (Brodkey, 1967, pp. 260–261). Any motion that might have a regular periodicity (e.g., that from an impeller in a mixer) could not be considered as part of the turbulent motion. Within this context the eddy cascade picture of turbulence and time-averaged models like the $k-\varepsilon$ model emerged. Frustration with this view has lead to the current concept of *coherent structures* in turbulence.

The coherent structure approach to turbulence is diametrically opposite to the statistical approach. Such coherent structures (e.g., ejections, sweeps, hairpin vortices, etc.) are to be distinguished from large scale organized motions that are forced upon the system externally. Today, coherent structures concepts are being extended to incorporate periodic structures generated by forcing or by geometry in the system. These forced structures can be generated, they evolve, and they interact with the natural turbulent coherent structures. In this context, coherent, regular structures are a feature of many turbulent flows, including mixing layers, and shed vortices can be included as part of our definition. To capture these structures, however, we are forced to adopt a more direct approach to the modeling, such as direct numerical simulation or large eddy simulation. Praturi and Brodkey (1978) offered the following commentary: "A mechanistic picture of turbulence cannot be treated on the average since such flows are dynamic. Many models can satisfy a long time-average picture. Emerging from this approach is the conclusion that turbulence can only be described as an evolving dynamic system. Reliable mechanistic models of turbulent shear flows that will enable reasonable predictions to be made should then be possible."

From the modeling perspective all flows, whether laminar, transitional, or turbulent, can be fully described by the Navier–Stokes equations with or without time dependency and with the restrictions of imposed geometry and appropriate boundary conditions. This suggests that there is no mechanistic difference between the flow regimes. Turbulent flow is simply a very complicated manifestation of the same physics that drives laminar flow.

Throughout this book, strong distinctions are made between laminar and turbulent mixing. The operation and design of mixing equipment in these two flow regimes are, in fact, quite different. Why? The flow for a given geometry and set of boundary conditions is a continuous development from very low Reynolds numbers (laminar operation) to very high ones (fully turbulent operation). At a low Reynolds number (Re), viscosity dominates, infinitesimal disturbances are damped out, and we have laminar flow. At a very high Re, inertial forces dominate, changes in viscosity have no effect on process results, and infinitesimal disturbances grow into a myriad of complex interacting structures so complex that we call it turbulence. With this complexity of interactions comes rapid dispersion and mixing. Somewhere between the extremes is a transitional region where both inertial and viscous forces play a role. Although our understanding of laminar mixing is imperfect and our understanding of turbulent mixing limited, our understanding of transitional flow and mixing is restricted to the simplest of cases.

Within this context, we offer the following working definitions of turbulence:

- *Turbulence* is a state of fluid motion where the velocity fluctuates in time and in all three directions in space. These fluctuations reflect the complex layering and interactions of large and small structural elements, such as vortices, sheets, ejections, and sweeps of a variety of shapes and sizes. In turbulent flows, scalar fields are rapidly dispersed compared to their laminar counterparts. At the time of writing, there is no completely acceptable way to model complex turbulent flow.
- *Fully turbulent flow* is an asymptotic state at very large Reynolds numbers. In fully turbulent flow, the velocity fluctuations are so intense that inertial forces overwhelm viscous forces. At all but the smallest scales of motion, viscous forces (and molecular diffusivity) become negligible. In fully turbulent flow, drag coefficients (e.g., friction factors and power numbers) and dimensionless blend times approach constant values. As is also the case in laminar flow, velocity profiles scale exactly with characteristic length and velocity scales. These conditions allow significant simplifications in modeling and design.

2-2.1.2 Mixing Mechanisms

- *Dispersion* or *diffusion* is the act of spreading out (B is dispersed in A).
- *Molecular diffusion* is diffusion caused by relative molecular motion and is characterized by the molecular diffusivity D_{AB}.
- *Eddy diffusion* or *turbulent diffusion* is dispersion in turbulent flows caused by the motions of large groups of molecules called *eddies*; this motion is measured as the turbulent velocity fluctuations. The turbulent diffusivity, D_t, is a conceptual analogy to D_{AB} but is a property of the local flow rather than of the fluid.
- *Convection* (sometimes called *bulk diffusion*) is dispersion caused by bulk motion.
- *Taylor dispersion* is a special case of convection, where the dispersion is caused by a mean velocity gradient. It is most often referred to in the case of laminar pipe flow, where axial dispersion arises due to the parabolic velocity gradient in the pipe.

2-2.1.3 Measures of Mixedness

- *Scale of segregation* is a measure of the large scale breakup process (bulk and eddy diffusivity) without the action of diffusion, shown in Figure 2-1*a*. It is the size of the packets of B that can be distinguished from the surrounding fluid A.
- *Intensity of segregation* is a measure of the difference in concentration between the purest concentration of B and the purest concentration of A in

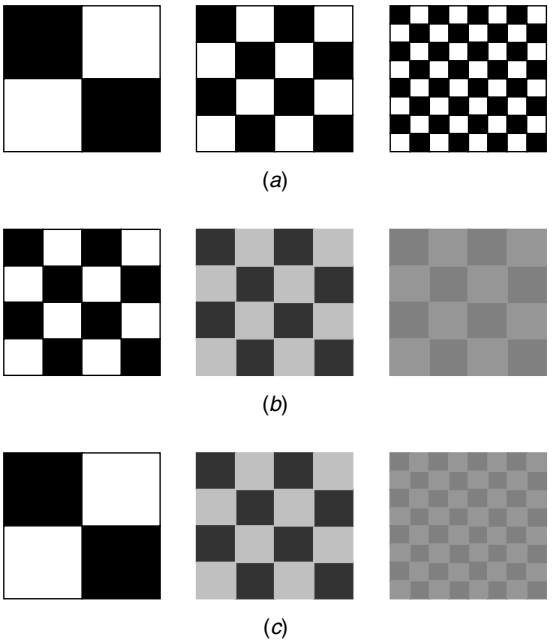

Figure 2-1 Intensity and scale of segregation: (*a*) reduction in scale of segregation; (*b*) reduction in intensity of segregation; (*c*) simultaneous reduction of intensity and scale of segregation.

the surrounding fluid[1] shown in Figure 2-1*b*. Molecular diffusion is needed to reduce the intensity of segregation, as even the smallest turbulent eddies have a very large diameter relative to the size of a molecule.

A reduction in intensity of segregation can occur with or without turbulence; however, turbulence can help speed the process by reducing the scale of segregation, thus allowing more interfacial area for molecular diffusion. The scale of segregation is typically reduced by eddy motion while molecular diffusion simultaneously reduces the intensity of segregation, as shown in Figure 2-1*c*. When diffusion has reduced the intensity of segregation to zero, the system is considered completely mixed.[2] Two examples illustrate the importance of the scale of segregation:

1. In a jet injection reactor with liquid or gaseous feeds and a solid product, the solid is formed at the interface between A and B. The final particle

[1] The term *intensity of segregation* is also used by Danckwerts as a measure of the age of a fluid at a point (i.e., the backmixing or residence time distribution problem).

[2] A more careful consideration of the completely mixed condition would have to consider the scale of the probe volume relative to the scale of the molecules, or the largest acceptable striation in the fluid.

size is a strong function of the rate of reduction of segregation in the reaction zone.

2. In the mixing of pigment into paint for automotive finishes, the color quality depends on the scale of segregation of the pigment. If the scale of segregation is too large, the color is uneven, but if the scale and intensity of segregation are too small, the color loses its brightness and becomes muddy. This result is perhaps surprising; it is due to the reduced ability of an individual pigment particle to scatter light.

2-2.1.4 Scales of Mixing

- *Macromixing* is mixing driven by the largest scales of motion in the fluid. Macromixing is characterized by the blend time in a batch system.
- *Mesomixing* is mixing on a scale smaller than the bulk circulation (or the tank diameter) but larger than the micromixing scales, where molecular and viscous diffusion become important. Mesomixing is most frequently evident at the feed pipe scale of semibatch reactors.
- *Micromixing* is mixing on the smallest scales of motion (the *Kolmogorov scale*) and at the final scales of molecular diffusivity (the *Batchelor scale*). Micromixing is the limiting step in the progress of fast reactions, because micromixing dramatically accelerates the rate of production of interfacial area available for diffusion.[3] This is the easiest way to speed up contact at the molecular level, since the molecular diffusivity is more or less fixed.[4]

We now proceed to our first exploration of turbulence in mixing applications: an evaluation of the time and length scales that are important for reactor design.

2-2.2 Length and Time Scales in the Context of Turbulent Mixing

For reactor design we would like to know how molecular diffusion and turbulent motions interact to bring molecules together. Turbulence can be used to break up fluid elements, reducing the scale of segregation. Energy is required for the generation of new surface area; so the limiting scale of segregation is associated with the smallest energy-containing eddies. These eddies are several times larger than the Kolmogorov scale,[5] η, and even the smallest scales of turbulence are much larger than a single molecule. As a result, even the smallest eddies will contain pockets of pure components A and B. Depending on the scale of observation, the fluid may appear well mixed; however, reaction requires submicroscopic

[3] The rate of diffusion is most frequently expressed as $k_{oL}a$. k_{oL} is essentially determined by physical properties of the fluids; a is increased by micromixing.

[4] For most liquids and gases the viscosity is greater than or equal to the molecular diffusivity ($Sc = \nu/D_{AB} \geq 1$), so it is easier to spread motion than molecules. Molten metals are a notable exception to this rule.

[5] See Section 2-3.

homogeneity, where molecules are uniformly distributed over the field. Molecules must be in contact to react. Turbulence alone cannot provide this degree of mixing. Molecular diffusion will always play an important role. Molecular diffusion, however, is very slow,[6] so the mixing process is critically dependent on both bulk mixing and turbulent diffusion to reduce the scales over which molecular diffusion must act. *To accomplish chemical reactions, we need the initial bulk mixing, efficient turbulence, and molecular diffusion for the final molecular contact.* Example 2-1 illustrates the impact of turbulence and molecular diffusion on mixing and reaction using a simplified physical model.

When mixing involves a chemical reaction, there are added complexities that depend on how the reactants are introduced into the mixing system. When a single stream is introduced and mixing occurs between fresh elements and older elements of the fluid, the mixing occurs in time and is called *self-mixing* or *backmixing*. When two streams enter a reactor and mixing occurs between the streams, two cases must be considered. If the reactants are all in one stream (*premixed* or *initially together*), the second stream acts as a diluent. With no mixing between the streams, the reaction proceeds as given by the kinetics. If, however, mixing dilutes the reactant concentrations and the order of the reaction is greater than 1, the dilution will depress the reaction rate. If the reactants are in separate streams (*unmixed* or *initially segregated*), molecular diffusion must take place for reaction to occur. In the last case, turbulence, molecular diffusion, and kinetics all interact to establish the course of the reaction. This is the critical turbulent mixing and kinetics problem that has received so much attention in the literature.

For chemical reactions in a known mixing field, the critical time scale depends on the relative rates of mixing and reaction. The limits of fast, slow, and intermediate reaction rates determine the relative importance of mixing and kinetics, as shown in Figure 2-2. Fast chemical reactions proceed as quickly as turbulence and molecular diffusion can bring the components together. The mixing rate dominates. Slow chemical reactions proceed much more slowly than any of the mixing time scales and are governed solely by reaction kinetics. For the important group of intermediate reaction rates, the reaction, diffusion, and mixing rates interact, and modeling is required. Example 2-2 illustrates these limits.

Example 2-1a: Y-Tube—Identifying the Role of Various Mixing Mechanisms. A mixing Y-tube configuration (Figure 2-3*a*) was suggested for mixing two gaseous streams. The original reaction was studied in a $\frac{1}{4}$ in. bench scale reactor. The experimental results showed excellent selectivity and excellent conversion. The final plant design was to be a 12 in. tubular reactor, requiring a 48 : 1 scale-up. Because of the large scale-up factor, it was decided that a pilot scale would be tested. For this, a 2 in. reactor was designed and built (Figure 2-3*b*), which amounted to an 8 : 1 scale-up.

A series of experiments in the pilot unit revealed that the pilot reactor performed poorly both in selectivity and in overall conversion. The flow rates were

[6] This applies for $Sc \geq 1$. See note 4.

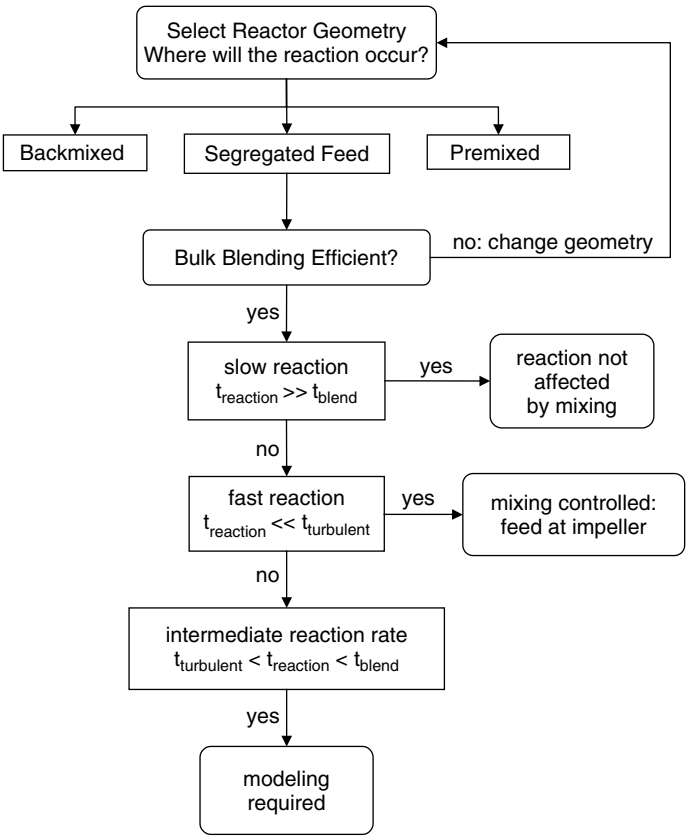

Figure 2-2 Relationship between mixing and reaction time scales for equipment design.

such that the flow was turbulent. Recognizing the need for turbulence in a turbulent mixing system, the experimenter modified the pilot plant unit by adding screens near the entry to promote mixing via turbulent generation, as shown in Figure 2-3*c*. Contrary to expectations, the conversion and selectivity were further reduced by the turbulence-promoting screens. We now revisit the problem, considering not just the *amount* of turbulence, but also the *spectrum* of turbulence length scales.

Chemical reaction carried out in combination with mixing of the reactants has, as a first requirement, the large scale bulk dispersion of A into B. Only after this occurs can the finer scale mixing and molecular diffusion occur at a reasonable rate. In the bench scale reactor, the two incoming streams interacted vigorously and a grossly uniform mixture was obtained (Figure 2-3*a*). In sharp contrast, the results for the 2 in. reactor (Figure 2-3*b*) showed material segregation. The reaction occurred only on the interacting surface between the two streams. When the turbulence generation screens were added (Figure 2-3*c*), the

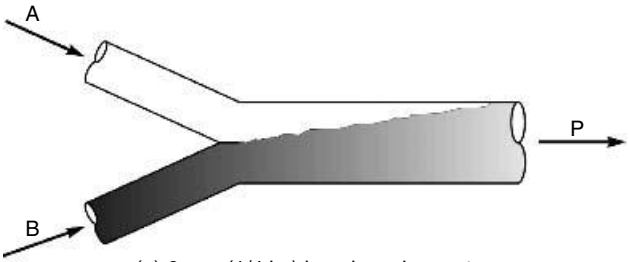

(*a*) 6 mm (1/4 in.) bench scale reactor

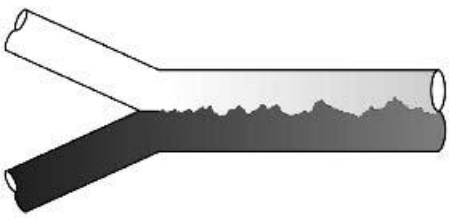

(*b*) Pilot scale mixing in 50 mm (2 in.) reactor without screens

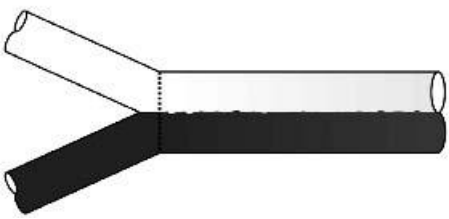

(*c*) Pilot plant mixing in 50 mm (2 in.) reactor with screens

Figure 2-3 Mixing and reaction carried out in a Y-tube.

screens eliminated the large scale interactions, providing a less contorted surface for reaction and thus further reduction of conversion. As a consequence of the screens, the pilot scale reactor provided extremely well-mixed material A and extremely well-mixed material B, but failed to bring A and B into contact. The Y-tube configuration has poor bulk mixing and thus fails the first test in Figure 2-2. An alternative geometry, such as a static mixer, T-junction, or stirred tank must be used for large scale dispersion (see, e.g., Monclova and Forney, 1995, or Wei and Garside, 1997). The key criterion for success in bulk mixing in a pipe is that the largest scale of segregation in the feed must be smaller than the largest scale of motion in the mixing geometry (Hansen et al., 2000).

This simple geometry provides us with an opportunity to explore the importance of various mixing mechanisms. We have already seen the disastrous impact of poor bulk mixing. Now, taking the length scale of the pipe, the problem is broken down into simplified models of pure molecular diffusion and pure eddy dispersion to clarify the interactions between these mixing mechanisms.

Example 2-1b: Y-Tube—Limiting Case with No Eddy or Bulk Diffusion. What time would be required to achieve 99% mixing in the Y-tube if the only active mechanism was molecular diffusion? In this case there is poor bulk mixing between the layers, as observed above, and there is no turbulent enhancement of any mixing that does occur. Since we seek only the relative time scales, we reduce the problem to the case of plug flow with no turbulent fluctuations. This is clearly nonphysical,[7] but it will isolate the scales of mixing due to pure molecular diffusion. Since the materials are gaseous, we will assume equal-molal counter diffusion with equal diffusivities of the two components.

The diffusion is one dimensional in the x-direction; thus the rate of diffusion of A is written

$$\frac{\partial C_A}{\partial t} = D_{AB}\frac{\partial^2 C_A}{\partial x^2} \tag{2-1}$$

where C_A is the concentration of species A. This is a common problem in chemical engineering, and solutions can be found in Brodkey and Hershey (1988). Probably the easiest approach for our purposes is to use the generalized chart solutions based on the original work by Gurney and Lurie (1923) and further improved upon by Heisler (1947). For our problem, each component must diffuse across a half width (from the centerline to the wall). To create the conditions required for 99% conversion of the reactants, we can take the "unaccomplished change" as 0.01, the centerline or half-width position ($n = 1$), and no resistance to transfer at the interface ($m = 0$). From the chart in Brodkey and Hershey (1988, pp. 670–672), the dimensionless time for these conditions is

$$\tau_D = \frac{D_{AB}t}{L^2} = 2.0 \tag{2-2}$$

We have been told that the diffusivity of our gases is about 25% greater than that of CO_2 in air; thus, we use $D_{AB} = 2 \times 10^{-5}$ m^2/s. We use as the scale, L, the half-width of the system. For the $\frac{1}{4}$ in. bench unit, the diffusion time would be about 4 s. This would increase to a little over 1 min for the 2 in. diameter and to nearly 40 min for the 12 in. diameter commercial unit. At a Reynolds number of 2000, these times would correspond to pipe lengths of 5, 40, and 230 m, respectively. Clearly, mixing by pure molecular diffusion is an upper limit and would result in very long reactors.

If the mixing involves liquids rather than gases, the effect is more pronounced. The molecular diffusion for liquids would be very much lower (i.e., $D_{AB} = 1 \times 10^{-9}$ m^2/s. Since t is inversely proportional to D_{AB}, the time required will increase by a factor of 2×10^4. The velocity in the liquid system will be lower

[7] If there are no fluctuations, the flow is laminar and the velocity profile is parabolic. The parabolic velocity profile will alter the diffusion characteristics, so this analysis is limited to a thought experiment. The superficial velocity from plug flow is needed to convert the required diffusion time to a distance down the reactor. To simplify the geometry without affecting the length scales significantly, we consider two dimensional plug flow between parallel plates, rather than the tubular geometry in the pipe.

Table 2-1 Limiting Case of Equimolar Counterdiffusion

Slab Thickness	6 mm ($\frac{1}{4}$ in.)	50 mm (2 in.)	305 mm (12 in.)
Air: $D_{AB} = \mathbf{O}(2.00 \times 10^{-5})\, m^2/s$, $v = 1.50 \times 10^{-5}\ m/s^2$, $Re = 2000$, $Sc = \mathbf{O}(1)$			
Time to 99% diffused	1 s	1.1 min	39 min
Velocity in plug flow	4.7 m/s	0.6 m/s	0.1 m/s
Length of reactor	4.8 m	38 m	230 m
Water: $D_{AB} = \mathbf{O}(1.00 \times 10^{-9}) m^2/s$, $v = 1.00 \times 10^{-6} m/s^2$, $Re = 2000$, $Sc = \mathbf{O}(1000)$			
Time to 99% diffused	5.6 hours	15 days	1.5 years
Velocity in plug flow	0.3 m/s	4 cm/s	7 mm/s
Length of reactor	6.3 km	50.8 km	305 km

by a factor of 15, because the kinematic viscosity of water is 15 times lower than that for air at the same Re. This does not make up for the slower diffusion and would result in a bench scale unit over 6 km long! The results are summarized in Table 2-1.

Example 2-1c: Y-Tube—Limiting Case with No Molecular Diffusion But Very Small Turbulent Eddies. Components A and B must come into contact on a molecular scale to react. If there is *no diffusion*, only a very thin monolayer of the product will form at the interface in Figure 2-3*c*. Once formed, it blocks any further reaction, since A and B cannot diffuse across the monolayer boundary. The familiar organic chemistry experiment where nylon is formed at the interface between sebacyl-chloride in tetrachloro-ethylene and an aqueous solution of hexamethylene diamine is a practical example of such a system. It is a simple geometric problem to obtain the interfacial area available per unit of length in our model reactor. Taking the molecular thickness to be ($d_m = 1$ Å) with a monolayer of reacted molecules at the interface gives a conversion of 8×10^{-10} in the full scale reactor. This is an extremely small fraction of the molecules present!

Let us allow instead extremely effective turbulence, and suggest that the smallest scale of turbulence in our gas system is about ($l_t = 0.1$ mm). You might call this the smallest energy-containing eddy, if we knew what an eddy was. We could also assume that this "eddy" is spherical, and that the volume of A inside the eddies equals the volume of B outside the eddies. In our simplified physical model, we assume that the reduction in scale of segregation happens immediately on entering the pipe. It will quickly become clear that the length of pipe required to accomplish the reduction in scale is not the limiting factor for our "perfectly turbulent" nondiffusing reactor.

To calculate the maximum conversion in the perfectly turbulent reactor, we calculate the volume of product on the surface of the eddies. The volume of product is

$$V_{\text{product}} = \frac{\pi}{6}[l_t^3 - (l_t - d_m)^3] = 1.57 \times 10^{-18}\ \text{m}^3$$

and the remaining volume of A inside the eddy is

$$V_A = \frac{\pi}{6}(l_t - d_m)^3 = 5.24 \times 10^{-13}\ m^3$$

which leaves a total remaining volume of reactants

$$V_{A+B} = 2V_A$$

Taking the ratio of volumes gives the conversion (assuming all molecules are approximately the same size)

$$\text{conversion} = \frac{V_{product}}{V_{A+B}} = 1.5 \times 10^{-6}$$

Diffusion and other physical properties are not a factor in this estimate of conversion. As long as the same Reynolds numbers and relative geometries are maintained, it will not matter if the system is a gas or liquid.

This conversion is clearly not good enough, so we decide to increase the turbulence and decrease the length scale, l_t, by a factor of 10 ($l_t = 10\ \mu m$). This improves the conversion by a factor of 10, to 1.5×10^{-5}. The increase in power consumption, however, increases with l_t^4, so the power requirement per unit mass jumps from 33.75 W/kg to 0.3 MW/kg if our fluid is a gas.[8] If our fluid is a liquid, things are somewhat better because of the lower viscosity. In this case the power consumption jumps from 0.01 W/kg to 100 W/kg. While pure molecular diffusion was too slow, pure reduction of length scales gives disastrously low conversions, regardless of the length of the reactor.

Before moving on, we need to remind ourselves that we have used a simplified model of the physics. Our estimate ignores the fact that the packing of the molecules in the volume and on the surface may be different. One expects that this would be a small factor and not important in order-of-magnitude estimates. It also assumes an eddy diameter that is very small and is near the lower limit of turbulence, the Kolmogorov scale. Another possible estimate could use an *average* eddy diameter. On the other hand, the dynamic nature of turbulence will provide mixing *between* eddies, which can increase the effective surface area by several orders of magnitude. Despite these approximations, this estimate shows that very little reaction will occur without molecular diffusion. Now we consider the case where initial bulk mixing, efficient turbulence, and molecular diffusion for the final molecular contact are all present.

Example 2-1d: Y-Tube—Molecular Diffusion with Very Small Static Eddies. This time, let us assume that diffusion can occur in the very small eddies formed in Example 2-1c. Let us again assume that the smallest scale of turbulence is

[8] This calculation is based on η as discussed in Section 2-3, with the same fluid properties as those used in Example 2-1.

($l_t = 0.1$ mm) and that the eddy is spherical. The spherical surface containing A + B becomes thicker as a result of molecular diffusion. We assume that all molecules within this thick surface will react.

For this example we combine the approaches used in Examples 2-1b and 2-1c, neglecting turbulent dispersion (see Section 2-3). Since the eddies are all assumed to be at their minimum size, all we need to determine is the time needed for the diffusion across an eddy radius ($l_t/2 = 0.05$ mm) for 99% diffusion. If the turbulence in the various test and commercial units does not change, the calculation will be the same for all cases, as it is based on a fixed eddy size, not on the system size. Of course, the total power will increase with the volume of the system. The only real difference from Example 2-1b is that we need to consider a sphere rather than a slab. The value of $D_{AB}t/L^2$ drops from 2.0 to 0.56 (see Brodkey and Hershey, 1988, p. 680), giving a diffusion time of

$$\tau = \frac{D_{AB}t}{L^2} = \frac{D_{AB}t}{(l_t/2)^2} = 0.56$$

$$t = \frac{(0.56)(1 \times 10^{-4}\ \text{m}/2)^2}{2 \times 10^{-5}\ \text{m}^2/\text{s}} = 7 \times 10^{-5}\ \text{s}$$

on all scales of operation. This is, of course, a limiting estimate, which assumes that the same thing happens in all eddies at the same rate. For any practical gas reactor problem, this suggests that the combination of very efficient turbulence with molecular diffusion on the smallest scales will provide a very efficient reactor. Even if a more conservative eddy diameter of 1 mm is used, the time needed for the gaseous system is 0.001 s, still small enough for any practical reactor.

For a liquid system the time needed to reach the mixing conditions for 99% conversion is 1.4 s for the 0.1 mm diameter eddy and well over 2 min for an *average* eddy size of 1 mm. Although the reduction in scale due to the simple static model of turbulence has dramatically reduced the time needed to reach 99% diffusion, the time required is still long relative to the time scale of a fast reaction. Although this model contains dramatic simplifications of the physics for the purposes of a thought experiment, better models of the turbulence based on scaling arguments can be implemented successfully for simple geometries (Forney and Nafia, 2000). More realistic models of the turbulence are needed for complex reactor design, and these are discussed in later sections. Before moving to this discussion, we consider the impact of reaction kinetics on the problem, given good bulk blending.

2-2.2.1 Interaction of Mixing Mechanisms: Summary of Example 2-1

- In the case of segregated feed of reactants A and B to a reactor, the bulk mixing of the system needs to be addressed. The reactants need to be dispersed rapidly across the system and over a range of scales from the scale

of the equipment to the point where individual molecules come into contact. Localized fine scale mixing of streams that remain segregated on the large scale contributes nothing to the overall mixing. (Example 2-1a)

- Diffusion alone, even in gas systems, is almost infinitely slow. (Example 2-1b)
- No diffusion results in essentially no reaction, even with a very dramatic reduction in the scale of segregation. (Example 2-1c)
- Adding molecular diffusion without eddy diffusion allows a crude estimate of the combined effects of (static) turbulence and molecular diffusion. The reduction in the time required for mixing on the molecular scale over previous cases is dramatic. For a gas system, this model is fast enough to reach practical limits. For liquids, the improvement is large, but not large enough to be realistic. (Example 2-1d)
- Although this example gives a dramatic illustration of the importance of all three mechanisms (bulk mixing, turbulent reduction of the scale of segregation, and molecular diffusion) to efficient mixing, a more realistic model of the turbulence is needed for accurate analysis.

2-2.3 Relative Rates of Mixing and Reaction: The Damkoehler Number

The outcome of a chemical reaction will depend on the rate of mixing compared to the rate of reaction. Figure 2-2 shows the interaction of the process and the key points to be considered. When the rate of reaction is slow compared to the mixing time, the reaction is not affected by mixing because the mixing is complete by the time significant reaction occurs (Example 2-2a). When the rate of reaction is fast compared to the rate of mixing, the kinetics are mixing limited, and the kinetics observed are effectively the mixing kinetics (Example 2-2b). Where the rate of reaction is similar to the rate of mixing, there will be strong interactions between the two rates (Example 2-2c). The relevant mixing time scales and reaction time scales are needed to determine the importance of mixing for a given reaction. In this chapter, only singular bimolecular reactions are considered. Also of considerable interest are bimolecular reactions that are either parallel-competitive ($A + B \rightarrow R, A + C \rightarrow S$) or series-competitive ($A + B \rightarrow R, B + R \rightarrow S$). These cases are discussed further in Chapter 13. It should be noted that what is said for the present single bimolecular case will apply equally well to the first reaction of the more complex cases.

Example 2-2: Relative Rates of Mixing and Reaction. To illustrate the role played by the turbulent scales across many different reactions, Toor (1969) and Mao and Toor (1971) obtained experimental conversion data in two different pipe flow reactors for a series of bimolecular reactions. Their results are combined with velocity measurements made in identical reactors by McKelvey et al. (1975). This allows us to compare various definitions of mixing time scales for pipe flow.

The defining number for this discussion is the Damkoehler number (Da), the ratio of mixing time to reaction time:

$$\mathrm{Da} = \frac{\text{mixing time}}{\text{reaction time}} = \frac{\text{reaction rate}}{\text{scalar dissipation rate}} = k_r C_{B0} \frac{L_{1/2}}{u} = k_r C_{B0} t_{\text{mixing}} \quad (2\text{-}3)$$

In the case of a bimolecular reaction with the concentration of A in large excess, the term $k_r C_{B0}$ is the reciprocal time required for the fraction of B remaining to fall to one-half of the initial concentration. To obtain Da = 1 when the mixing time is just equal to the reaction time, Mao and Toor (1971) defined the mixing length as equal to $L_{1/2}$ and the mixing time as equal to $L_{1/2}/U$, where U is the superficial velocity in the pipe. Their $L_{1/2}$ must be determined from mixing studies or from the equivalent fast reaction measurements.

It would be more convenient to use a mixing time that is not geometry specific. A number of such times and Damkoehler numbers were compared by Brodkey and Kresta (1999) using various local turbulence scales in the Toor reactor. All of these times use local turbulence parameters or characteristic times. The position at which these are evaluated for the two multitube reactors is at the point of coalescence of the feed jets. It turns out that this is very close to Mao and Toor's (1971) characteristic half mixing length.

Independent of the turbulent time scale chosen, two distinct dividing points appeared in the Damkoehler number, allowing the identification of the two limiting cases of interest. Two of these measures are presented in Table 2-2 and Figure 2-4. The first measure is the microscale time, given by $t_\lambda = (\lambda^2/\varepsilon)^{1/3}$, and the second is the eddy dissipation time, given by $t_e = k/\varepsilon$. The eddy dissipation time (Spalding, 1971) is often used in reaction models (e.g., Forney and Nafia, 1998). Results such as these are a clear indication of the general value of these time constants, which in turn are based on turbulence scaling arguments. Turbulence scaling arguments are addressed in more detail in Section 2-3. For now, we accept these as given and focus on the three categories of reaction rate.

(a) Slow reactions. This is the case where the reaction time is much longer than the time needed to blend the reactants. There is plenty of time to complete the mixing before the reaction makes any significant progress. Vassilatos and Toor (1965) measured the progress of a slow reaction and were able to predict the results accurately by assuming a homogeneous concentration field and applying only the reaction kinetics. McKelvey et al. (1975) compared homogeneous calculations with calculations made using a known turbulent field. Their comparisons showed that the effect of turbulence was indeed negligible. Mao and Toor (1971) expressed the results in terms of a Damkoehler number based on the pipe diameter ($\mathrm{Da} = k_r C_{B0} D_p/u$) such that for Da below 0.016, slow reaction conditions will apply. For all of the Damkoehler numbers defined in Table 2-2, the lower limits are on the order of 0.01. In this limit, turbulence is not important; the reactor is truly well mixed and a homogeneous kinetic calculation is sufficient.

Table 2-2 Damkoehler Numbers Based on Different Mixing Times

Mixing Time Scale		Mao and Toor	Taylor	Eddy Dissipation
Definitions				
Reaction rate (s^{-1})		k_rC_{B0}	k_rC_{B0}	k_rC_{B0}
Mixing time (s)		$t_M = L_{1/2}/u$	$t_\lambda = (\lambda^2/\varepsilon)^{1/3}$	$t_e = k/\varepsilon$
Da		$Da_M = k_rC_{B0}\frac{L_{1/2}}{u}$	$Da_\lambda = k_rC_{B0}t_\lambda$	$Da_k = k_rC_{B0}t_e$
Limits Based on Experimental Results				
Da_u (fast reaction limit)		100	30	150
Da_l (slow reaction limit)		0.02	0.009	0.01
Experimental Results from Toor (1969) and Mao and Toor (1971), References Therein				
Reaction	k_r (L/mol·s)	Da_M	Da_λ	Da_k
Fast Reactions (Diffusion Controlled)				
HCl–NaOH	1.4×10^{11}	1.7×10^7 -8.8×10^7	5.2×10^6 -1.2×10^7	3.2×10^7 -7.2×10^7
Maleic acid–OH^-	3×10^8	3.3×10^4	1.0×10^4	6.2×10^4
Nitrilotriacetic acid–OH^-	1.4×10^7	2.2×10^3	6.7×10^2	4.1×10^3
Intermediate Reactions				
CO_2–2NaOH	8.32×10^3	3.05–6.94	0.93	5.7
CO_2–nNH_3	5.85×10^2	~0.1	0.023	0.030
Slow Reaction (Kinetics Controlled)				
$HCOOCH_3$–NaOH	4.7×10^1	~0.01	0.0023	0.0030

(b) Fast reactions. When reactions are extremely fast, the time needed for a reaction to occur is much smaller than the time needed to blend the reactants. If two molecules can be brought together, they will react instantaneously. The controlling mechanism is the mixing due to both turbulence and diffusion. If the reactants are fed in stoichiometric balance, Toor (1962) has shown that the extent of the reaction is a direct measure of the mixing. The upper limit for Mao and Toor's (1971) definition of the Damkoehler number ($Da = k_rC_{B0}D_p/u$) is on the order of 100. For the definitions of Da in Table 2-2, the upper limit ranges from 30 to 150. Above this limit, fast reaction conditions apply. Acid-base reactions, which fall in this category, are often used as a means of measuring mixing times.

In addition to considering the limit of fast reactions, there is an effect of stoichiometry on the results, assuming that reactants are fed in stoichiometric ratio. Keeler et al. (1965) measured both mixing and fast reaction in the wake of a grid over a range of stoichiometric feed ratios. The effect of stoichiometry was also examined by Vassilatos and Toor (1965), who first assumed that mixing and very fast reaction results were equivalent for a stoichiometry of unity and then predicted the reaction at other stoichiometric ratios.

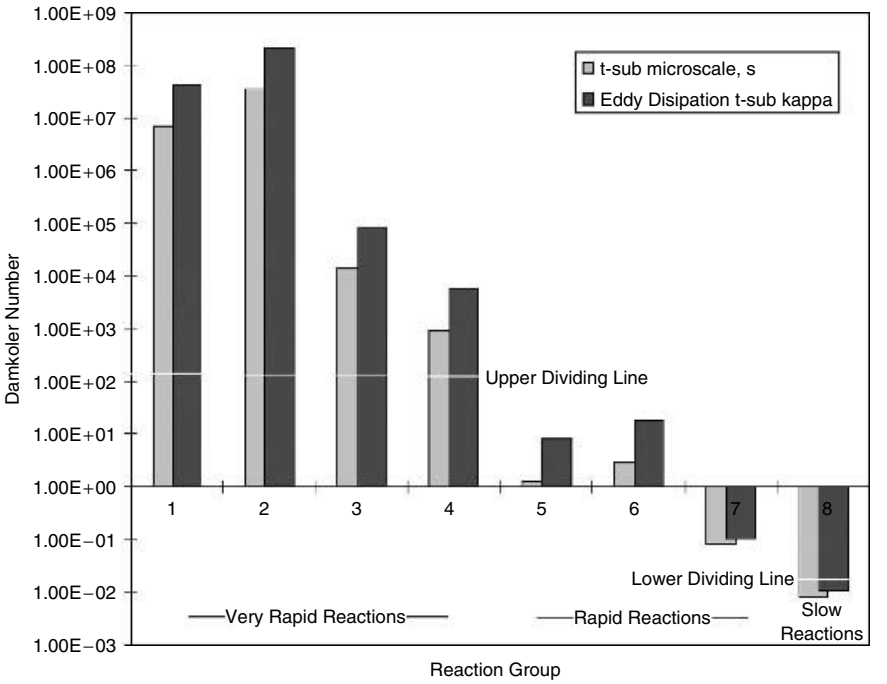

Figure 2-4 Comparison of limits of Damkoehler number based on two different time scales.

(c) *Intermediate rates of reaction*. In the outer limits of very slow and very fast reactions, either mixing or kinetics becomes controlling and the other part of the physics can be ignored in the model. This simplifies the problem dramatically. In many real processing problems, however, both mixing and kinetics influence the course of reaction. In this example, the relatively simple case of a reaction in a pipe is used to illustrate our needs for the study of turbulent mixing.

Models reported in the literature have tended to focus on one of two parts of the problem. Simple reaction models (e.g., reacting slabs, random coalescence-dispersion, or multienvironment models) are designed to fit overall reaction data. More complex theoretical approaches require a model of the turbulence (see Section 2-5). The problem here is the adequacy of the turbulence model over a wide range of flow conditions. There still is no theory that takes into account structural aspects of turbulence with or without superimposed chemical reaction, although steady progress is being made in this direction [some current approaches are discussed by Fox (1998)].

As an example of what is needed, consider the models developed by McKelvey et al. (1975) using kinetic data from Toor (1969) and Mao and Toor (1971). McKelvey et al. (1975) measured the velocity field and mixing characteristics in exactly the same multinozzle pipe reactor that was used by Toor and co-workers to measure the kinetics. McKelvey et al. had two objectives. The first was to

establish the velocity and concentration fields in reactors used by Vassilatos and Toor (1965) to verify that turbulent mixing could be predicted from knowledge of the turbulent field. The second was to model the progress of a single second-order irreversible reaction where there is a significant impact of the dynamics of mixing on the observed reaction kinetics.

McKelvey et al. first consider the mass balance equation for a second-order reaction between species A and B [$A + nB \rightarrow (n+1)P$]. The equation for an individual species A in a differential control volume is

accumulation of A + net bulk convection of A

= net diffusion of A − disappearance of A due to reaction

$$\frac{\partial C_A}{\partial t} + (\mathbf{U} \cdot \nabla)C_A = D_{AB}\nabla^2 C_A - k_r C_A C_B \tag{2-4}$$

C_A and C_B are the concentrations of species A and B. D_{AB}, the diffusion coefficient, and k_r, the reaction rate, are constant. The system is assumed incompressible and isothermal, and the scalar field has no effect on the velocity field (variations in concentration, for example, do not induce velocity gradients). Reynolds decomposition is used to separate the velocity and concentration fields into an average and fluctuating part. When these terms are substituted into eq. (2-4), the resulting equation can be averaged[9] to give

accumulation of A + mean convection due to mean gradients of A

+ convection due to cross-fluctuations of velocity and concentration

= bulk diffusion − reaction due to (mean field + fluctuating field)

$$\frac{\partial \overline{C_A}}{\partial t} + (\overline{\mathbf{U}} \cdot \nabla)\overline{C_A} + (\nabla \cdot \overline{\mathbf{ua}}) = D_{AB}\nabla^2 \overline{C_A} - k_r(\overline{C_A C_B} + \overline{ab}) \tag{2-5}$$

McKelvey et al. reduced this to a simplified form for the one dimensional experimental reactor

mean convection in the x-direction = molecular diffusion in the x-direction

− reaction due to (mean field + fluctuating field)

$$\overline{U_x}\frac{d\overline{C_A}}{dx} = D_{AB}\frac{d^2\overline{C_A}}{dx^2} - k_r(\overline{C_A C_B} + \overline{ab}) \tag{2-6}$$

The term $\overline{ab}$ is the fluctuating component of the concentration field. It is related to the intensity of segregation and thus depends directly on the turbulent mixing field. The axial change in C_A cannot be determined without $\overline{ab}$; however, if $\overline{ab}$ could be estimated, the equation could be numerically integrated. Toor

[9] See Brodkey and Hershey (1988, pp. 214–223) for a detailed presentation of the Reynolds averaging procedure.

(1969) showed that $\overline{ab}$ was the same for very slow reactions and very fast, stoichiometrically fed, second-order reactions. The former is dominated by kinetics, and the latter by mixing. With this as background, Toor hypothesized that "$\overline{ab}$ is independent of the speed of the reaction when the reactants are fed in stoichiometric proportion." He pointed out that this could not be exactly true for nonstoichiometric mixtures.

Based on this hypothesis, the measured intensity of segregation (I_s, discussed further in Section 2-3) was used for $\overline{ab}$ and the equation numerically integrated by McKelvey et al. (1975). They examined three of five experiments performed by Vassilatos and Toor (1965). The measured velocity and intensity of segregation were used for $\overline{U_x}$ and I_s in the integration. The stoichiometric ratio varied from 1.0 to nearly 3.9. The agreement between the computations and the conversion experiments, shown in Figure 2-5, is remarkable, so for the simple second-order homogeneous reaction where both mixing and kinetics are of importance, the hypothesis of Toor clearly allows adequate predictions to be made. Mao and Toor's (1971) Damkoehler number should be between ($0.02 < Da < 100$) for the intermediate reaction conditions to apply.

For more complex reactions that are consecutive in nature, a fully adequate analysis is still lacking, but progress is being made. To adequately model the progress of a reaction, the terms equivalent to $\overline{ab}$ must be determined, and these depend in turn on the turbulent mixing. Where reactions depend on highly localized concentrations, the time average fluctuations, $\overline{ab}$, need to be modeled in

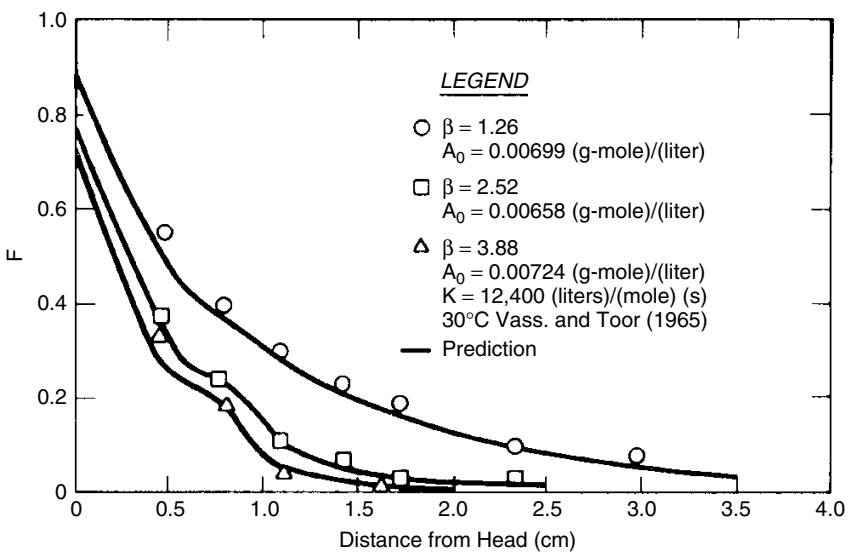

Figure 2-5 Predicted conversion of an intermediate reaction where the turbulent mixing field is known. (From McKelvey et al., 1975.)

terms of probability density functions (PDF's) and other properties of the fluctuations. The simplified model used for the thought experiment in Example 2-1d is hopelessly inadequate because it neglects both the dynamics and the range of length scales present in a turbulent flow.

2-2.3.1 Importance of Turbulence in Modeling Reactions: Summary of Example 2-2

- In very fast reactions, the measured rate of reaction is wholly dependent on the rate of mixing. In this case, the mixing time is much longer than the reaction time. (Example 2-2b)
- In very slow reactions, the mixing time has no effect on the kinetics of reaction. The reaction takes much longer than the mixing. (Example 2-2a)
- Various Damkoehler numbers can be defined, preferably based on turbulence characteristics rather than on geometry-dependent variables. Regardless of the definition selected, there are definite limits of Da for the two limiting cases of fast and slow reactions. (Example 2-2)
- For intermediate reaction rates, modeling of the turbulence is essential, as the local concentration field is a function of the velocity field. The concentration field will change, and the velocity field may change, as the reaction proceeds. The fluctuating concentration field, in concert with the reaction kinetics, determines the progress of the reaction. (Example 2-2c)

Turbulent mixing covers a broad spectrum of applications beyond the field of reactions and reactor design, all of which are affected by the turbulence. Drop breakup, off-bottom solids suspension, gas dispersion, bulk blending, and heat transfer are all affected by the turbulent field. Without a better understanding of this part of the physics, it is difficult to make progress in these areas. With this broader objective clearly in mind, we now move forward to describe the key characteristics of turbulent flow.

2-3 CLASSICAL MEASURES OF TURBULENCE

In this section we review the classical approaches to the problem of turbulence and how they are applied in the field of mixing. For more detailed treatments, see Brodkey (1967, Chap. 14), Tennekes and Lumley (1972), Hinze (1975), Baldyga and Bourne (focusing on reactions in turbulent flows, 1999), Mathieu and Scott (2000), and Pope (2000). We begin with a description of turbulence, building up the model from the simple reduction of scale explored in Example 2-1c to something that is more realistic. This realistic picture is very difficult to model in its full complexity, so various ways of reducing the full physical complexity to a manageable scale of difficulty must be considered. First, the idea of the turbulence spectrum is discussed. This is a fingerprint of the scales of motion which are present in a flow. The turbulence spectrum provides us with a simplified image of

the flow[10] and allows us to observe some general characteristics of turbulent transport. These simplifications, in turn, lead to some special cases of turbulence (e.g., homogeneous, isotropic, or locally isotropic) which underlie most turbulence modeling approaches used in computational fluid dynamics (CFD), and many experimental approaches as well. Finally, scaling arguments are developed and applied. The characteristic length and time scales that arise from scaling arguments depend on the physics outlined earlier in the chapter. The simplicity of the equations belies the challenges involved in successful scale-up and scale-down: our objective is to provide some physical understanding of scaling principles and some ground rules for their application. Now, we begin at the beginning with a physical model of turbulence.

2-3.1 Phenomenological Description of Turbulence

Development of an understanding of turbulence requires consideration of the details of turbulent motion. Much of our intuitive sense of fluid flow is based on what we can observe with the naked eye, and much of this intuitive sense can be applied to an understanding of turbulence, if we proceed with some care. We begin with the classical definition of simple shear flow, as shown in Figure 2-6. In this figure a Newtonian fluid is placed between two flat plates. The top plate moves with velocity V_x, requiring a force per unit area of plate surface (F/A) to maintain the motion. The force required is in proportion to the fluid viscosity,

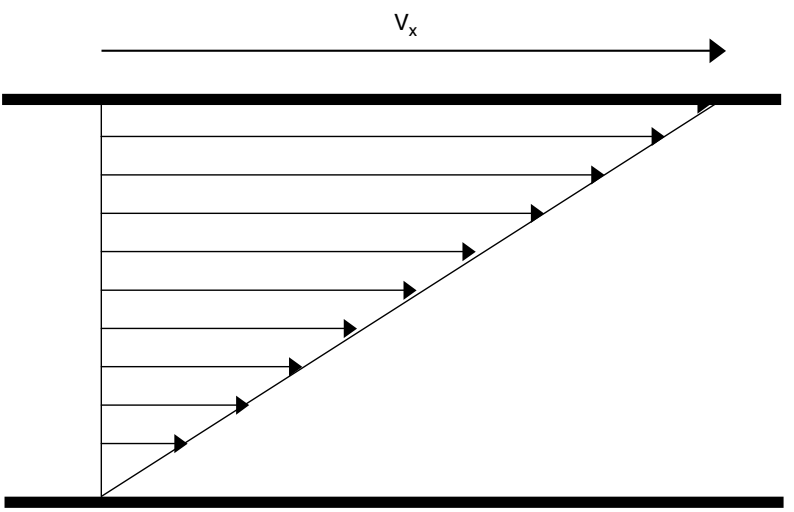

Figure 2-6 Simple shear flow.

[10] See Brodkey (1967, pp. 273–278) for a full development of the meaning of the spectrum.

returning Newton's law of viscosity:

$$\tau_{yx} = \frac{F}{A} = \mu \frac{\partial U}{\partial y} = \mu \frac{\Delta U}{\Delta y} \tag{2-7}$$

For the simple laminar shear flow between two flat plates, a probe placed anywhere in the flow will register a velocity that is constant in time (Figure 2-7). A probe placed in a stationary laminar recirculation zone will return the same result.

Now consider a stationary particle held in position by a stream flowing upward at just the terminal velocity of the particle, as shown in Figure 2-8. The fluid far away from the particle is in laminar flow, but in the wake of the particle,[11] eddies form. A two dimensional slice of the flow provides a picture that is similar, in our intuitive context, to the surface currents behind a rock in a flowing stream. The eddies are relatively stationary in space and are easy to observe. They are typically round (or elliptical) in cross-section and maintain their size, which invites our intuition to jump to the idea of a coherent[12] spherical (or ellipsoidal) eddy. We need to examine a general turbulent flow more carefully before making that assumption.

The trademark of a turbulent or transitional flow is that the velocity fluctuates in time,[13] as shown in Figure 2-7. These fluctuations occur as eddies change or

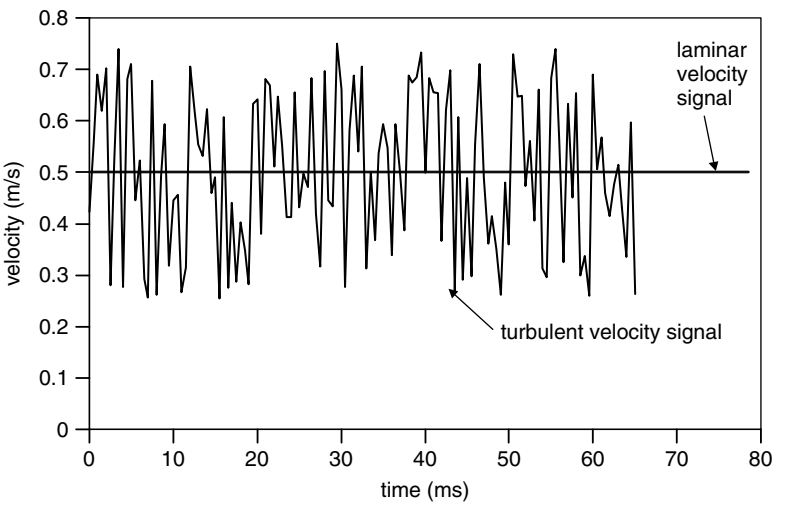

Figure 2-7 Velocity as a function of time in laminar and turbulent flow.

[11] The wake is the downstream side of the particle, where the fluid flow is affected by the presence of the particle.

[12] A coherent structure in a flow field is one that maintains its shape but may evolve over time. If the structure grows, the velocity will decay as a requirement of the conservation of momentum. Stable coherent structures that maintain their shape, size, and velocity are often observed in lower Reynolds number flows.

[13] We defer the definition of transitional flow to Section 2-5.

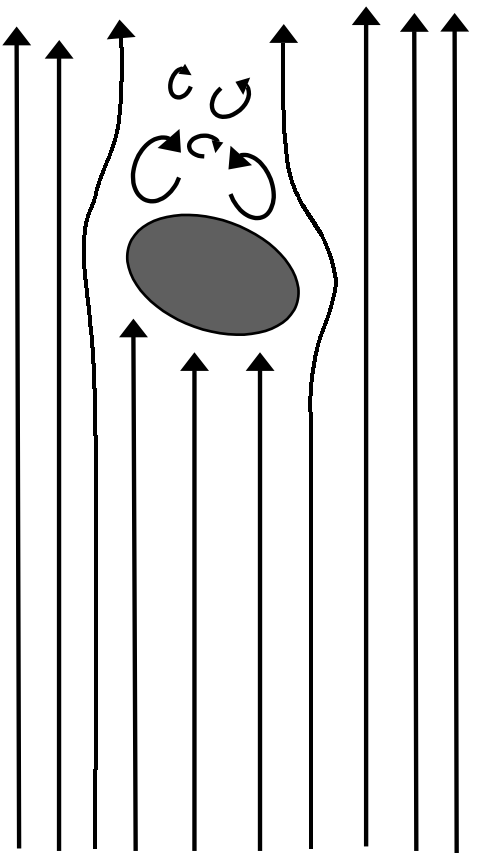

Figure 2-8 Turbulence in the wake of a particle: two dimensional cross-section.

move past the probe. Returning to our observations in a flowing stream or in a pipe, a constant superficial velocity or local mean velocity can also be defined. At any point in the flow, the signal can be averaged to give a repeatable mean, although the details of the velocity signal fluctuations in any record are unique. We might represent this situation as a series of rotating simple shear flows of varying size, as shown in Figure 2-9, which are convected along with a velocity U_c. In the figure, a very limited size range is shown, and the velocity profiles are all linear. In a more realistic turbulent flow, a much broader range of eddy sizes is observed, and the velocity profiles take on various nonlinear shapes in response to the surrounding eddies. This image is left to the reader's imagination.

The idea of many miniature shear flows that are rotating in space and being convected across a probe seems like a useful one. This may allow us to make a link between the three flow regimes (laminar, transitional, and turbulent), but before adopting it, let's clarify the assumptions that underlie this model. First, we've assumed that the eddies do not change as they are convected along in the

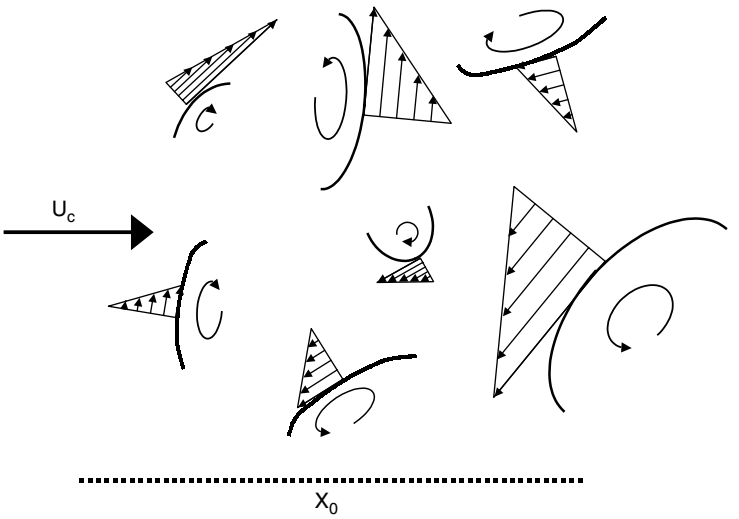

Figure 2-9 Eddies of various sizes and velocities, each containing a component of simple shear. The convective velocity, U_c, and the integral length scale, X_0, are arbitrary.

flow. If this were true, we could take a set of signals collected at X_0 and back out an exact picture of the flow at an instant in time. We could then calculate instantaneous mean shear and deformation rates over the cross-section. This is known as *Taylor's hypothesis* (1921):

$$\frac{\partial u_i}{\partial x} = -\frac{1}{U_c}\frac{\partial u_i}{\partial t} \tag{2-8}$$

On average, Taylor's hypothesis will turn out to be quite useful, but it is a dangerous one for the development of our intuition. Taylor's hypothesis locks the turbulent eddies into two dimensional symmetrical shapes, which stay in the same place relative to each other as they rotate through space. To expand on our intuitive images and understand the dynamic three dimensional component of turbulence, we need to observe eddies in clouds on a windy day, or in stack plumes and car exhausts on a cold day. The eddies are highly three dimensional. If one eddy is observed as it is convected along at U_c, it rotates, changes shape, changes size, and exchanges material with the surrounding fluid as it moves downstream. Its life cycle is extremely dynamic. These characteristics are critical for turbulent mixing, as they allow much more rapid cutting, folding, and incorporation of new material than does Taylor's image of frozen turbulence.[14]

The critical characteristics in our discussion of turbulence so far are that it contains three dimensional eddies which have a wide range of sizes and shapes

[14] To be fair to G. I. Taylor, he clearly limited this hypothesis to very short sampling times, thus minimizing some of these problems. His hypothesis is often applied as the best available approximation over times that exceed the valid limits.

and which change dramatically over time. To complete the discussion, we need to investigate the three dimensional aspect of the problem a bit more closely.

Return to the particle suspended in upward flow, but now instead of a particle, consider a cylinder that is very long, placed perpendicular to U_c. A pragmatic example of this is a dip pipe or cross-flow heat exchanger. At low Reynolds numbers, the two dimensional wake of the cylinder will look the same in cross-section as the particle wake in Figure 2-8, but the three dimensional eddy is quite different from the deformed ellipsoid behind a particle. Now it is a long unstable tube behind a pipe. The tubular eddy has a diameter similar to that of the pipe, but it is very long in the third dimension. As the Reynolds number increases, the wake will shed eddies of various sizes, many of them long and skinny. If the velocity fluctuations are measured in the streamwise direction, the signal will be similar to that in the particle wake, but in the transverse direction, the signal will be affected by the long dimension of the eddies parallel to the pipe.

Another example of a three dimensional eddy arises in the boundary layer close to the wall. In this layer, horseshoe eddies, turbulent spots, and turbulent bursts separate from the wall and are swept into the bulk flow. Many of these eddies have highly distorted dimensions, as shown in the simple example in Figure 2-10. It is easy to imagine that for the single illustrated eddy, at least three distinct

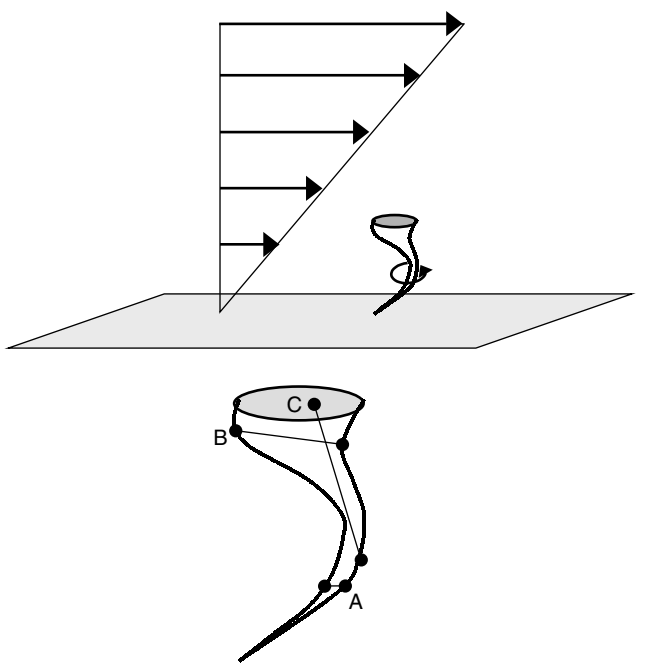

Figure 2-10 Vortex in a boundary layer showing the different length scales (A, B, and C) or wavenumbers contained in a single extended eddy: the wavelength ($1/k = U_c/2\pi f$) is a single arbitrary dimension of a three dimensional time-varying structure.

length scales (also measured as frequencies, or wavenumbers) could be observed for different one dimensional slices through the flow at A, B, and C.

Next consider what will happen to a drop of immiscible fluid that is injected into a turbulent velocity field. At the beginning, the drop may be spherical or ellipsoidal, but it will quickly respond to the velocity field, and we assume that the fluid and surface properties are such that it may deform very quickly in response to the motion of surrounding eddies. When the drop is embedded in an "eddy" that is much larger than its own characteristic diameter, it will be convected along in the eddy with very little deformation (Figure 2-11*a*). However; when the drop encounters eddies close to its own size, it will be deformed due to the interactions between the drop and the eddies. It may be either torn apart by two co-rotating eddies (Figure 2-11*b*) or elongated as it is squeezed between two counterrotating eddies, (Figure 2-11*c*). Finally, when the drop encounters small eddies, packets of its volume are torn away to mix with the surrounding fluid (Figure 2-11*d*). If there is no molecular diffusion, the minimum drop sizes will be limited to the scale of the Kolmogorov eddies and the drop fragments generated on breakup. Some of the drop fragments can be much smaller than the Kolmogorov scale (Zhou and Kresta, 1998). The drop size distribution characterizes discrete drops of fluid and reaches an equilibrium distribution after some (long) time. If, on

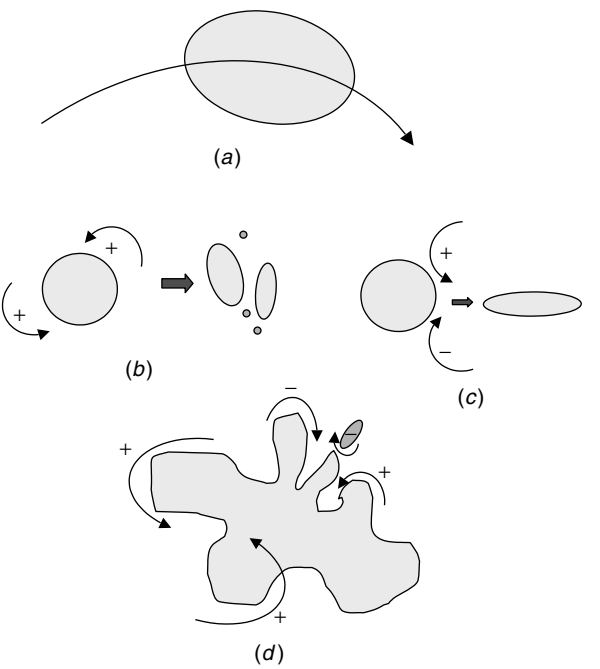

Figure 2-11 Scalar deformation in a turbulent field with surface tension between the two phases: (*a*) convection by large eddies; (*b*) erosion by co-rotating eddies; (*c*) elongation by counterrotating eddies; (*d*) multiple scales of deformation.

the other hand, there is significant molecular diffusion and no surface tension between the two fluids, as is the case for blending of miscible liquids, the blob of scalar fluid will deform continuously without breaking and the edges of the blob will be smoothed out by molecular diffusion at the same time as turbulent eddies deform and break the blob. After a fairly short time, no discrete blobs will be observed. Both of these cases are illustrated in the drop breakup and blending videos on the Visual Mixing CD affixed to the back cover of the book.

In the same way that relative length scales of eddies and blobs affect the breakup of blobs, in multiphase flows the relative response times of particles and eddies determine how particles interact with eddies (Tang et al., 1992). Although we do not discuss this issue in detail, it is important to recognize two things: (1) the relevant length scales for multiphase flows can be much more difficult to scale accurately because of the complicated interactions between turbulence and particles; and (2) where tracer particles are used in experiments, the scales of motion that can be observed are a function of the particle size and characteristic response time.

2-3.1.1 Nature of Turbulence: Summary of Section 2-3.1

- Turbulence is a dynamic three dimensional multiscaled phenomenon.
- Eddies *are not spherical*, and turbulence length scales are not characteristic dimensions in the usual sense.
- Turbulence interacts with both scalars (dye, reactants) and dispersed phases (bubbles, drops, and particles) according to the relative length and time scales involved.
- The smaller the turbulent length scales, the finer the scale of micromixing, and the faster the rate of mixing at the smallest scales of motion.

If we can hold onto some sense of the three dimensional dynamic character of turbulent eddies, including the range of sizes that appear and how quickly the eddies change in time, we can start to extract the questions we must ask for applications of turbulence in mixing. In the next section we examine more formal ways of characterizing turbulence.

2-3.2 Turbulence Spectrum: Quantifying Length Scales

In Section 2-2, we used Figure 2-7 to illustrate the instantaneous velocity versus time signal and the mean velocity. A third velocity used widely for turbulent flows is the root-mean-square (RMS) velocity, or the standard deviation of the instantaneous velocity signal. Because the average fluctuation is zero by definition, the RMS velocity gives us an important measure of the amount or intensity of turbulence, but many different signals can return the same mean velocity and RMS fluctuating velocity,[15] so more information is needed to characterize the turbulence.

[15] The RMS velocity is exactly equivalent to the statistical measure known as the standard deviation.

If the velocity record is mean centered and transformed from the time domain to the frequency domain using a Fourier transform, we obtain the energy spectrum. The energy spectrum is a measure of the amount of energy present at each scale of motion. This allows us to take a fingerprint of the dominant frequencies in the flow in terms of their energy content (E), or power spectral density (PSD), as a function of wavenumber (k, in m^{-1}) or frequency (f, in Hz or s^{-1}). The spectrum gives the energy contained at each wavenumber, so the integral of the three dimensional spectrum returns the turbulent kinetic energy (2k or q), and the integral of the one dimensional spectrum (in the j-direction) over all wavenumbers returns the (j component of) RMS velocity, u_j^2.

The length scales of turbulence are contained in the measured frequencies, but the frequencies are a function of the mean velocity as well as of the rate of fluctuation. To obtain a more scalable picture of the length scales of turbulence, the measured frequencies are converted to wavenumbers using the mean convective velocity and Taylor's hypothesis:

$$k = \frac{2\pi f}{\overline{U}_c} \tag{2-9}$$

This application of Taylor's hypothesis is not quite the same as the faulty example given earlier, where we collected velocity versus time at X_0 and used it to back out the flow field at one instant in time. Now we are quantifying the time-averaged conditions in the flow, using Taylor's hypothesis to scale the spectrum with the mean convective velocity. The turbulence spectra, which develop at different mean velocities, can now be compared in terms of the wavenumbers (length scales) that are present in the turbulent part of the flow. We only have to assume that the eddies are coherent long enough to convect the largest length scale across X_0 in some *repeatable time-averaged* sense to justify using Taylor's hypothesis for scaling the spectrum.

To get a sense of the meaning of a wavenumber, consider a perfectly spherical eddy. As the eddy is convected past a probe at a constant velocity, it will give many different wavenumbers (frequencies), depending on where the sensor cuts through the sphere. The measured spectrum of lengths for a sphere will range from close to zero up to the diameter of the sphere. The three dimensional irregular dynamic multiscaled eddies present in fully turbulent flows will produce an analogous range of results. Wavenumbers are not physical lengths in the way we are used to thinking about them, but they will prove very useful as a means of scaling turbulence.

A typical spectrum for a stirred tank is shown in Figure 2-12*b* (Michelet, 1998). This spectrum is measured close to a Rushton turbine, where there are strong fluctuations in the velocity due to the moving blades and the trailing vortices, shown in Figure 2-12*a* (Yianneskis et al., 1987). The spectrum in Figure 2-12*b* is scaled with f_p, the blade passage frequency, so the blade passage frequency and its harmonics are evident as sharp peaks in the spectrum at 1 and at 2. The blade passages have a strong directional preference and are often

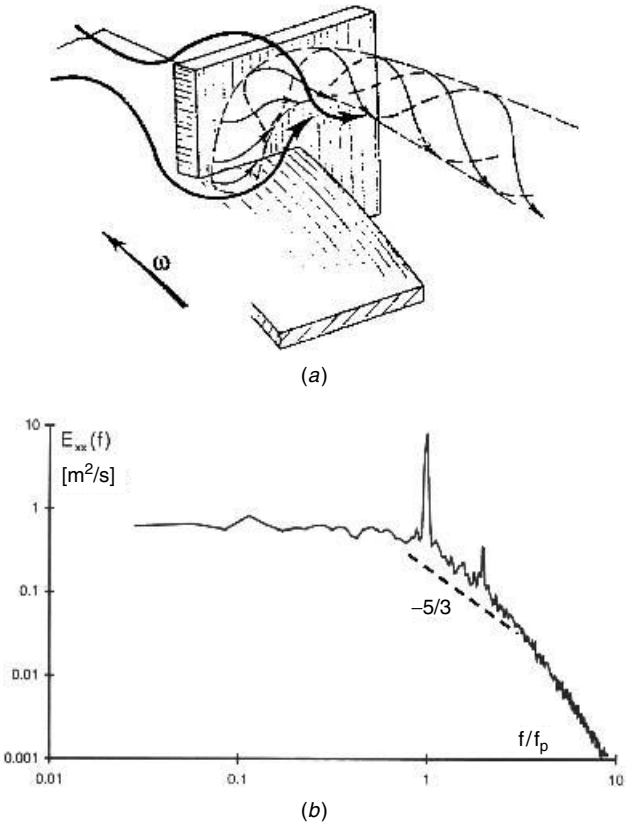

Figure 2-12 Trailing vortex behind the blade of a Rushton turbine shown in (*a*) (Yianneskis et al., 1993) has a mirror image on the lower side of the blade. The frequency spectrum in (*b*) is normalized with the blade passage frequency and shows two peaks due to the blade passages. The trailing vortices are shown in motion on the Visual Mixing CD affixed to the back cover of the book.

removed from the signal before analysis of the turbulence. The reasons for this are discussed in detail in Example 2-5. In some configurations, an additional lower frequency is present at some fraction of the impeller speed, which must also be removed before the turbulence can be accurately quantified (Roussinova et al., 2000). Note that the range of *length scales* in the tank extends from T (the largest dimension) over at least three orders of magnitude (a factor of 1000) to η, and the measured *frequencies* in Figure 2-12*b* extend over a similar range. Using log scales allows us to cover the wide range of both power and wavenumbers.

The slope of the spectrum at frequencies higher than the blade passage frequency gives information about the distribution of energy across the turbulent scales of motion. If the energy distribution is in equilibrium, all the energy that enters the turbulent motion at large scales (i.e., in the form of low frequencies

at the impeller) is dissipated at the same rate at the smallest scales of motion, where viscous dissipation is most effective. Where equilibrium exists, the slope in the equilibrium region must be $-\frac{5}{3}$ on a log-log scale.[16] It is evident from the figure that this criterion is satisfied only over a small range of frequencies close to the blades of a Rushton turbine.

The smallest scales of motion, or the smallest eddy dimensions, are characterized using the *Kolmogorov length scale:*

$$\eta = \left(\frac{\nu^3}{\varepsilon}\right)^{1/4} \tag{2-10}$$

At this length scale, the viscous forces in the eddy are approximately equal to the inertial forces due to turbulent velocity fluctuations. Somewhere close to this length scale, the dissipation of energy becomes rapid, and the slope of the spectrum increases dramatically, as shown in Figure 2-13. The Kolmogorov length, η, is a *defined* length equal to the inverse of the Kolmogorov wavenumber. It is used as a point of reference so that various conditions can be compared in a consistent way, but it is only one of a whole range of turbulent length scales which are present in any turbulent flow.

So what is the characteristic length scale of turbulence? This question is analogous to asking, "What is the diameter of an elephant?" We might say that the Kolmogorov scale is analogous to the diameter of the elephant's tail. Many

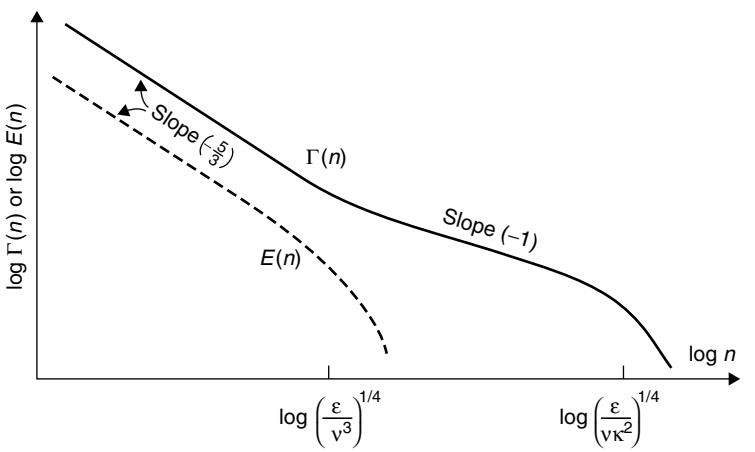

Figure 2-13 Spectrum of velocity [E(n)] and temperature or concentration [Γ(n)] fluctuation wavenumbers (m^{-1}) in the equilibrium range of homogeneous isotropic turbulence for the case of large Sc or Pr (modified from Batchelor, 1959). In the Batchelor scale, κ is either the thermal diffusivity ($k/\rho C_p$) or the molecular diffusivity (D_{AB}).

[16] Note, however, that the converse is not true: A $-\frac{5}{3}$ slope is not proof that equilibrium, or isotropy, exists.

other equally valid turbulent length scales have been defined, and we could say that they are analogous to the size of the elephant's trunk, ears, and legs. All of these length scales are related to each other and to the size of the elephant (the total energy in the spectrum) in a consistent and highly correlated way from one elephant to the next. Despite this, no single length scale can uniquely define the diameter of the elephant. In many cases of practical interest, the entire range of length scales is important to the process, and apparently small changes in the spectrum can make large changes in the process. An elephant without a tail is a perfectly good elephant, unless the elephant's main objective is to swat flies!

2-3.2.1 Spectral Arguments for Scalar Mixing and Mass Transfer. Batchelor (1959) used scaling arguments to determine the size of a pure sphere of dye that will diffuse in exactly the time it takes the energy in an eddy of size η to dissipate. This is called the *Batchelor scale:*

$$\lambda_B = \left(\frac{\nu D_{AB}^2}{\varepsilon}\right)^{1/4} \quad \text{and} \quad \frac{\eta}{\lambda_B} = Sc^{1/2} = \left(\frac{\nu}{D_{AB}}\right)^{1/2} \tag{2-11}$$

This analysis is limited to cases where the molecular diffusivity is slow relative to the momentum diffusivity (kinematic viscosity), so that $Sc \geq 1$. In the same way that the Kolmogorov scale provides a limit where turbulent stresses are balanced by viscous stresses, the Batchelor scale provides a limiting length scale where the rate of molecular diffusion is equal to the rate of dissipation of turbulent kinetic energy. Below this scale, distinct packets of dye will quickly be absorbed into the bulk fluid by molecular diffusion, where our meaning of "quickly" is now consistent between the energy dissipation and molecular diffusion.

Figure 2-13 shows the gross characteristics of the velocity and concentration spectra. For a low viscosity liquid, Sc can be on the order of 1000, so the Batchelor scale can be 30 times smaller than the Kolmogorov scale. The ultimate scale of mixing needed for reaction is the size of a molecule, so in liquid-phase reactions, molecular diffusion is critically important for the final reduction in scale. For a gas, Sc is closer to 1, so the ratio is closer to 1, and the competition between the turbulent reduction in scale and molecular diffusion occurs at the same range of wavenumbers. The various length scales shown in Figure 2-13 are also summarized in Table 2-3

So far, our discussion of length scales has focused on the smallest scales of motion. At the larger scales of motion, Taylor (1921) considered the turbulent dispersion of fluid particles by homogeneous isotropic turbulence in the absence of molecular diffusion. In his model, each fluid particle leaving a point source in a uniform velocity field is expected to deviate from the linear mean path in a random manner, depending on the local nature of the turbulence. The RMS deviation of the particle paths is observed as a continued divergence, spread, or dispersion as the particles are carried downstream. *This eddy motion occurs even*

Table 2-3 Useful Time and Length Scales Arising from Spectral Arguments

Usual Notation	Name	Physical Meaning
$\eta = \left(\frac{\nu^3}{\varepsilon}\right)^{1/4}$	Kolmogorov length scale	Eddy size at which the viscous forces are equal to the inertial forces. Viscous dissipation becomes important. Some authors place the dissipation limit at 5η, where the viscous forces reach 20% of the inertial forces of turbulence.
$t_K = \left(\frac{\nu}{\varepsilon}\right)^{1/2}$	Kolmogorov time scale	Time it takes to dissipate the energy contained in the smallest (η-sized) eddies.
$t_B = t_K \propto \frac{\eta^2}{D_{AB}}$	Batchelor time scale	Time required for a pure scalar blob of A to diffuse into pure B if the blob diameter is η.
$\lambda_B = \left(\frac{D_{AB}^2 \nu}{\varepsilon}\right)^{1/4}$	Batchelor length scale for mass transfer where Sc is large	Size of a pure scalar blob that will diffuse into pure surrounding fluid in exactly t_K.

in the absence of molecular diffusion. The spread of the plume size, L, for large times (relative to the smallest scales of turbulence) can be approximated by

$$\frac{d(L^2)}{dt} = 2u^2\tau_E \approx \frac{k^2}{\varepsilon} \tag{2-12}$$

where τ_E is the integral of the particle velocity autocorrelation function (constant for large integration times, but varying locally in the flow), and u, k, and ε are local values that must be integrated over the path of the plume. The use of k^2/ε in this context should be considered a scaling approximation. It assumes that the turbulence in the plume is at least locally isotropic and that it is uniform across the plume at any constant distance from the source. Inside the spreading plume, whether or not molecular diffusion plays an important role, the time-averaged concentration distribution will be Gaussian, making the reaction kinetics aspect of the problem more complicated.[17] This model is often the

[17] A colleague working in the area of pollutant dispersion notes an important weakness of the time-averaged approach: If the maximum concentration is a critical parameter, the average concentration is not a useful result. Take, for example, the dispersion of H_2S: If the local instantaneous concentration exceeds a toxic limit, people on the ground will die. "Alive on the average" is not a useful result, even if the average is very accurately determined! The necessary details of the distribution of concentrations can be extracted from statistical or PDF models which account for the time-varying characteristics of the concentration fluctuations.

best we can do with the available data, but it is clearly a simplified view of the physics.[18]

Taking a somewhat different approach, Corrsin (1957, 1964) considered the overall decay of concentration fluctuations, c(t), in a homogeneous turbulent field at high Re. In this case, the RMS fluctuations follow an exponential decay of the form

$$\overline{c^2(t)} = \overline{c^2(0)} \exp\left(\frac{-t}{\tau}\right) \tag{2-13}$$

τ can be related to the physical properties of the fluid, ν and Sc, and the largest scales of concentration fluctuations, L_s, as well as the rate of dissipation of turbulent kinetic energy, ε. Corrsin integrated the approximate spectrum from the wavenumber corresponding to the size of the largest blobs of pure A (k_0) to beyond $1/\lambda_B$ to obtain an estimate of the mixing time constant. The resulting equations for both low and high Sc are given in Table 2-4. For liquids, Sc is large, λ_B is smaller than η, and diffusion is very slow. The time constant increases due to the action of diffusion (second term in the expression for τ), but this second term is often small when compared to the magnitude of the first term, particularly for low viscosity fluids. When Sc is near unity, as for gases, λ_B is approximately equal to η, and the approximate spectrum is integrated from k_0 to beyond η. For the resulting equation to apply, Sc needs to be in the vicinity of 1; otherwise, the equation will predict infinite mixing time.

Corrsin's analysis was developed for an isotropic homogeneous turbulent field but has been very successfully applied in pipe flow, both in terms of the shape of the spectrum and in terms of the overall mixing time (see Example 2-1e). Others have applied Corrsin's scaling arguments in mixing tanks to determine the correct dimensionless groups to apply for blend time correlations (see Example 2-3). The key concept to understand from Table 2-4 is the relationship between the concentration fluctuation field and the velocity fluctuation field. This relationship is different for gases and liquids. The mixing time estimates in Table 2-4 allow us to make some useful arguments about the length scales that are retained on scale-up, and about the mass transfer time scales compared to the reaction time scales in cases where micromixing dominates the process.

[18] Going one step further, the combination of molecular diffusion with Taylor dispersion has also been treated in Brodkey (1967, p. 326). Turbulent eddies carry what has to be mixed from one part of the fluid to another, which accelerates the breakdown of blobs of pure A. At the same time, molecular diffusion is enhanced by the increase in surface area and the steep gradients of concentration that occur due to the action of the turbulent eddies. Using a statistical approach, the enhancement of mixing due to turbulent dispersion can be described with a simple first-order solution:

mean-squared displacement of the interface = turbulent dispersion

+ result of interaction between turbulence and molecular diffusion

$$L^2 = L_0^2 + 2D_{AB}t$$

This equation describes the mean spread of a plume in uniform (plug) flow and is most relevant for cases involving the dispersion of gases.

Table 2-4 Effect of Schmidt Number on Concentration Length Scales and on Blend Time

Schmidt Number $Sc = \nu/D_{AB}$	Relative Length Scales $Sc^{1/2} = \eta/\lambda_B$	Time Constant for Decay of Concentration Fluctuations
$Sc \ll 1$ Molecular diffusivity faster than momentum diffusivity	$\eta < \lambda_B$ Smallest length scales are in the velocity field; not realizable	
$Sc = 1$ or small Equal diffusivities of mass and momentum: typical of gases	Equal length scales	Governed by turbulence: $\tau = \left(\frac{5}{\pi}\right)^{2/3} \frac{2}{3 - Sc^2} \left(\frac{L_s^2}{\varepsilon}\right)^{1/3}$
$Sc \gg 1$ Molecular diffusion slow: typical of liquids	$\eta > \lambda_B$ Smallest length scales are in the concentration field	Mixing is slowed down by the effects of molecular diffusion: $\tau = \frac{1}{2}\left[3\left(\frac{5}{\pi}\right)^{2/3}\left(\frac{L_s^2}{\varepsilon}\right)^{1/3} + \left(\frac{\nu}{\varepsilon}\right)^{1/2} \ln(Sc)\right]$ The effect of Sc is usually small, particularly for low viscosity liquids

Example 2-1e: Realistic Models of Turbulent Mixing. Now that we have some additional understanding of turbulent mixing of scalars, we can return to Example 2-1 to consider a more realistic analysis. Example 2-1d considered molecular diffusion across a single frozen eddy length scale. When we treat the turbulent eddies as a fixed reduction in the scale of segregation, the dynamic multiscaled nature of the turbulence is neglected. What we really need to know is how eddies across the entire spectrum of length scales interact dynamically with the concentration field in space and time. Because little is known about modeling these dynamics directly, the problem is formulated in terms of statistical averages in the theories developed by Taylor and by Corrsin.

Corrsin's (1957, 1964) theory considers the time scale, τ, required for the decay of the concentration fluctuations. This can be expressed in terms of the intensity of segregation:

$$I_s = \frac{\overline{c'^2}}{\overline{c_o'^2}} = e^{-t/\tau} \tag{2-14}$$

The intensity of segregation is a measure of the mixing accomplished. The intensity is 1 when the components are unmixed and zero when they are fully mixed (zero fluctuations). This intensity is a point measurement, not an average over

the entire vessel. The time constants, τ, for low and high Sc are taken from Table 2-4.

The macroscale of mixing, L_s, is not well established, so estimates for this, and for ε, are needed. Brodkey (1967, p. 351) suggests

$$\left(\frac{5}{\pi}\right)^{2/3}\left(\frac{L_s^2}{\varepsilon}\right)^{1/3} = 0.341\frac{r_0}{u} \tag{2-15}$$

for a pipe, where r_0 is the radius of the feed pipe and u is the streamwise RMS velocity. We will return to discuss the scaling arguments related to this expression in the next section, but first we would like to test the estimate using experimental evidence. McKelvey et al. (1975) established the velocity and concentration fields in the same pipe reactor as that used by Vassilatos and Toor (1965; Example 2-2c). Their objective was to test the time constants for mixing as predicted from velocity field measurements. This involved showing that there was an equivalence of the mixing and very fast reaction rates in Toor's reactor.[19] Figure 2-14 shows extremely good agreement between the mixing model based on velocity measurements and the reaction rate results from Vassilatos and Toor.

The general equivalence of time constants estimated over a wide variety of experiments involving gases and liquids and a variety of geometries was shown in a review by Brodkey (1975). He showed that nearly a 10 000 fold range in mixing times could be adequately estimated if one has some idea as to the proper value of r_0 (the characteristic dimension) to be used. This lends some credibility to Corrsin's theory and motivates further examination of L_s and ε.

2-3.3 Scaling Arguments and the Energy Budget: Relating Turbulence Characteristics to Operating Variables

To relate the Kolmogorov scale, η, to operating variables, we need to get a measure of the rate of dissipation of turbulence kinetic energy per unit mass, ε. The easiest way to do this is via scaling arguments and the use of characteristic length and velocity scales. These scales are an important tool in engineering fluid mechanics and deserve some explanation.

In fully turbulent flow, viscous forces become negligible relative to turbulent stresses and can be neglected (except for their action at the dissipative scales of motion). This has an important implication: above a certain Reynolds number, *all velocities* will scale with the tip speed of the impeller, and the flow characteristics can be reduced to a single set of dimensionless information, *regardless of the fluid viscosity*. One experiment in the fully turbulent regime[20] can be applied for all tanks that are exactly geometrically similar to the model, at all Reynolds numbers

[19] Toor (1962) hypothesized that mixing and very fast reaction rates are equivalent when the reactants are stoichiometrically fed, and their stoichiometric ratio is 1.

[20] See the discussion of whether the tank is fully turbulent when the impeller region is fully turbulent in Section 2-5.

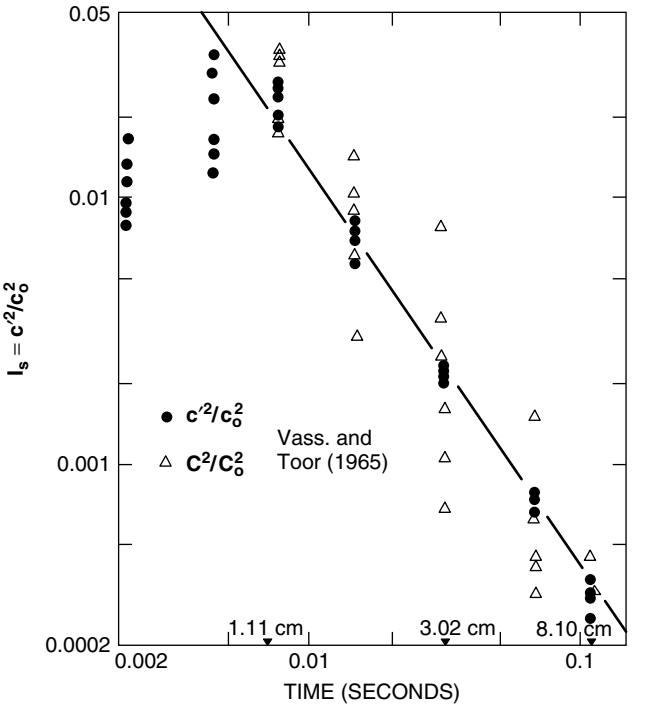

Figure 2-14 Predicted intensity of segregation-based Corrsin-type analysis and Toor's hypothesis. (Data from McKelvey et al., 1975.)

in the fully turbulent regime, and for the full range of Newtonian working fluids. For the stirred tank, the characteristic turbulent velocity and length scales are

$$u_c = C'_u V_{TIP} = C_u ND$$
$$L_c = C_L D \tag{2-16}$$

For now, the characteristic length scale L_c is assumed to scale with the impeller diameter, not the tank diameter.[21] If geometric similarity is observed and all impeller dimensions are scaled with the impeller diameter (including details such as blade thickness), the characteristic length scale ($C_L D$) will scale any of the impeller dimensions equally well; only C_L will change. The constants C_u and C_L are a function of the impeller and tank geometry selected. For now, however, we retain them as constants.

The dissipation, ε, is the rate of dissipation of turbulent kinetic energy. The turbulent kinetic energy must scale with u_c^2. The rate of dissipation of energy is

[21] As long as strict geometric similarity is maintained, the only difference between D and T is a constant. See Example 2-3 for further discussion.

taken to scale with u_c/L_c, the characteristic time scale of the flow. This gives

$$\varepsilon \propto \frac{u_c^3}{L_c} = \frac{C_u^3 N^3 D^2}{C_L} = A\frac{C_u^3 N^3 D^2}{C_L} \tag{2-17}$$

Note the large sensitivity of ε to C_u, relative to its sensitivity to C_L and A! When the dissipation is estimated from experimental data, A is taken to be equal to 1, u_c is measured, and L_c is either determined from an integral energy balance, or is estimated as some fraction of the impeller diameter. Direct measurements of the dissipation are extremely difficult [see review by Kresta (1998)].

A second estimate of turbulence characteristics, which avoids the need for C_u, is the power per unit mass of fluid in the tank. If the liquid depth, H, is equal to the tank diameter, T:

$$\frac{P}{\rho V_{tank}} = \frac{4N_p \rho N^3 D^5}{\rho \pi T^2 H} \propto N_p N^3 D^2 \left(\frac{D}{T}\right)^3 \tag{2-18}$$

This scaling, however, introduces a factor of $(D/T)^3$. This may work well where the bulk characteristics of the flow dominate, but it is not an accurate measure of turbulence if local characteristics are needed. For the same power input per unit tank volume, or holding eq. (2-18) constant with variations in impeller type, diameter, and off-bottom clearance, Zhou and Kresta (1996a) provided an extensive set of data and showed that the local dissipation can vary by up to a factor of 100. This is illustrated for the Intermig on the Visual Mixing CD affixed to the back cover of the book. The best order-of-magnitude estimate of the maximum dissipation uses the swept volume of the impeller instead of the total tank volume:

$$\frac{P}{\rho V_{impeller}} \propto \frac{N_p \rho N^3 D^5}{\rho D^3} = N_p N^3 D^2 \tag{2-19}$$

and gives the same scaling with N and D as the original estimate of the dissipation. Note that this scaling suggests that the effect of C_u^3/C_L is characterized by the power number, and that some fraction of the total energy is dissipated in the impeller swept volume. This fraction depends on the impeller geometry (Zhou and Kresta, 1996b). Figure 2-15 applies this scaling approach to measured estimates of ε_{max} for various tank geometries, showing that this scaling estimate is accurate within a factor of 2 for four different impellers with power numbers ranging from 0.3 to 6. The importance of using the swept diameter in calculations, particularly for a PBT, is illustrated in the example below from Weetman (2002).

Example 2-3: Swept Diameter Calculation. In this example we consider two PBT's. The first is a standard geometry ($W/D = 0.2$, 45° blade angle or tip chord angle). The second is a PBT with $W/D = 0.5$ and a tip chord angle (TCA) of

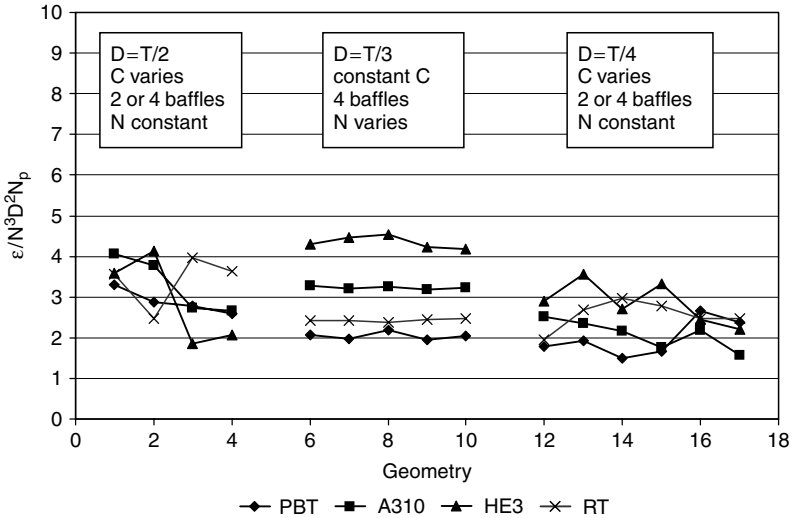

Figure 2-15 Scaling of maximum local dissipation with the power per impeller swept volume across a range of geometries. Use of the power per tank volume with exact geometric similarity will give a similar result; however, when the geometry is varied, values of the local dissipation can vary dramatically from one tank to another, even at the same power per tank volume. (Modified from Zhou and Kresta, 1996b.)

30° to the horizontal. The blade length plus the hub radius is the perpendicular dimension, but the swept diameter must be corrected for the projection of the tip of the blade beyond the perpendicular radius.

Standard impeller (W/D = 0.2; TCA = 45°; blade thickness = t_b = 0.01D):

$$\frac{D_{swept}}{D} = \frac{1}{\{1 - [W\cos(TCA)/D + t_b \sin(TCA)/D]^2\}^{0.5}} = 1.0112$$

$$\frac{P_{swept}}{P} = \frac{N_p \rho N^3 D_{swept}^5}{N_p \rho N^3 D^5} = \left(\frac{D_{swept}}{D}\right)^5 = 1.057$$

$$\frac{\varepsilon_{swept}}{\varepsilon} = \frac{N_p N^3 D_{swept}^2}{N_p N^3 D^2} = \left(\frac{D_{swept}}{D}\right)^2 = 1.022$$

30°, Wide-blade impeller (W/D = 0.5; TCA = 30°; t_b = 0.01D):

$$\frac{D_{swept}}{D} = \frac{1}{\{1 - [0.5\cos(30^\circ) + 0.01\sin(30^\circ)]^2\}^{0.5}} = 1.112$$

$$\frac{P_{swept}}{P} = (1.112)^5 = 1.703$$

$$\frac{\varepsilon_{swept}}{\varepsilon} = (1.112)^2 = 1.237$$

For a standard PBT the error is on the order of 5% if the perpendicular distance is used. For the large-bladed impeller with a shallower angle, the errors are up to 70%! This D also makes sense when measuring the primary flow with a laser Doppler velocimeter for determination of the flow number (see Chapter 6). It is very important in a mixing installation when one has to be concerned with clearances from the tips of the blades.

Where does this leave us? We have three ways to estimate the dissipation and the Kolmogorov length scale: The first requires experimental information for C_u, C_L, and A; the second uses the power number and the impeller swept volume to get an estimate of the maximum local dissipation; the third uses the total volume of the tank to get an estimate of the gross average dissipation and introduces a factor of $(D/T)^3$ into the equation. More recent detailed studies on the Rushton turbine in particular (Michelet, 1998; Escudier, 2001) have shown that these estimates are reasonably accurate over some portion of the impeller discharge stream. All three methods will allow us to assess trends on scale-up, where physical properties often remain constant, but dimensions and rotational speeds change. The power per impeller swept volume is recommended as the best practice estimate.

Example 2-4a: Blend Time. Now that we have ways to estimate ε and the characteristic length scale L_s, we return to Corrsin's equations in Table 2-4. Probably the *most important practical point* is that the time constant of mixing scales with $(L_s^2/\varepsilon)^{1/3}$. All the rest of the terms in the equation for $(Sc \gg 1)$ are either constants or relatively minor effects of the Schmidt number. For mixing in a pipe, we take the radius of the feed pipe, r_0, as the initial integral length scale, and the fluctuating velocity, u, as a measure of the turbulent energy. Thus we can write

$$\varepsilon \propto \frac{u^3}{r_0}$$

$$\tau \propto \left(\frac{L_s^2}{\varepsilon}\right)^{1/3} \propto \left(\frac{r_0^2 r_0}{u^3}\right)^{1/3} = \frac{r_0}{u}$$

What are the practical implications of this result? The time constant goes up (longer mixing times are needed) directly with an increase in the size of the system and down with an increase in the turbulent RMS fluctuations. Stated in dimensionless terms, the mixing length, L/D, depends on the turbulence intensity in the pipe, U/u.

What about our underlying assumptions? We know from experimental measurements that u/U is a weak function of Reynolds number. We can assume that it is approximately constant. On scale-up at constant Reynolds number, the dimension increases and U decreases; thus u must decrease also. For the same scale-up, the largest concentration scales must also increase, as they scale with r_0. Substituting this back into the equation for τ, we see that the mixing time will scale with the characteristic dimension squared. The mixing length is not quite

so bad, as it will scale with τU, where U decreases on scale-up at constant Re. This means that the mixing length will scale with the characteristic dimension, L/D = constant. This is essentially a requirement of geometric similarity. The only way to maintain a constant mixing time on scale-up is to increase the turbulence. Keeping our eye on the important scale-up parameters certainly helps us to understand mixing better.

Applying the same scaling arguments in a stirred tank, L_s is equal to some fraction of D and ε is estimated using the power per impeller swept volume. This gives

$$\tau \propto \left(\frac{L_s^2}{\varepsilon}\right)^{1/3} \propto \left(\frac{D^2}{N_p N^3 D^2}\right)^{1/3} = \frac{1}{N_p^{1/3} N}$$

Compare this with the general form of correlation for blend time in the tank from Chapter 9, where the exponent n is 2 for axial impellers:

$$\theta_B \propto \frac{1}{N_p^{1/3} N} \left(\frac{T}{D}\right)^n \tag{2-20}$$

The correct dependence of θ_B on N_p and N is suggested by the scaling arguments. The effect of T/D can be extracted if we use a minimum dissipation instead of the maximum dissipation, and set the integral length scale equal to the tank diameter at the fully mixed conditions in the bulk:

$$u_{c,max} \propto (\varepsilon_{max} D)^{1/3} \propto (N_p N^3 D^2 D)^{1/3} = N_p^{1/3} N D$$

$$u_{c,min} \propto N_p^{1/3} N D \frac{D}{T} \quad \text{due to jet decay, so} \quad \varepsilon_{min} \propto \frac{u_{c,min}^3}{T} \propto \frac{N_p N^3 D^6}{T^4}$$

$$\tau_{max} \propto \left(\frac{L_s^2}{\varepsilon_{min}}\right)^{1/3} \propto \left[\frac{T^2}{N_p N^3 D^2 (D/T)^4}\right]^{1/3} = \frac{1}{N_p^{1/3} N} \left(\frac{T}{D}\right)^2$$

Where T/D is held constant on scale-up, this result reduces to $1/(N_p^{1/3} N)$. There are many different ways to make the scaling arguments (see, e.g., Grenville et al., 1995; Grenville and Tilton, 1996, 1997; or Nienow, 1997). The point is that the end result agrees well with Corrsin's approach. The most important thing to recognize is that L_s^2/ε, *however it is estimated, must be constant on scale-up to maintain constant blend time*. If the dissipation (ε) is held constant on scale-up, the blend time will always increase.

Example 2-4b: Scale-up with Exact Geometric Similarity. In this example we consider the relationship between the spectrum of velocity fluctuations and the micromixing scales. At the lab scale, a T = 0.25 m vessel is used to formulate a homogeneous reaction in an aqueous phase. The fully baffled vessel is equipped with a Rushton turbine impeller of D = T/2 at C = T/3 with $N_p = 5.0$. The

reaction proceeds as desired at N = 240 rpm. Scale-up to the plant vessel follows exact geometric similarity, with T = 2 m. What is the appropriate N to use in the plant?

We could calculate the bulk blend time in the lab and in the plant, but in this case the process result requires a reaction. The reaction kinetics and molecular diffusivity are constant on scale-up, so we must ensure that the Batchelor scale is also preserved. The Batchelor scale can be defined using an estimate for the dissipation:

$$\varepsilon \propto \frac{(\pi ND)^3}{L_c} \propto N_p N^3 D^2$$

$$\lambda_B = \left(\frac{\nu D_{AB}^2}{N_p N^3 D^2}\right)^{1/4}$$

Setting the Batchelor scale equal in the lab and the plant gives

$$N^3D^2 = \text{constant} = \left(\frac{240}{60\ \text{s}}\right)^3 \left(\frac{0.25\ \text{m}}{2}\right)^2 = 1.0\ \text{m}^2/\text{s}^3$$

$$N_{\text{plant}} = \left[\frac{1.0\ \text{m}^2/\text{s}^3}{(2\ \text{m}/2)^2}\right]^{1/3} \left(60\ \frac{\text{s}}{\text{min}}\right) = 60\ \text{rpm}$$

So the use of N = 60 rpm (or higher) and exact geometric similarity will ensure that the Batchelor length scale for scalar mixing is preserved on scale-up.

Now check the Reynolds number and power consumption:

$$\text{Re}_{\text{plant}} = \frac{ND^2}{\nu} = \frac{(1\ \text{s}^{-1})(1\ \text{m})^2}{1 \times 10^{-6}\ \text{m}^2/\text{s}} = 10^6$$

$$\text{Re}_{\text{lab}} = \frac{(4\ \text{s}^{-1})(0.125\ \text{m})^2}{1 \times 10^{-6}\ \text{m}^2/\text{s}} = 6.25 \times 10^4$$

Both vessels are in the fully turbulent regime, so the scaling rules will hold. Thus,

$$\left(\frac{P}{V_{\text{tank}}}\right)_{\text{plant}} = \frac{4N_p \rho N^3 D^5}{\pi T^2 H} = \frac{(4)(5.0)(1000\ \text{kg/m}^3)(1\ \text{s}^{-1})^3(1\ \text{m})^5}{(3.14)(2\ \text{m})^2(2\ \text{m})}$$

$$= 796\ \text{W/m}^3$$

$$\left(\frac{P}{V_{\text{tank}}}\right)_{\text{lab}} = \frac{(4)(5.0)(1000\ \text{kg/m}^3)(4\ \text{s}^{-1})^3(0.125\ \text{m})^5}{(3.14)(0.25\ \text{m})^2(0.25\ \text{m})} = 796\ \text{W/m}^3$$

Since we required a constant D/T and ε on scale-up, the power per unit volume is also forced to remain constant. The power consumption provides what is considered intense agitation in both vessels.

Notice that the value for the molecular diffusivity was never used in this problem, because the physical properties were retained on scale-up!

Example 2-4c: Scale-up where Exact Geometric Similarity Is Not Maintained. A more difficult case is one where geometric similarity is not maintained on scale-up. In this case the lab scale vessel is a round-bottomed flask with a magnetic stirrer, and an existing vessel with a PBT (T = 1 m, D = T/4, C = T/4, four baffles, $N_p = 1.2$) is to be used in the plant. The initial operating conditions set N at 45 rpm ($Re = 4.7 \times 10^4$), but there is excessive formation of by-product. The chemists agree to run some scale-down experiments. The first experiment uses exact geometric similarity and the same scaling principles as outlined in Example 2-4b. The resulting product distribution matches the one obtained in the plant. The new conditions in the lab are T = 160 mm, D = 40 mm, C = 40 mm, and N = 152 rpm.

On increasing N to 400 rpm in the lab, the desired product distribution is obtained. *This is an indication that there is interaction between the reaction kinetics and the mixing.* To keep N^3D^2 constant, N in the plant must be 118 rpm. Unfortunately, the plant mixer has a fixed rpm. To keep a constant microscale, we decide to change the impeller diameter:

$$N_p N^3 D^2 = \text{constant} \qquad N = 45 \text{ rpm}$$

$$(400 \text{ rpm})^3 (0.04 \text{ m})^2 = (45 \text{ rpm})^3 D^2 \qquad D = 1.06 \text{ m}$$

This is larger than the existing tank diameter, so it is necessary to change the impeller geometry to something with a larger power number. Selecting a Rushton turbine (RT), N_p is taken equal to 5.0 (conservative), so

$$(1.2)(400 \text{ rpm})^3 (0.04 \text{ m})^2 = 5.0(45 \text{ rpm})^3 D^2 \qquad D = 0.52 \text{ m}$$

This impeller diameter will fit in the existing tank. Now consider the relative blend times:

$$\theta_{B,\text{lab}} = \frac{5.2}{(400/60 \text{ s})(1.2)^{1/3}} \left(\frac{0.16 \text{ m}}{0.04 \text{ m}} \right)^2 = 11.7 \text{ s}$$

$$\theta_{B,\text{plant}} = \frac{5.2}{(45/60 \text{ s})(5.0)^{1/3}} \left(\frac{1.0 \text{ m}}{0.52 \text{ m}} \right)^2 = 15 \text{ s}$$

We expect to see a longer blend time in the plant, so this is probably acceptable. Both Reynolds numbers are in the turbulent regime and the fluids are the same, so this looks like a feasible design. One remaining problem is that we have moved from an axial impeller to a radial impeller, so the circulation patterns will change dramatically. It will be much cheaper to test the effect of this change in a scaled-down geometry than on the full plant scale! To complete the problem, we need

to check the torque for the RT design versus the current operating conditions and make sure that the equipment can support the increased load.

2-3.3.1 Summary of Scaling Arguments

- In applying Corrsin's theory to real problems, we find that L_s^2/ε, however it is estimated, must be constant on scale-up. For a pipe, this requires scaling with r_o/u; for a tank where geometric similarity is preserved, it requires scaling with $1/N_p^{1/3}N$. (Example 2-4a)
- Scale-up with exact geometric similarity (or scale-down) requires very little empirical information. (Example 2-4b)
- Changing geometry on scale-up is a very complex undertaking that should be avoided wherever possible. (Example 2-4c)
- The crux of any problem is to determine the critical length scales and then to scale them correctly. (Example 2-4)

2-4 DYNAMICS AND AVERAGES: REDUCING THE DIMENSIONALITY OF THE PROBLEM

In turbulent flow, mixing is to a large extent controlled by the turbulence. Consequently, an understanding of turbulence per se is necessary before we can analyze transport phenomena. Recalling our phenomenological description from Section 2-3.1, turbulence is three dimensional, dynamic, and multiscaled, even in its most ideal form. In a stirred tank, the picture is further complicated by

- Chaotic macroinstabilities on the scale of the tank turnover time
- Anisotropic, coherent trailing vortices on the scale of the blade width
- The potential lack of fully turbulent flow (failure of Reynolds number scaling) in regions distant from the impeller
- The presence of internals and either gas or solid phases in the tank, which further complicate the generation and dissipation of turbulence

These additional variables make the stirred tank extremely versatile, but also make generalizations both difficult and dangerous. In this section we discuss various ways of simplifying our descriptions of the flow and the turbulence and illustrate where these simplifications have been applied successfully.

Example 2-5: Solids Suspension versus Uniform Distribution. It is sometimes difficult to sort out exactly how each of the various length and time scales can dominate a process. To investigate this idea, consider solids suspension versus solids distribution in a tank. In the first case, our main interest is in making sure that all the solids are suspended. This is the constraint, for example, in solids dissolution, or leaching. In the second case it is important to have uniform solids distribution throughout the tank. This would be the constraint for a slurry catalyst or for continuous operation with slurry withdrawal at one point in the tank.

Consider the results for off-bottom solids suspension first. In 1958, Zwietering developed a correlation for the just suspended speed (N_{js}) of solids in a stirred tank. Despite numerous attempts to improve on the correlation, the result remains substantially unchanged. In 1978, Baldi et al. redeveloped the equation starting from an analysis of the fluctuating velocities in the boundary layer at the bottom of the tank. They argued that only the turbulent fluctuations can lift the solids off the bottom so that they can be convected into the main flow. The close agreement between their equation and Zweitering indicates that *the governing mechanism for off-bottom suspension is the scaling of turbulent fluctuations in the boundary layer at the bottom of the tank.*

A related problem is that of *uniform solids distribution* in the tank. Even when the N_{js} criterion is met, solids are often not uniformly distributed throughout the tank. The vertical distribution of solids is still not well understood. In some cases, a sharp, stable interface forms above which there are few solids. The slip velocity between the particles and the fluid will certainly play a role in solids distribution, as will the upward velocity at the tank wall. To resolve this problem, a better understanding of the *vertical flow and macroinstabilities at the wall* is needed.

A third case is the rate of solids dissolution: once the solids are fully suspended ($N > N_{js}$), the rate of dissolution does not change significantly even if N is increased. Why? The mass transfer at the surface of the particle is determined by the boundary layer on the particle. The relative velocity between the particle and the fluid is the slip velocity, and this is not strongly affected by the fluid velocity. Once the particles are suspended, the slip velocity is approximately constant and no significant further gains can be made. *The governing mechanism for solids dissolution is the slip velocity between the particle and the fluid.*

These three cases illustrate the importance of considering the correct governing mechanism when trying to determine the most useful simplification of the flow.

2-4.1 Time Averaging of the Flow Field: The Eulerian Approach

Before the advent of fast computers, the time-averaged approach to the flow field was the only reasonable way to approach turbulent flows. In this approach, data taken at a single point are averaged over a sampling time long enough to provide a repeatable mean and RMS result. The only information available about transient behavior is the statistics of the signal (rms velocity) and the frequency spectrum. As long as the time scale of the process is longer than the time scale of the averaging, this approach is likely to be successful. In some other limiting cases (see Example 2-2b) the kinetics of the process are so fast that the mean mixing rate is the governing rate, and once again progress can be made.

For a basic analysis of the problem, we can use the Reynolds equations, which are the time-averaged form of the Navier–Stokes equations (see Section 2-5 and Chapter 5). The major problem is to simplify the equations and obtain additional relations between the unknowns. One idea to provide simplification is to assume that turbulent fluctuations are random in nature and can therefore be treated by

means of statistics. Thus we approach the problem from a rigorous statistical theory into which we can introduce certain simplifying assumptions that will allow us to reduce the equations and solve for some of the variables of interest. The most important of these assumptions are defined and discussed in this section. The models of turbulence that result are discussed in Section 2-5.

2-4.2 Useful Approximations

A necessary objective in turbulence analysis is to define a limited number of simplifying assumptions that will simplify the problem while introducing only small errors in the solution. Any assumption is permissible as long as the limitations of the assumption are understood and taken into account. Let us begin by assuming that eddies range continuously in size from the very smallest to the largest, which are typically the same scale as the equipment. In the most ideal case, the boundaries influence only the large eddies and transfer energy to or from them. The larger eddies transfer their energy to the smaller eddies, and so on, until the energy is transferred to the smallest of eddies. These smallest eddies lose their energy by viscous dissipation. The five most useful assumptions required to build and work with this model are:

1. *Fully turbulent flow*. At very high Reynolds numbers, the inertial forces due to fluctuating velocities overwhelm the viscous forces, so the flow field becomes independent of fluid viscosity. Mean velocity profiles scale with a characteristic velocity and length scale, and drag coefficients (e.g., the power number) become independent of Reynolds number.
2. *Homogeneous turbulence*. The turbulence is completely random and is independent of position (i.e., RMS of u, v, w are constant over the field). The three fluctuating components u, v, and w are not necessarily equal.
3. *Full isotropy*. The fluctuations have no directional preference at any scale of motion. No gradients exist in the mean velocity.
4. *Local isotropy*. This assumption can be applied over a limited range of frequencies or eddy sizes (not a limited volume of space). Over this restricted range of eddy sizes, isotropy prevails. Eddies outside this range can be highly anisotropic, and mean velocity gradients are permitted.
5. *Turbulent shear flow*. This flow is a modification of completely homogeneous flow to allow for shear stresses and for well-defined mean velocity gradients, such as those found in a jet, a mixing layer, or a boundary layer. Usually, one or two of the Reynolds shearing stresses (Section 2-5) are zero.

The term *homogeneous turbulence* implies that the statistical characteristics of the turbulent velocity fluctuations are independent of position. We can further restrict the homogeneous system by assuming that the velocity fluctuations are independent of the axis of reference (i.e., invariant to axis rotation and reflection).

This is equivalent to saying that there is no directional preference in the fluctuating field. This restriction leads to *isotropic turbulence*, which by its definition is always homogeneous. To illustrate the difference between the two types of turbulence, consider the RMS velocity fluctuations. In homogeneous turbulence, the three components of the RMS velocity can all be different, but each value must be constant over the entire turbulent field. In isotropic turbulence, spherical symmetry requires that the fluctuations be independent of the direction of reference, or that all the RMS values be equal. A bowl of peanuts or pretzels is isotropic in a two dimensional sense: It is the same no matter how you look at it or where you place the reference axis. The same is true (in three dimensions) for isotropic turbulence. The branches and leaves on a tree, on the other hand, have a specific arrangement, so moving the axis changes the image. The tree is highly anisotropic.

True *isotropic homogeneous flow* requires that there be no directional preference in the three dimensional flow. There can be no mean velocity gradients, thus no shearing stresses. All three normal stresses must be equal, and all nonnormal stresses ($\overline{uv}$, $\overline{vw}$) must be equal to zero. If the flow has no directional preference and no coherent organized structures, there can be no correlation between components of the fluctuating velocity. The normal components ($\overline{uu}$, $\overline{vv}$, $\overline{ww}$), on the other hand, will always be positive because they are squared terms. Experimentally, such a flow can be obtained approximately in the turbulence developed behind a properly designed grid. This restriction excludes consideration of the trailing vortices in mixing vessels, which have a clearly defined orientation; it also excludes flow anywhere in the tank where velocity gradients exist. There is no possibility of seeing truly isotropic turbulence in a stirred tank.

While the fully isotropic assumption is not a good match to physical reality, the implications of isotropy are profound for turbulence modeling and measurements. Isotropy allows the entire turbulent spectrum to be defined from one component of fluctuating velocity, because the flow is perfectly without directional preference. It allows simplification of the equations to include only the normal stresses. It also allows one to make spectral arguments to simplify the measurement of the dissipation. This assumption is so powerful that it is often invoked *in the hope that it will be good enough for a first approximation*, despite the fact that it is a poor match for the full physical reality.

The area of turbulent study that holds the greatest interest for engineers is *turbulent shear flow*. This flow is a modification of completely homogeneous flow to allow for shear stresses and mean velocity gradients. Usually, one or two of the Reynolds shearing stresses are zero. Turbulent shear flow in turn may be divided into flows that are *nearly homogeneous* in the direction of flow and those that are *inhomogeneous* in the direction of flow. It has been found experimentally that the nearly homogeneous flows are those that are bounded, as in pipe flow, while the inhomogeneous shear flows are unrestricted systems, such as jets. Longitudinal homogeneity (or homogeneity in the direction of flow), arises from the fact that in pipe flow, turbulence is generated along the wall and there is no decay. Longitudinal decay arises from the dispersion of momentum and

the decay of streamwise velocity, as is observed in jets. One flow of importance that has characteristics of both confined and free shear flows, depending on the location of study, is boundary layer flow. The area near the wall is nearly homogeneous in the direction of flow, and that near the bulk of the fluid is inhomogeneous and spreads as the boundary layer grows. Turbulent shear flow cannot be fully isotropic, but it may be locally isotropic.

Many misunderstandings have arisen due to a lack of care in distinguishing the *locally isotropic* assumption from the *isotropic* or fully isotropic assumption. The restriction of *local isotropy* can be applied over a limited range of frequencies or eddy sizes (not a limited volume of space). The conditions for local isotropy state that if the local Reynolds number (based on the turbulent length scale and the fluctuating velocity, not on the equipment length scale D and the mean velocity) is high enough, there may be a range of eddy sizes over which the turbulence energy cascade is in equilibrium. Under these conditions, energy enters at the top of the locally isotropic range of eddy sizes and is dissipated at the smallest locally isotropic scales of motion with no losses of energy at the intermediate scales. Over this range of eddy sizes, no memory of the oriented large scale motions (i.e., the trailing vortices) remains, and there is no directional preference in the flow. This condition extends up the cascade to some large eddy size l. Below this limiting length scale, the flow can be treated as locally isotropic. Eddies larger than l may still be highly anisotropic. It should be understood that any conclusions that are valid for locally isotropic turbulence, are also valid for fully isotropic turbulence over the same range of wavenumbers.

This discussion of the basic simplifying assumptions used to describe different types of turbulence prepares the way for a better understanding and further interpretation of turbulence in mixing vessels. The next example involves applications of the five simplifying assumptions.

Example 2-6: Applications of the Simplifying Assumptions

(a) *Homogeneous turbulence.* Is $\varepsilon = P/\rho V_{tank}$? In the early days of mixing research, there were very few data on the flow field, and some initial scaling variables were needed. Based on the first law of thermodynamics, the energy put into the tank can only be dissipated, since there is no energy out. Taking the power input at the shaft and dividing it by the mass of fluid in the tank ($P/\rho V_{tank}$) returns the same units as the rate of dissipation of turbulent kinetic energy per unit mass. It is not a big leap to abbreviate $P/\rho V_{tank}$ to ε, but is this physically meaningful? Is it a useful representation of the turbulence?

When the jump is made from $P/\rho V_{tank}$ to ε, an assumption that the turbulence is *homogeneous* is implied. This assumption is clearly a poor one in a stirred tank, where the levels of turbulence can vary by a factor of 100 from the impeller to the bulk. Generation and dissipation are vastly different between the impeller region and the regions away from the impeller. For shear-sensitive materials such as cells, their survival depends more on the maximum shear they see than on the average. In such cases, using $P/\rho V_{tank}$ as some kind of an average dissipation is

about as informative as saying that the average velocity in the tank is zero. So why does $P/\rho V_{tank}$ work so well as a correlating variable?

The success of $P/\rho V_{tank}$ is actually restricted to cases where *exact geometric similarity* is maintained. If this restriction is satisfied, $P/\rho V_{tank}$ *is really a scaling basis, not an average dissipation*. The local dissipation roughly scales with $N_p N^3 D^2$, or the power per impeller swept volume, which differs by a factor of $(D/T)^3$ from $P/\rho V_{tank}$. If D/T is constant, the two approaches are equivalent. There are many other good reasons for maintaining geometric similarity on scale-down, so this is not a bad restriction to keep—we just have to be careful of the basis for the argument.

Where the objective is to uncover the governing physics in the problem, the effects of the local dissipation must be separated from the effects of other variables. To accomplish this, geometric similarity will often not be maintained, and the best available scaling for the local dissipation is $N_p N^3 D^2$, or the power input per unit of *impeller* swept volume.

(b) *Fully turbulent flow*. Scaling variables work when the flow is *fully turbulent* and exact geometric similarity is maintained. When these two conditions are true, the effect of fluid viscosity is negligible. The flow field can be made dimensionless using a characteristic length scale and a characteristic velocity scale. Once fully developed turbulence is satisfied, dimensionless velocities scale exactly with the characteristic velocity. In a stirred tank, this velocity is the tip speed of the impeller. Figure 2-16*a* shows the radial velocity profile in the discharge stream of a Rushton turbine, scaled with the tip speed of the impeller. The velocity profile is measured at three different rotational speeds and in three different fluids. All of the data collapse onto one line. In Figure 2-16*b*, the local dissipation, ε, below an Lightnin A310 impeller is scaled in the same way. Note that the last place to attain this scaling in the impeller discharge is the velocity peak at the tip of the impeller blades.

In Figure 6-14 the power number is constant and independent of Re for $Re > 2 \times 10^4$. Similarly, the blend time scales exactly with N above the fully turbulent Re (see Chapter 9). Viscosity no longer has any effect on the velocity field or on the power draw. These dramatic simplifications are true only where the flow is fully turbulent. *Fully turbulent* does *not* mean that the turbulence will be fully homogeneous and the same everywhere. Processes that depend on local conditions, such as cell survival and apparent chemical kinetics, will be affected by the local variations that exist in mixing systems. Average quantities will work only if they reflect the distribution of the quantity as well as the average quantity (i.e., an average tank dissipation may be a valid parameter if when the average is doubled, the maximum is also doubled). For this reason, maintaining exact geometric similarity on scale-down is often critical.

(c) *Local isotropy*. Consider pipe flow at some relatively high Reynolds number. Throughout the pipe, the viscous forces along the wall provide the conditions necessary for turbulence formation. Rotation, very large vortices, or large eddies arise from the interaction of the mean flow with the boundary. In a mixing vessel,

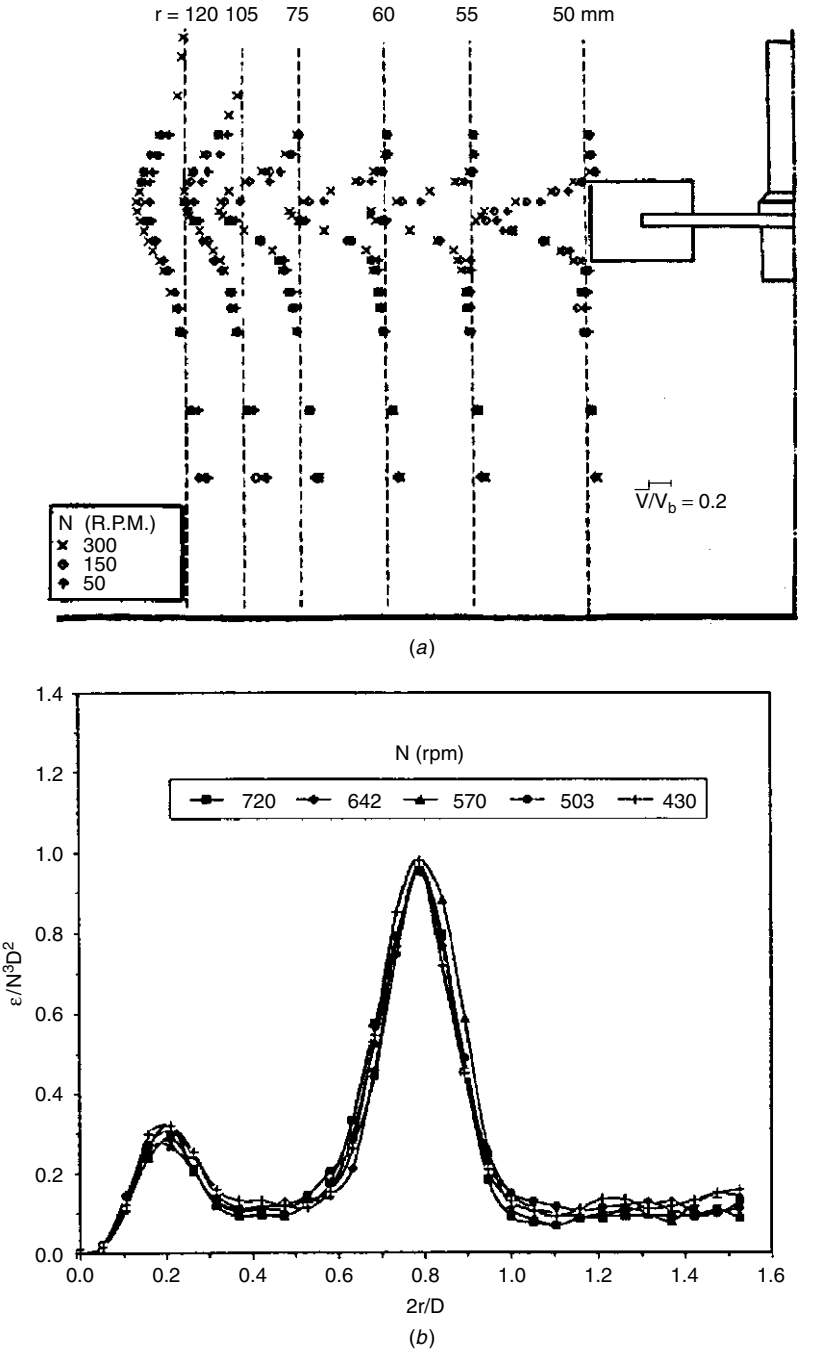

Figure 2-16 Scaling of flow characteristics. (*a*) Scaling of velocity profiles with tip speed in fully turbulent flow. (From Nouri et al., 1987.) (*b*) Scaling of dissipation with N^3D^2 for the Lightnin A310 impeller, D = 0.475T. (From Zhou and Kresta, 1996b.)

the equivalent viscous forces and large eddies are generated at the impeller and baffles. The scale of these large eddies would be comparable to the pipe diameter, the impeller diameter, or the tank diameter. In the earlier section on locally isotropic turbulence, a model was proposed involving a cascade of energy from large to progressively smaller eddies. Now consider that the walls affect the largest fluid structures most strongly and lose their effect as the process moves down the chain. At very high wavenumbers or small eddy sizes, the effect of the boundaries is lost completely or is negligible. The small eddies are considered independent of the boundaries or mean flow. Even though the system may be inhomogeneous on the large scale, it may well be locally isotropic on the small scale, and thus an equilibrium range and inertial subrange might still be found. *Over this range*, and at the same local Re, the characteristics of the turbulence in the pipe and the turbulence in the stirred tank should be indistinguishable.

Several indicators are used to assess whether the assumption of local isotropy may be applied: the first is a high local Reynolds number, the second is a $-\frac{5}{3}$ slope in the frequency spectrum of the velocity signal, as tested in Figure 2-12, and the third is equality of the three RMS components of velocity. The final rigorous test of local isotropy is to transform the one dimensional energy spectrum measured for one component of velocity (xx) to another direction (yy or zz), and compare the results with the spectrum measured in that (yy or zz) direction. Michelet (1998) performed the first test of this condition for the flow in a stirred tank. Partial results from his work are shown in Figure 2-17. When applied to the flow closer to the impeller, as shown in Figure 2-17*a* and *c*, local isotropy must be considered an engineering approximation over a limited range of frequencies. As the probe is moved out into the discharge stream in Figure 2-17*b* and *d*, however, agreement quickly becomes very good. A similar growth in the extent of the $-\frac{5}{3}$ region was shown by Lee and Yianneskis (1998).

(d) *Turbulent shear flow*. As a first step, a very brief contemporary picture of turbulence in boundary layers and wall regions is provided. The flow can be divided into a wall region, outer region or regions away from walls, and the interactions that occur between the two regions. In wall regions (which would include impellers and baffles), the production of turbulent kinetic energy occurs. There are extensive studies of this for a variety of geometries. Often, there are intermittent periods when the Reynolds stresses are high. This is associated with an ordered sequence of events of *ejections* of low momentum fluid outward from the boundary, *interaction events*, and *sweeps* of high momentum fluid toward the area. For pipe and boundary layer flows, the entire sequence has been called a *burst phenomenon*. The outer region is characterized by the overall flow. For large systems, where boundary layers can form, these are the features that determine the turbulent/nonturbulent interfaces. The highly three dimensional bulges along the interface of boundary layers are vortical motions. Extensive measurements have been made of the turbulence characteristics inside these structures. Studies on jets and on the plane turbulent mixing layer have helped to uncover the basic features of the large scale structures in these flows. Much of the flow in the stirred tank is similar to jets, and there are valuable analogies to be made between this model

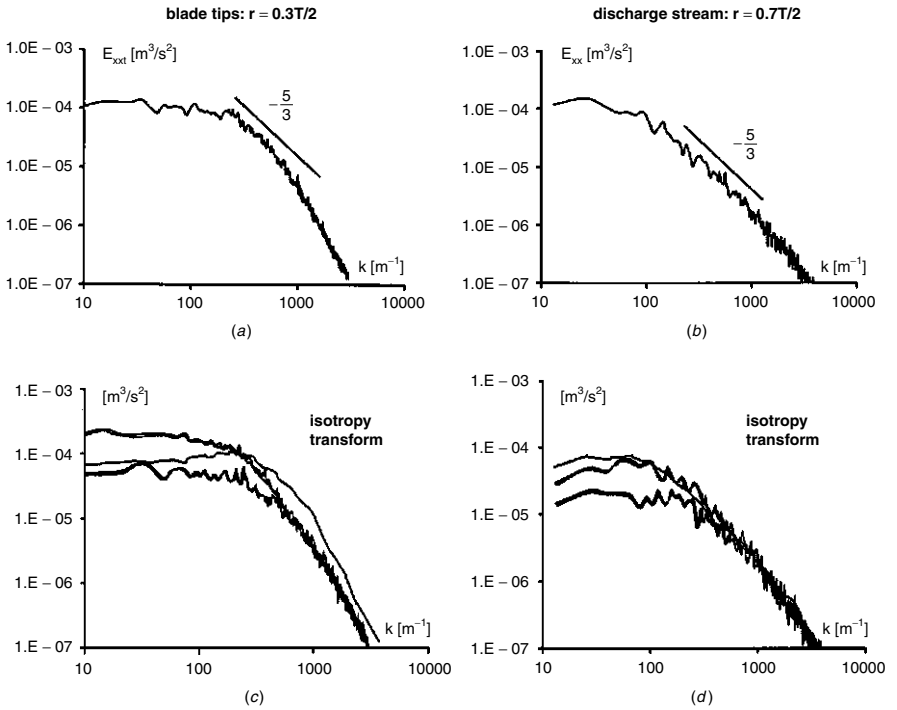

Figure 2-17 Typical wavenumber spectra for a D = T/3 Rushton turbine with the blade passages removed. Parts (*a*) and (*c*) are taken at the tip of the impeller blades (r = 0.3T/2). Figures (*b*) and (*d*) are in the discharge stream (0.7T/2). Parts (*a*) and (*b*) show only one component of the wavenumber spectrum, E_{xx}. Parts (*c*) and (*d*) show the transformation of the xx spectrum (smoother line) onto the measured yy and zz spectra. Local isotropy quickly penetrates to high wavenumbers. (From Michelet, 1998.)

flow and the complicated recirculating flow in the tank (Fort, 1986; Bittorf and Kresta, 2001; Bhattacharya and Kresta, 2002; Kresta et al., 2002), as illustrated in Figure 2-18, and discussed in Section 10-3.2 in Chapter 10.

2-4.3 Tracking of Fluid Particles: The Lagrangian Approach

The Eulerian approach fails when there are significant variations of temperature or concentration in the tank that affect the process kinetics. One example of this is bioreactors, where cells may experience severe oxygen deprivation over large parts of the tank, changing their growth kinetics (Yegneswaran et al., 1991). A second example is crystallization (also discussed in Chapter 17), where the supersaturation varies significantly from the feed zone to the bulk. The local supersaturation determines growth and nucleation rates and thus the final particle size distribution and morphology (Baldyga et al., 1995; Wei and Garside,

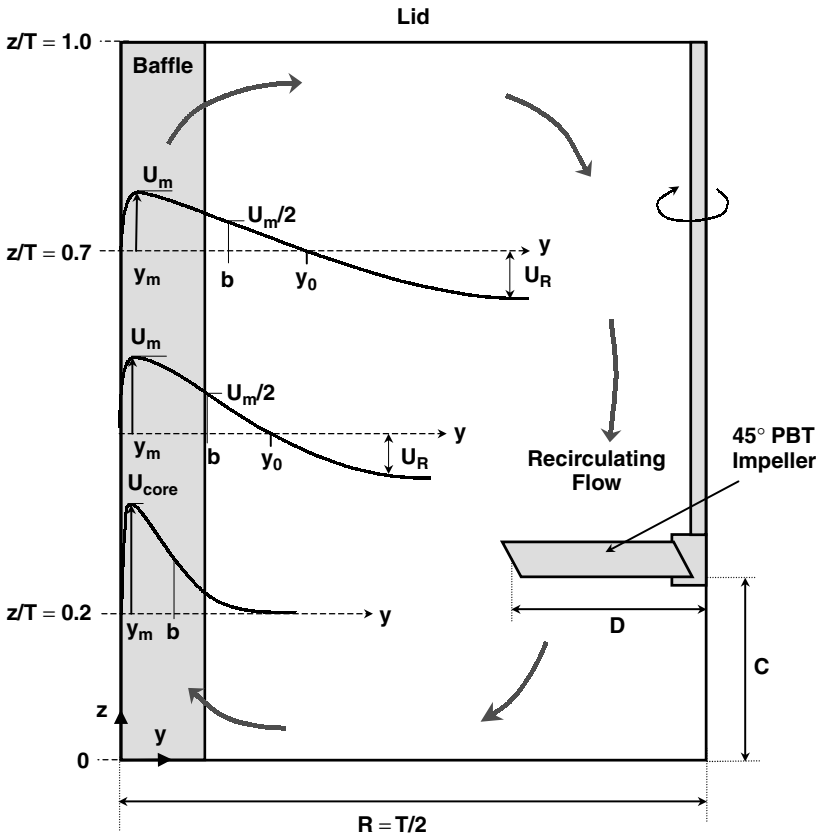

Figure 2-18 Wall jet driven by axial impellers. The velocity profile at the wall scales with U_m.

1997). To model the process results accurately in both these cases, the Lagrangian experience of a fluid particle must be considered.

The Lagrangian approach follows a fluid particle over time as it moves through the flow field. Simulated or experimental particles are injected into the field at an arbitrary time and location. The particles are then tracked as they move under the influence of the velocity field. The injected particles can be neutrally buoyant or given a different density than of the fluid. In their most precise form, computed particle paths should follow experimental full-field time-resolved velocity vector data. Zhao and Brodkey (1998a) have illustrated the importance of using time-resolved data for the opposed jet system. If the process time is long, the mean concentration gradients are large, and/or the transient data are not important, significant progress can be made using a time-averaged velocity field with simple turbulent dispersion models (Bourne and Yu, 1994; Vivaldo-Lima et al., 1998). A third approach is to use circulation time distributions (Yegneswaran, 1991; Roberts et al., 1995) with stochastic modeling to incorporate the effect of

variations in the particle path. Two of the greatest difficulties lie in defining accurate, reliable models of turbulent dispersion at intermediate (anisotropic) scales and in modeling complex higher-order kinetics. Both of these phenomena may well be present in cases where detailed modeling based on Lagrangian particle paths is warranted.

2-4.4 Experimental Measurements

The full resolution of a turbulent mixing problem would require full field measurements of three instantaneous velocity components over time [u(x,y,z,t), v(x,y,z,t), w(x,y,z,t)], plus full field concentration(s) for each component [c(x,y,z,t)]. This five dimensional space is not easily attainable with current methods, and the postprocessing requirements of this quantity of data suggest that some averaging will be required. In Section 2-3.4.1, we consider the various common experimental methods and what dimensions of this problem they measure.

2-4.4.1 Information Contained in Experimental Measurements

- *Pointwise velocity as a function of time* [u(t) or v(t) or w(t)]. *Laser Doppler velocimetry* (LDV) is a single-point time series measurement, typically of one or two velocity components. From these data we can extract mean and RMS velocities, spectral information, and in the case of a two-component instrument, a single Reynolds stress ($u_i u_j$). We cannot obtain much information about the shape of large structures, or macroinstabilities in the flow, because only one spatial location can be measured at a time.
- *Pointwise velocity relative to the impeller blade* [u(θ) or v(θ) or w(θ)]. *Angle- or phase-resolved* LDV is still a single-point measurement but with the addition of a shaft encoder, which records the shaft angle versus time. The velocity versus time data are then sorted by angular position to give the velocity *relative to the impeller blade*. These data can be used to uncover cyclically appearing structures, such as the trailing vortices, and to define angle-resolved values of the RMS velocity and (again if two components are available) a single Reynolds stress. This information suggests that the peak levels of turbulence are rotating with the blades in a very small area behind the blades. Understanding this is important if we are to address the mechanisms of drop breakup and cell destruction vis-a-vis the instantaneous turbulence field.
- *Two components of velocity as a function of time over a full plane of the flow* [u(x,y,t), v(x,y,t)]. Full-plane *particle image velocimetry* (PIV) provides a full plane of velocity data with two components of the velocity at once. The measuring volume is thin in the direction normal to the plane. This is a problem if the component normal to the plane is large because the particles will not stay in the illuminated plane long enough to register a velocity. There are ways around this if the plane can be oriented to match

the direction of the streamwise velocity, but in the highly three dimensional stirred tank, this requires significant insight into the flow. A newer extension of PIV can use two simultaneous views at two angles (stereoscopic imaging) to give the third component of the velocity, but still within a narrow plane.

- *Concentration as a function of time over a full plane of the flow* [c(x,y,t)]. *Laser-induced fluorescence* (LIF) provides a full plane of instantaneous concentration data and can be very valuable where the intermittency of concentration at the visible scales of motion must be understood. It has been applied successfully to several low Reynolds number mixing devices to elucidate mixing structures. Examples are given in Chapter 3. Quantitative analysis of the images can be done by converting light intensity to dye concentration at each pixel of data.
- *Three components of velocity as a function of position in three dimensional space* [u(x,y,z,t), v(x,y,z,t), w(x,y,z,t)]. *Particle tracking velocimetry* (PTV) tracks the image of several (up to 1000 (Guezennec et al., 1994; Zhao and Brodkey, 1998b)) particles in a three dimensional volume over time, giving the location of the particles over time. From the position records, three components of velocity can be extracted for each particle at each time step. If data are taken for a long enough time, the full time-averaged three dimensional velocity field can be extracted with all six Reynolds stresses. The time that is "long enough" can be very long if small numbers of particles are used, because at one instant in time only 2 views in the tank are measured, even though the full volume is recorded in the image. The success of PTV requires extensive image analysis, efficient tracking algorithms, and stereomatching techniques. The spatial resolution of this method is still low compared to PIV methods.
- *Three components of velocity as a function of position in three dimensional space* [u(x,y,z), v(x,y,z), w(x,y,z)]. *Scanning* PIV is a three dimensional extension of planar PIV at a higher spatial resolution than is possible with PTV. Time resolution in this method is more difficult than that for PIV, because a finite time is needed to scan the tank before the light sheet returns to the initial position. At least four of the six Reynolds stresses can be resolved with this approach. Another approach to this measurement is holographic PIV. None of these methods are commercially available at the time of writing.

2-5 MODELING THE TURBULENT TRANSPORT

Modeling can prove to be far less costly to use in the long run than actual mixing experiments, and may provide much more detailed information than is available from experiments, so there is a large incentive to develop reliable models of mixing processes. If the computed results do not adequately model the real physical system, they will not be of much use, so any useful model must be quantitatively validated.

A key part of any mixing process model will be the turbulence model, and an entire range of turbulence models has been developed in an effort to address this problem (Table 2-5). In these models there is a clear trade-off between complexity and representation of the underlying physics. The various theoretical approaches can be formulated in wavenumber space or physical space; can use long time averages, averages over specific structures, or no averages at all; and will usually involve some closure approximation based on statistical reasoning,

Table 2-5 Summary of Approaches to Turbulence Modeling[a]

Model	Physical Basis of the Model	Drawbacks
Boussinesq approximation • One equation with one adjustable parameter • Averaged over time and all length scales	• One length scale • Based on analogy to laminar transport and apparent viscosity	• Oversimplification of the physics • The apparent viscosity is a function of the flow field and of position
Prandtl mixing length • One equation with two adjustable parameters • Averaged over time and all length scales	• One length scale • Based on analogy to mean free path in the kinetic theory of gases	• Oversimplification of the physics • The assumption of a linear velocity profile does not match physical reality; however, the results are surprisingly good for the log-law region of a pipe
Two-equation models (taking the k−ε model as an example) • Two partial differential equations with five model constants • Averaged over time, with models for two locally varying turbulent quantities (k and ε)	• Assumes that the three normal stresses are equal and that all cross-correlated stresses are zero (cross stresses may be estimated after the fact) • Based on turbulent kinetic energy balance (k-equation) and a model for the rate of dissipation of turbulent kinetic energy (ε-equation) • Variations have been developed to model subclasses of flows	• Five model constants have been determined for simplified flows • Two-equation models cannot accurately model the effects of anisotropy on the large scale, although the form of the model may be useful for the locally isotropic range of turbulence • k−ε model tends to be overly diffusive

(*continued overleaf*)

Table 2-5 (*continued*)

Model	Physical Basis of the Model	Drawbacks
Full Reynolds stress models (ASM, RSM, or DSM) • Model all six Reynolds stresses • Averaged over time	• Treat anisotropy in the flow by modeling all six Reynolds stresses in their time-averaged form	• Computationally difficult • Subject to problems with convergence • Grid independence is difficult to attain
Large eddy simulations (LES) • Model large scales and small scales separately • Average small scales over time • Allow transient (direct) simulation of large scales	• Model the larger, anisotropic scales of turbulence using a DNS approach, following their motion directly as it varies in time • Treat the subgrid scales of turbulence as isotropic and in equilibrium: model these scales using a two-equation model of turbulence	• Requirements for data storage and data processing are outside the range of most users • No consensus has emerged on subgrid modeling requirements • Boundary conditions at solid surfaces are problematic
Direct numerical simulations (DNS) • Solve the full time varying Navier–Stokes equations for the three dimensional field of fluctuating velocities • No averaging required	• Using only the instantaneous form of the Navier–Stokes equations, solve the flow field at each instant in time, storing full three dimensional records of the fluctuating velocity • Sometimes called a "numerical experiment"	• Computationally intensive • Huge storage requirements; restricted to low Re • Commercial versions are unlikely

[a]Every time a new problem is attempted, model results must be validated. The level of complexity required in the model depends heavily on the level of accuracy and detail required in the results.

dimensional analysis, experimental evidence, or simplified conceptual modeling. Many facets of the physics need to be addressed to accurately represent any process of industrial importance. First, accurate models of the physics based on fundamental understanding are needed, and second, the inherent dynamics of turbulence, mixing, and reaction must be addressed.

2-5.1 Time-Resolved Simulations: The Full Solution

Since turbulence is by definition a time-varying phenomenon, the best hope for full resolution of the physics is in transient, or time-resolved, simulations. Both

direct numerical simulation (DNS) and large eddy simulations (LES) use the governing equations directly without time averaging. These equations are the Navier–Stokes equations, the continuity equation, the individual species balance equations, and the energy balance equations. In such an approach there are as many equations as unknowns, so the problem is deterministic and the equations are, in principle, closed. However, the partial differential equations are nonlinear, higher order, and coupled. Problems in numerical resolution can be extreme, especially when DNS calculations are used.

The problem is complicated by the large range of length scales which are relevant to the process results and by the highly three dimensional nature of the stirred tank flow field, so simulation results that are grid- and time step–independent can be extremely difficult to attain. At the time of writing, time-resolved simulations are still in the province of the expert user. Despite this, a good deal of insight into modeling issues can be gained from a brief explanation of this approach to turbulence modeling.

2-5.1.1 Direct Numerical Simulation. The Navier–Stokes equations describe a momentum balance on a differential control volume at any instant in time. They are exactly correct, at any instant in time, so in principle all that is needed to solve turbulent flow is a transient solution of the Navier–Stokes equations with appropriate initial and boundary conditions. This is the approach used in DNS.

In a high Reynolds number turbulent flow, the changes with time can be very rapid, and the range of scales is extreme. In Example 2-1c, the smallest eddy was taken as 0.1 mm in a system that could be as large as 30 cm overall. The range of length scales in this simple geometry is 1 : 3000. A full computational domain would be $3000^3 = 2.7 \times 10^{10}$ cells big, a number that is far too large for present computers. The task is even more impressive when one realizes that the simulation must be transient with adequate resolution in time. It takes a very large computer indeed to do such modeling, even at low turbulent Reynolds numbers. Present computations can only be applied to low Reynolds numbers in somewhat simple geometries. Despite the lack of ability to do extremely detailed space and time resolution calculations, calculations in more modest grid structures (still fine when compared to LES) can be of use. In particular, when the geometry is complex and local conditions (as discussed earlier) are not as critical, such calculations could be very helpful in design.

In an ideal world, one could use DNS to reproduce the experimental flow field that controls mixing, then obtain measures of the individual terms in the Navier–Stokes equations on scales down to a small multiple of the grid size. These terms determine the coupling between mixing (and of course kinetics and heat transfer) with the instantaneous flow field. The results of these detailed, fully coupled calculations could then be used to test and develop models for subgrid scales in LES, and for other computational fluid dynamics (CFD) calculations where average forms of the equations are used.

2-5.1.2 Large Eddy Simulation. The second approach is to use large eddy simulations. The limitations of this method are much less severe. The large scale motions are computed in a manner similar to DNS but on a much coarser grid. The scale might be as coarse as 1 : 30. The computational domain would then be $30^3 = 2.7 \times 10^4$, which would not be difficult with current machines. A grid several times as fine as this would not be out of the question, and initial LES simulations in stirred tanks have recently been reported (Bakker et al., 1998; Revstedt et al., 1998; Derksen and van den Akker, 1999; Roussinova et al., 2001).

This modeling approach computes the larger scales of turbulence directly as they vary in time and models the finer scales of turbulence. The LES modeling technique has few assumptions, all of which can be modified to provide a match between the experimental statistical measures and the more detailed large scale results. The advantage of LES is that it is far less computationally demanding than DNS, so that the computations can be pushed to higher Reynolds number flows. The problem is to decide which, if any, of the subgrid models and filtering techniques are adequate to represent the data. As in the DNS effort, one cannot expect to match the data on an instantaneous basis, since any instantaneous velocity record is expected to be unique; however, by tracking the statistics that are important to the mixing process, the critical information can (in principle) be extracted. Initial results are promising, showing excellent agreement between experiment and simulation for the trailing vortices associated with a Rushton turbine (Derksen and van den Akker, 1999) and macroinstabilities associated with a pitched blade impeller in its resonant geometry ($D = T/2$, $C/D = 0.5$, $f = 0.186/N$; Roussinova et al., 2001).

Example 2-7: Physical Implications of Large Scale Effects. Which eddies are large eddies for mixing processes? Are the additional resources required to resolve this level of detail, and to process detailed transient results, warranted? Bakker et al. (1996) did a comparative study between PIV and time-averaged CFD for the pitched blade impeller. While they were able to show good agreement between the time-averaged flow fields, as shown in Figure 2-19*a* and *b*, the instantaneous PIV results in Figure 2-19*c* show that the overall flow field does not resemble the time-averaged result. Roussinova et al. (2003) showed that there is a single dominant low frequency in the resonant geometry. Figure 2-19*d* shows the scaling of the macroinstability frequency for the resonant tank geometry (PBT, $D = T/2$, $C = T/4$, $St = f_{MI}/N = 0.186$). When the off-bottom clearance is changed, the frequency persists, but other frequencies may also appear. These macroinstabilities can induce strong vibrations of the tank and in some cases can cause breakage of vessel internals such as baffles, coupling bolts, and impeller shafts. Recent LES animation results from Roussinova et al. (2003), included on the Visual Mixing CD show the full complexity of this large scale variation. If the desired process result responds on a longer time scale than the scale of the time averaging (on the order of 10 s), as would be the case for a slow reaction or for bulk blending, the additional details are averaged into the result. If, however, the time scale of the process is shorter than the lifetime of these large eddies

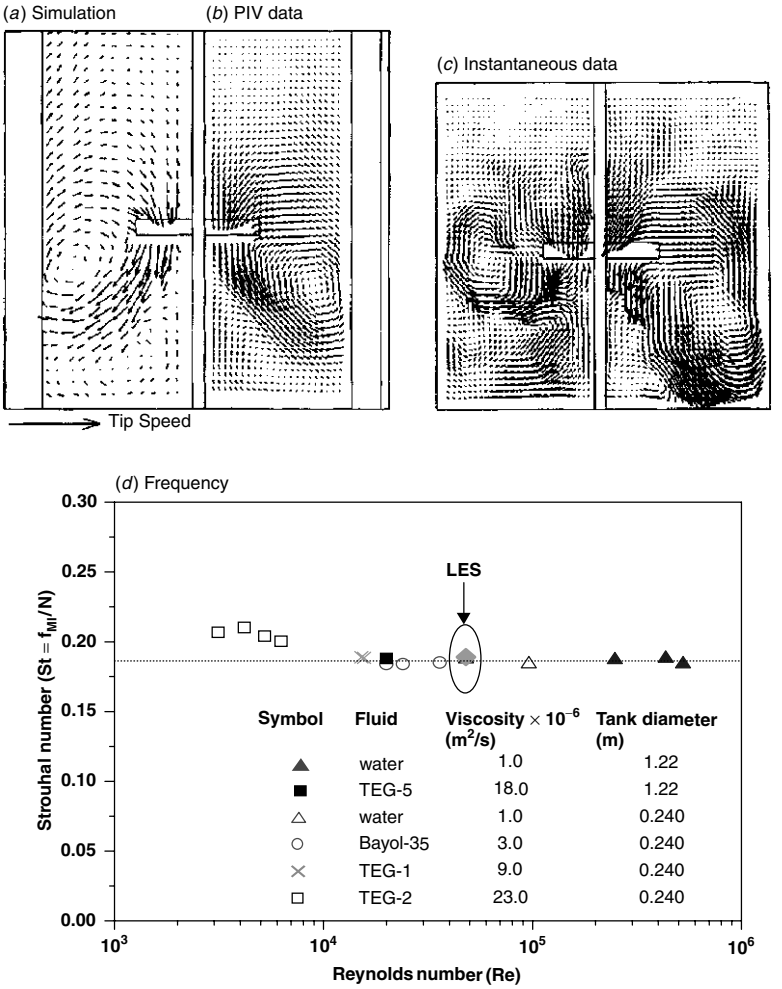

Figure 2-19 Comparison of (*a*) time-averaged simulation with (*b*) time-averaged PIV data and (*c*) instantaneous PIV data. (From Bakker et al., 1996.) (*d*) Scaling of the frequency of the macroinstability for the resonant geometry (PBT impeller: $D = T/2$, $C/D = 0.5$, four baffles, $f_{MI} = 0.186N$; Roussinova et al., 2003). The Strouhal number $St = f_{MI}/N = 0.186$. An animation of the macroinstability is included on the Visual Mixing CD affixed to the back cover of the book.

but longer than the smallest scales of turbulence (e.g., intermediate reaction rates with higher-order kinetics), the process result may be affected by the mesoscales and it will be necessary to characterize these scales in order to make progress. Feed stream jet intermittency, a good example of how mesomixing is affected by large scale flow instabilities, is discussed further by Jo et al. (1994), Baldyga et al. (1997), and Houcine et al. (1999).

The next smallest scale of motion is the trailing vortices, shown in Figure 2-12 and animated on the Visual Mixing CD affixed to the back cover of the book. These are well predicted by explicit impeller modeling, sliding mesh, and DNS methods (Derksen and van den Akker, 1999). These coherent structures have stimulated ongoing debate about allowable ways to model turbulence in stirred tanks and have motivated many of the efforts to push this field forward. While the long time scales involved in the transient breakup of liquid–liquid dispersions point to the importance of these vortices and their presence certainly affects the analysis of turbulence for the Rushton turbine, their physical implications for other process results remain largely unexplored. For impellers other than the Rushton turbine, these vortices are much weaker, or even nonexistent (Roussinova et al., 2000).

The smallest intermediate scales that there is strong motivation to examine with LES (or DNS) are the larger inertial or mesomixing scales. These feed into the probability density functions used extensively by Fox (1998) to model the interactions between turbulence and chemical reactions.

2-5.2 Reynolds Averaged Navier–Stokes Equations: An Engineering Approximation

To reduce the modeling problem to a single steady solution, Reynolds formulated time-averaging rules. Application of these rules yields a time-averaged form of the Navier–Stokes and other equations, known as the Reynolds averaged, or RANS, equations. These equations now relate time-averaged quantities, not instantaneous time-dependent values. For this simplification, we pay a dear price in that there are now more unknowns than equations.

The additional unknowns are the six Reynolds stresses, which are the normal or mean-squared values (autocorrelations) and cross-correlations of the three components of fluctuating velocity:

$$\text{Reynolds stresses} = \rho \begin{bmatrix} \overline{uu} & \overline{uv} & \overline{uw} \\ \overline{vu} & \overline{vv} & \overline{vw} \\ \overline{wu} & \overline{wv} & \overline{ww} \end{bmatrix} \tag{2-21}$$

The terms on the diagonal are the normal stresses or variances, and these squared terms will always be positive. In an idealized flow with no directional preferences, they will all be equal. The off-diagonal elements are symmetric ($\overline{uv} = \overline{vu}$), so only three of them are unique. If the turbulence has no directional preference and there are no velocity gradients in the flow, the individual fluctuations will be completely random and the covariances will be equal to zero. This assumption of "no directional preference" or "isotropic turbulence" is an important concept for understanding the different classes of time-averaged turbulence models.[22] With these two conditions, the six unknowns can be reduced to a single unknown:

$$k = \tfrac{1}{2}(\overline{uu} + \overline{vv} + \overline{ww}) \tag{2-22}$$

[22] See a more complete discussion of isotropy in Section 2-4.3.

It turns out that this degree of simplification is too severe, and some way of treating the cross-correlations must also be considered. Although complete texts (Pope, 2000), and regular review articles (see, e.g., Launder, 1995) are written on the subject of turbulence modeling, the reader will benefit from understanding two important subsets of models. The simplest approach makes an initial assumption that the Reynolds stresses can be modelled using k and its rate of dissipation: these are the two-equation isotropic models, including the k−ε model. A more general, but more complex approach models each of the Reynolds stresses separately, allowing the development of anisotropy, or orientation of eddies, in the flow.

2-5.2.1 Two-Equation Models of Turbulence. On application of Reynolds time averaging, six new unknowns (the Reynolds stresses) appear in the momentum equations. There are now more unknowns than equations, so the system of equations is no longer closed. This is the closure problem of turbulence. Physical flow models for the Reynolds stresses are needed to close the equations. Many logical closure schemes have been proposed and have met with some success for certain classes of flows, but there is no standard, fully validated approach to the modeling of Reynolds stresses.

A stable starting point for the kinds of flows encountered in a stirred tank is the k−ε model. This model assumes that the normal stresses are roughly equal and are adequately represented by k. Two differential equations are used to model the production, distribution, and dissipation of turbulent kinetic energy: the k-equation, and the ε-equation. These equations were developed for free shear flows, and experimentally determined constants are established for the model parameters. One of these constants is used to relate local values of k and ε to an estimate of $(\overline{uv})$ using a modified turbulent viscosity approach:

$$\overline{uv} = \nu_t \frac{\partial \overline{U}}{\partial y} = 0.09 \frac{k^2}{\varepsilon} \frac{\partial \overline{U}}{\partial y} \tag{2-23}$$

Many variations on the k−ε model have been proposed and used, with varying degrees of success. Some of them are designed for the prediction of separation points, others incorporate some degree of anisotropy for cases where the flow is highly swirling (e.g., cyclones), and still others are being developed for application in multiphase flows. When a fully converged simulation using the k−ε equation does not predict the physical phenomena of interest to the desired degree of accuracy, other models should be considered.

One school of thought maintains that if the results do not have the desired degree of accuracy, the model constants should be tuned to improve agreement with experimental data. If the physical basis for the constants is considered carefully, and the adjustments based on an identifiable physical reason, the new constants might have some hope of general usefulness. On the other hand, when model constants are used as fitting parameters, the physical meaning of the turbulence model is reduced and the objective of the simulations (hopefully, one of

validating the models to allow prediction of the flow field under new conditions) should be reassessed.

Example 2-8: Prediction of Gross Circulation Patterns Using CFD. If the main objective of CFD modeling is determination of the mean flow patterns in the tank or of macroscopic quantities such as the power number, RANS simulations can provide good indications of the effects of changes in tank geometry and impeller geometry on the time-averaged results. Agreement for laminar flow is very good (Jaworski et al., 1998; Lamberto et al., 1999), while for fully turbulent flow the reported results vary, with the quality of the results dependent partially on the turbulence model and partially on the details of the grid and computational techniques. In general, one may expect good qualitative prediction of experimental trends where *accurate* experimental boundary conditions are used to model the impeller (Kresta and Wood, 1991; Fokema et al., 1994; Bakker et al., 1996; Coy et al., 1996; Harris et al., 1996; Armenante et al.,1997; Jaworski et al., 1998); where the impeller is simulated directly using multiple reference frames (Harris et al., 1996; Harvey and Rogers, 1996; Ranade and Dommeti, 1996; Ranade, 1997; Bhattacharya and Kresta, 2002); and where a sliding mesh is used to obtain transient solutions (Jaworski et al., 1998; Micale et al., 1999).

Several conditions are needed for accurate RANS simulation of gross circulation patterns:

- There must be fully turbulent flow at the impeller; $\mathrm{Re} > 2 \times 10^4$.
- If impeller boundary conditions are used, they should be obtained for exactly the same geometry as is used in the simulation (Fokema et al., 1994).
- If a sliding mesh simulation is used, 20 or more rotations of the impeller are needed for convergence (Jaworski et al., 1998).
- Even with a good preprocessor, the user must pay careful attention to the layout of the grid. This is the single biggest factor affecting both convergence and accuracy of the results. The bottom line is that more cells are needed where large gradients are expected, usually close to the impeller and close to the baffles. Each impeller modeling method has its own gridding constraints in addition to the computational constraints listed above.

2-5.2.2 Full Reynolds Stress Models. Full Reynolds stress modeling retains all six Reynolds stresses throughout the solution of the balance equations. The equations for these stresses are highly coupled and convergence is difficult. The advantage of this approach is that all of the stresses are available to play a role in the development of the flow field, and the transport of energy between components can develop strong directional preferences and coherent structures. This level of complexity in modeling is essential for very difficult, highly anisotropic flows, such as those found in a cyclone.

2-5.3 Limitations of Current Modeling: Coupling between Velocity, Concentration, Temperature, and Reaction Kinetics

Even with the rapid progress currently underway in the modeling of velocity fields for fully turbulent flow, the real objective remains the process result. The critical physics lies in interactions between equations of motion and scalar transport and the kinetics of reactions, crystal precipitation and growth, and other core processes. These are coupled higher order sets of equations that need to be solved simultaneously in a truly rigorous solution.

The alternative to this full solution is to take detailed velocity field calculations and extract critical information that can be applied over simplified zones. The reacting fluid particle is then tracked as it moves through the time-averaged (Eulerian) flow field. This Eulerian–Lagrangian approach has been followed by several authors (Bourne and Yu, 1994; Wei and Garside, 1997), with impressive results. The reader is referred to the review by Baldyga and Pohorecki (1995) the text by Baldyga and Bourne (1999), and Chapter 13 for more discussion and information about coupling reaction kinetics information to flow characteristics.

2-6 WHAT HAVE WE LEARNED?

- Turbulent blobs and their scalar counterparts are three dimensional, time-varying structures of arbitrary shape. They are represented by the wavenumber spectrum. Various portions of the spectrum, but not the whole spectrum, can be retained on scale-up.
- Models that account for all of the physics of turbulence cannot presently be solved for problems of practical interest. Turbulence models that can be solved do not contain all the physics needed to accurately predict all aspects of the velocity and turbulence fields.
- The effect of turbulence on scalars in the flow (c, T, reaction kinetics) is strong, and is sensitive to the details of the velocity and turbulence fields. Models that have been formulated to solve the combination of velocity and scalar fields have not yet accounted for the multiplicity of interactions between the fields, especially when complex reaction kinetics exist. Steady progress continues in the application of full PDF models to these problems.
- With a good phenomenological understanding of turbulence, many of the gross problems in design and operations can be addressed, despite our incomplete understanding of the physics. As engineers, it is often enough to have a good understanding of the process. Once the crucial issues have been identified, simpler scaling arguments can often provide a satisfactory engineering solution to the problem.

NOMENCLATURE

a	fluctuating concentration of A (mol/L)
A	proportionality constant, 1.0 for isotropic turbulence (−)
b	fluctuating concentration of B (mol/L)
c	concentration fluctuation (mol/L)
C_A	mean concentration of A (mol/L)
C_{B0}	concentration of B at time 0 (mol/L)
C_L	length scale proportionality constant (−)
C_u	velocity scale proportionality constant (−)
d_m	molecular diameter (m)
D	impeller diameter (m)
Da	Damkoehler number (−)
D_{AB}	molecular diffusivity of A in B (m^2/s)
D_p	pipe diameter (m)
D_t	turbulent diffusivity (m^2/s)
E	energy content, or PSD power spectral density
f	frequency (s^{-1})
H	liquid depth (m)
I_s	intensity of segregation (−)
k	turbulent kinetic energy per unit mass (m^2/s^2)
k	wavenumber [$2\pi f/U_c$ in eq. (2-9)] (m^{-1})
k_0	wavenumber corresponding to largest scale of concentration (m^{-1})
k_r	reaction rate constant (units vary)
l_t	smallest turbulent scale (Example 2-1c) (m)
L	length scale (m)
L_c	characteristic length scale (m)
L_s	Corrsin integral length scale (m)
$L_{1/2}$	Mao and Toor mixing length (m)
N	impeller rotational speed (rps)
N_{js}	just suspended speed, solids (rps)
N_p	power number (−)
r	distance in the radial direction (m)
r_0	feed pipe radius (m)
Re	Reynolds number (−)
Sc	Schmidt number, ν/D_{AB} (−)
t	time (s)
t_e	eddy dissipation time scale, k/ε (s)
t_k	Kolmogorov time scale, $(\nu/\varepsilon)^{1/2}$ (s)
t_λ	time scale based on Taylor microscale, $(\lambda^2/\varepsilon)^{1/3}$ (s)
T	tank diameter (m)
u	streamwise fluctuating velocity component (m/s)
u_c	characteristic turbulent velocity scale (m/s)
U	mean velocity in the streamwise direction (m/s)
U_c	convective velocity (m/s)

v	cross-stream fluctuating velocity component (m/s)
V_{TIP}	impeller tip speed, πND (m/s)
V	volume (m^3)
$V_{impeller}$	impeller swept volume (m^3)
V_{tank}	tank volume (m^3)
w	cross-stream fluctuating velocity component (m/s)
x	distance in the x-direction (m)
y	distance in the y-direction (m)
z	distance in the z-direction (m)

Greek Symbols

ε	rate of dissipation of turbulent kinetic energy per unit mass (m^2/s^3)
η	Kolmogorov scale, $(\nu^3/\varepsilon)^{1/4}$ (m)
θ_B	blend time (s)
λ	Taylor microscale of turbulence (m)
λ_B	Batchelor length scale, $(\nu D_{AB}^2/\varepsilon)^{1/4}$ (m)
μ	absolute viscosity (kg/m·s)
ν	kinematic viscosity (m^2/s)
ρ	density (kg/m^3)
τ	mixing time constant (s)
τ_D	dimensionless time for unsteady mass transfer [eq. (2-2)]
τ_{yx}	shear stress on the y-plane in the x-direction (Pa)

REFERENCES

Armenante, P. M., C. Luo, C. Chou, I. Fort, and J. Medek (1997). Velocity profiles in a closed, unbaffled vessel: comparison between experimental LDV data and numerical CFD predictions, *Chem. Eng. Sci.*, **52**, 3483–3492.

Bakker, A., K. J. Myers, R. W. Ward, and C. K. Lee (1996). The laminar and turbulent flow pattern of a pitched blade turbine, *Trans. Inst. Chem. Eng.*, **74A**, 485–491.

Bakker, A., H. Haidari, and E. Marshall (1998). Numerical modeling of mixing processes—What can LES offer? *Paper 238j*, presented at the AIChE Annual Meeting, Miami Beach, FL, Nov. 15–20.

Baldi, G., R. Conti, and E. Alaria (1978). Complete suspension of particles in mechanically agitated vessels, *Chem. Eng. Sci.*, **42**, 2949–2956.

Baldyga, J., and J. R. Bourne (1999). *Turbulent Mixing and Chemical Reactions*, Wiley, Chichester, West Sussex, England.

Baldyga, J., and R. Pohorecki (1995). Turbulent micromixing in chemical reactors: a review, *Chem. Eng. J.*, **58**, 183–195.

Baldyga, J., W. Podgorska, and R. Pohorecki (1995). Mixing-precipitation model with application to double feed semibatch precipitation, *Chem. Eng. Sci.*, **50**, 1281–1300.

Baldyga, J., J. R. Bourne, and S. J. Hearne (1997). Interaction between chemical reactions and mixing on various scales, *Chem. Eng. Sci.*, **52**, 457–466.

Batchelor, G. K. (1959). Small scale variation of convected quantities like temperature in turbulent fluid: Discussion and the case of small conductivity, *J. Fluid Mech.*, **5**, 113–133.

Bhattacharya, S., and S. M. Kresta (2002). CFD simulations of three dimensional wall jets in stirred tanks, *Can. J. Chem. Eng.*, **80**(4), 695–709.

Bittorf, K. J., and S. M. Kresta (2001). Three dimensional wall jets: axial flow in a stirred tank, *AIChE J.*, **47**, 1277–1284.

Bourne, J. R., and S. Yu (1994). Investigation of micromixing in stirred tank reactors using parallel reactions, *Ind. Eng. Chem. Res.*, **33**, 41–55.

Brodkey, R. S. (1967). *The Phenomena of Fluid Motions*, Dover, Mineola, NY.

Brodkey, R. S. (1975). Mixing in turbulent fields, in *Turbulence in Mixing Operations: Theory and Applications to Mixing and Reaction*, R. S. Brodkey, ed., Academic Press, New York, pp. 49–119.

Brodkey, R. S., and H. C. Hershey (1988). *Transport Phenomena: A Unified Approach*, McGraw-Hill, New York.

Brodkey, R. S., and S. M. Kresta (1999). Turbulent mixing and chemical reactions in an ideal tubular reactor, presented at Mixing XVII, Banff, Alberta, Canada, Aug. 20–25.

Corrsin, S. (1957). Simple theory of an idealized turbulent mixer, *AIChE J.*, **3**, 329–330.

Corrsin, S. (1964). The isotropic turbulent mixer: II. Arbitrary Schmidt number, *AIChE J.*, **10**, 870–877.

Coy, D., R. LaRoche, and S. Kresta (1996). Use of sliding mesh simulations to predict circulation patterns in stirred tanks, presented at AIChE Annual Meeting, Chicago, Nov. 10–15.

Derksen, J., and H. E. A. van den Akker (1999). Large eddy simulations of the flow driven by a Rushton turbine, *AIChE J.*, **45**, 209–221.

Escudier, R. (2001). Structure locale de l'hydrodynamique générer par une turbine de Rushton, Ph.D. dissertation, INSA, Toulouse, France.

Fokema, M. D., S. M. Kresta, and P. E. Wood (1994). Importance of using the correct impeller boundary conditions for CFD simulations of stirred tanks, *Can. J. Chem. Eng.*, **72**, 177–183.

Forney, L. J., and N. Nafia (1998). Turbulent jet reactors: mixing time scales, *Trans. Inst. Chem. Eng.*, **76A**, 728–736.

Forney, L. J., and N. Nafia (2000). Eddy contact model: CFD simulations of liquid reactions in nearly homogeneous turbulence, *Chem. Eng. Sci.*, **55**, 6049–6058.

Fort, I. (1986). Flow and turbulence in agitated vessels, Chapter 14 in *Mixing: Theory and Practice*, V. W. Uhl and J. B. Gray, eds., Academic Press, Toronto.

Fox, R. O. (1998). On the relationship between Lagrangian micromixing models and computational fluid dynamics, *Chem. Eng. Process.*, **6**, 521–535.

Grenville, R. K., and J. N. Tilton (1996). A new theory improves the correlation of blend time data from turbulent jet mixed vessels, *Trans. Inst. Chem. Eng.*, **74A**, 390–396.

Grenville, R. K., and J. N. Tilton (1997). Turbulence or flow as a predictor of blend time in turbulent jet mixed vessels, *Recent Prog. Genie Proc., Paris*, **11**, 67–74.

Grenville, R., S. Ruszkowski, and E. Garred (1995). *Blending of miscible liquids in the turbulent and transitional regimes*, presented at Mixing XV, Banff, Alberta, Canada.

Guezennec, Y., R. S. Brodkey, N. Trigui, and J. C. Kent (1994). Algorithms for fully automated three-dimensional particle tracking velocimetry, *Exp. Fluids*, **17**, 209–219.

Gurney, H. P., and J. Lurie (1923). Charts for estimating temperature distributions in heating or cooling solid shapes, *Ind. Eng. Chem.*, **15**, 1170–1172.

Hansen, L., J. E. Guilkey, P. A. McMurtry, and J. C. Klewicki (2000). The use of photoactivatable fluorophores in the study of turbulent pipe mixing: effects of inlet geometry, *Meas. Sci. Tech.*, **11**, 1235–1250.

Harris, C. K., D. Roekaerts, F. J. J. Rosendal, F. G. J. Buitendijk, Ph. Dakopoulos, A. J. N. Vreenegoor, and H. Wang (1996). CFD for chemical reactor engineering, *Chem. Eng. Sci.*, **51**, 1569–1594.

Harvey, A. D., and S. E. Rogers (1996). Steady and unsteady computation of impeller stirred reactors, *AIChE J.*, **42**, 2701–2712.

Heisler, M. P. (1947). Temperature charts for induction and constant temperature; heating, *Trans. ASME*, **69**, 227–236.

Hinze, J. O. (1975). *Turbulence*, 2nd ed., McGraw-Hill, Toronto.

Houcine, I., E. Plasari, R. David, and J. Villermaux (1999). Feedstream jet intermittency phenomenon in a continuous stirred tank reactor, *Chem. Eng. J.*, **72**, 19–30.

Jaworski, Z., M. L. Wyszynski, K. N. Dyster, V. P. Mishra, and A. W. Nienow (1998). A study of an up and a down pumping wide blade hydrofoil impeller: II. CFD analysis, *Can. J. Chem. Eng.*, **76**, 866–876.

Jo, M. C., W. R. Penny, and J. B. Fasano (1994). Backmixing into reactor feedpipes caused by turbulence in an agitated vessel, in *Industrial Mixing Technology: Chemical and Biological Applications*, G. B. Tatterson, ed., AIChE Symp. Ser., **90**, 41–49.

Keeler, R. N., et al. (1965). Mixing and chemical reaction in turbulent flow reactors, *AIChE J.*, **11**, 221–227.

Kresta, S. M. (1998). Turbulence in stirred tanks, anisotropic, approximate, and applied, *Can. J. Chem. Eng.*, **76**, 563–576.

Kresta, S. M., and P. E. Wood (1991). Prediction of the three dimensional turbulent flow in stirred tanks, *AIChE J.*, **37**, 448–460.

Kresta, S. M., K. J. Bittorf, and D. J. Wilson (2002). Internal annular wall jets: radial flow in a stirred tank, *AIChE J.*, **47**, 2390–2401.

Lamberto, D. J., M. M. Alvarez, and F. J. Muzzio (1999). Experimental and computational investigation of the laminar flow structure in a stirred tank, *Chem. Eng. Sci.*, **54**, 919–942.

Launder, B. E. (1995). Modeling the formation and dispersal of streamwise vortices in turbulent flow, 35th Lanchester Lecture, *Aeronaut. J.*, **99**(990), 419–431.

Lee, K. C., and M. Yianneskis (1998). Turbulence properties of the impeller stream of a Rushton turbine, *AIChE J.*, **44**, 13–24.

Mao, K. W., and H. L. Toor (1971). A diffusion model for reactions with turbulent mixing, *AIChE J.*, **16**, 49–52.

Mathieu, J., and J. Scott (2000). *An Introduction to Turbulent Flow*, Cambridge University Press, New York.

McKelvey, K. N., H. Yieh, S. Zakanycz, and R. S. Brodkey (1975). Turbulent motion, mixing and kinetics in a chemical reactor configuration, *AIChE J.*, **21**, 1165–1176.

Micale, G., A. Brucato, F. Grisafi, and M. Ciofalo (1999). Prediction of flow fields in a dual impeller stirred vessel, *AIChE J.*, **45**, 445–464.

Michelet, S. (1998). Turbulence et dissipation au sein d'un reacteur agité par une turbine Rushton: vélocimètrie laser Doppler a deux volume de mesure, Ph.D. dissertation, Institut National Polytechnique de Lorraine, France.

Monclova, L. A., and L. J. Forney (1995). Numerical simulation of a pipeline tee mixer, *Ind. Eng. Chem. Res.*, **34**, 1488–1493.

Nienow, A. W. (1997). On impeller circulation and mixing effectiveness in the turbulent flow regime, *Chem. Eng. Sci.*, **52**, 2557–2565.

Nouri, J. M., J. H. Whitelaw, and M. Yianneskis (1987). The scaling of the flow field with impeller size and rotational speed in a stirred reactor, presented at the 2nd International Conference on Laser Anemometry, Advances and Applications, Strathclyde, Scotland, Sept. 21–23.

Pope, S. B. (2000). *Turbulent Flows*, Cambridge University Press, New York.

Praturi, A. K., and R. S. Brodkey (1978). A stereoscopic visual study of coherent structures in turbulent shear flow, *J. Fluid Mech.*, **89**, 251–272.

Ranade, V. V. (1997). An efficient computational model for simulating flow in stirred vessels: a case of Rushton turbine, *Chem. Eng. Sci.*, **52**, 4473–4484.

Ranade, V. V., and S. M. S. Dommeti (1996). Computational snapshot of flow generated by axial impellers in baffled stirred vessels, *Trans. Inst. Chem. Eng.*, **74A**, 476–484.

Revstedt, J., L. Fuchs, and C. Tragardh (1998). Large eddy simulations of the turbulent flow in a stirred reactor, *Chem. Eng. Sci.*, **53**, 4041–4053.

Roberts, R. M., M. R. Gray, B. Thompson, and S. M. Kresta (1995). The effect of impeller and tank geometry on circulation time distributions in stirred tanks, *Chem. Eng. Res. Des.*, **73A**, 78–86.

Roussinova, V., B. Grgic, and S. M. Kresta (2000). Study of macro-instabilities in stirred tanks using a velocity decomposition technique, *Chem. Eng. Res. Des.*, **78**, 1040–1052.

Roussinova, V. T., S. M. Kresta, and R. Weetman (2003). Low frequency macroinstabilities in a stirred tank: scale-up and prediction based on large eddy simulations, *Chem. Eng. Sci.* **58**, 2297–2311.

Spalding, D. B (1971). Mixing and chemical reaction in confined turbulent flames, presented at the 13th International Symposium on Combustion, Combustion Institute, Pittsburgh, PA, pp. 649–657.

Tang, L., F. Wen, Y. Yang, C. T. Crowe, J. N. Chung, and T. R. Troutt (1992). Self-organizing particle dispersion mechanism in a plane wake, *Phys. Fluids A*, **4**, 2244–2251.

Taylor, G. I. (1921). Diffusion by discontinuous movements, *Proc. London Math. Soc.*, **20**, 196–212.

Tennekes, H., and J. L. Lumley (1972). *A First Course in Turbulence*, MIT Press, Cambridge, MA.

Toor, H. L. (1962). Mass transfer in dilute turbulent and nonturbulent systems with rapid irreversible reactions and equal diffusivities, *AIChE J.*, **8**, 70–78.

Toor, H. L. (1969). Turbulent mixing of two species with and without chemical reaction, *Ind. Eng. Chem. Fundam.*, **8**, 655–659.

Vassilatos, G., and H. L. Toor (1965). Second order chemical reactions in a nonhomogeneous turbulent fluid, *AIChE J.*, **2**, 666.

Vivaldo-Lima, E., P. E. Wood, A. E. Hamielec, and A. Penlidis (1998). Calculation of the PSD in suspension polymerization using a compartment mixing model, *Can. J. Chem. Eng*., **76**, 495–505.

Wei, H., and J. Garside (1997). Application of CFD modeling to precipitation systems, *Trans. Inst. Chem. Eng*., **75A**, 219–227.

Weetman, R. W. (2002). Personal correspondence.

Yegneswaran, P. K., B. G. Thompson, and M. R. Gray (1991). Experimental simulation of dissolved oxygen fluctuations in large fermentors: effect on Streptomyces clavuligerus, *Biotechnol. Bioeng.*, **38**, 1203–1209.

Yianneskis, M., Z. Popiolek, and J. H. Whitelaw (1987). An experimental study of the steady and unsteady flow characteristics of stirred reactors, *J. Fluid Mech*., **175**, 537–555.

Zhao, Y., and R. S. Brodkey (1998a). Averaged and time resolved, full-field (three-dimensional), measurements of unsteady opposed jets, *Can. J. Chem. Eng*., **76**, 536–545.

Zhao, Y., and R. S. Brodkey (1998b). Particle paths in three-dimensional flow fields as a means of study: opposing jet mixing system, *Powder Technol.*, **100**, 161–165.

Zhou, G., and S. M. Kresta (1996a). Distribution of energy between convective and turbulent flow for three frequently used impellers, *Chem. Eng. Res. Des*., **74A**, 379–389.

Zhou, G., and S. M. Kresta (1996b). Impact of geometry on the maximum turbulence energy dissipation rate for various impellers, *AIChE J.*, **42**, 2476–2490.

Zhou, G., and S. M. Kresta (1998). Evolution of drop size distribution in liquid-liquid dispersions for various impellers, *Chem. Eng. Sci*., **53**, 2099–2113.

Zwietering, T. N. (1958). Suspending of solid particles in liquid by agitators, *Chem. Eng. Sci*., **8**, 244–253.